



A University of Sussex PhD thesis

Available online via Sussex Research Online:

<http://sro.sussex.ac.uk/>

This thesis is protected by copyright which belongs to the author.

This thesis cannot be reproduced or quoted extensively from without first obtaining permission in writing from the Author

The content must not be changed in any way or sold commercially in any format or medium without the formal permission of the Author

When referring to this work, full bibliographic details including the author, title, awarding institution and date of the thesis must be given

Please visit Sussex Research Online for more information and further details

WHAT THE AVIAN EYE TELLS ITS BRAIN:
PROCESSING OF CHROMATIC AND
ACHROMATIC INFORMATION AT THE LEVEL
OF CHICKEN RETINAL GANGLION CELLS

Marvin Seifert

Submitted for the degree of Doctor of Philosophy

University of Sussex

May 2022

Declaration

The thesis entitled “WHAT THE AVIAN EYE TELLS ITS BRAIN: PROCESSING OF CHROMATIC AND ACHROMATIC INFORMATION AT THE LEVEL OF CHICKEN RETINAL GANGLION CELLS” submitted for the degree of Doctor of Philosophy only presents my own work. Collaborative work and external data are explicitly stated throughout the manuscript.

Contributions by others:

Paul A. Roberts developed and implemented the clustering algorithm that was used to identify clusters of function RGC types.

George Kafetzis established the phase lock analysis used to determine the quality of chirp responses.

Previously published work:

Parts of the introduction, summarizing the literature on the morphology of the chicken retina has been published as review in a peer-reviewed journal and was adapted by Marvin Seifert for this thesis:

Seifert, M., Baden, T., Osorio, D., 2020. The retinal basis of vision in chicken. Seminars in Cell & Developmental Biology. <https://doi.org/10.1016/j.semcdb.2020.03.011>

I hereby declare that this thesis has not been and will not be, submitted in whole or in part to another University for the award of any other degree.

Brighton, 30.04.2022

Abstract

Birds have highly sophisticated vision, including tetrachromacy but it is unknown how visual information is processed within the retina. Using a high density multielectrode, stimulus driven extracellular electrical signals of multiple retinal ganglion cells (RGC) were measured in parallel. Twenty-seven functionally distinct RGC types were identified by clustering, revealing major principles of avian RGC electrophysiology:

Firstly, most RGCs were excited by both ON and OFF steps, and had complex chromatic sensitivities and opponency responses, often in combination with wavelength dependent and long response latencies in the ON channel. These RGCs resemble small bistratified (blue-ON) RGCs in the primate retina.

A second group of RGCs showed OFF dominant responses, faster response latencies, and simpler spectral sensitivities, likely matching double cones. These cells potentially form a classical achromatic contrast pathway, like primate alpha/parasol RGCs.

Focusing on wavelength dependent response latencies, we found that except for near UV responses, long wavelength ON-responses yielded the shortest latency and most synchronised responses, consistently followed by shorter wavelengths. Combining these insights, we used principal component analysis of flash-responses to reveal that greyscale and “colour” stimuli are encoded in a near-orthogonal manner.

We tentatively suggest that birds use a combination of time- and opponency-coding to represent spectral information, while a smaller proportion of cells act as fast greyscale OFF channels which serve achromatic vision.

TABLE OF CONTENTS

List of Figures	6
List of Tables	6
Acknowledgments.....	7
Abbreviations and terms.....	8
Chapter 1: Introduction	11
Vision.....	12
The vertebrate retina.....	12
The structural diversity of vertebrate retinas.....	13
Visual processing in the vertebrate retina.....	14
Contrast vision	15
Colour vision	16
Avian vision	20
The red junglefowl	20
The structure of the chicken retina	20
Photoreceptors	21
Horizontal cells.....	26
Bipolar cells.....	28
Amacrine cells	29
Retinal ganglion cells.....	30
Retinal function.....	33
Thesis aims.....	33
Chapter 2: Methods	35
Animal handling	35
Dark adaptation and sacrifice	35
MEA experiments.....	35
Dissection.....	35
Light stimulation	37
General setup.....	37
Stimuli	39
Recordings.....	40
MEA.....	40
Software.....	40
General data analysis.....	41
Spike sorting.....	41

First quality control	42
Stimulus and spike alignment	42
Second quality control	42
Clustering	42
Specific data analysis	44
On OFF analysis	44
Tuning curves	45
Identification of kernel types	45
Chirp analysis	45
Photoreceptor modelling	45
First spike analysis.....	46
Statistics	46
Chapter 3: Chicken retina MEA recordings.....	46
Summary	46
Introduction	47
MEA introduction.....	47
MEA studies on chicken retina.....	48
Results.....	48
Dissection protocol	49
Recordings.....	50
Discussion.....	51
Dissection	51
Recordings.....	51
Temperature	51
Spike sorting.....	52
Chapter 4: General RGC responses.....	59
Short summary.....	59
Introduction	59
Results.....	60
ON OFF responses.....	60
Chromatic responses.....	61
Chromatic opponent responses.....	62
Chirp responses.....	64
Discussion.....	66
Key findings	66
ON and OFF responses.....	66

Chromatic responses.....	67
Response kinetics.....	68
Chirp responses.....	68
Limitations of the methods.....	69
Chapter 5: Functional RGC types	83
Short summary.....	83
Introduction	83
Results.....	85
Part 1: Functional RGC types.....	85
Part 2: Photoreceptor inputs	91
Discussion.....	92
Functional RGC types	92
Chromatic functional RGC types	94
Limitations.....	96
Chapter 6: Response Shapes.....	115
Summary	115
Introduction	115
Results.....	116
Response shape	116
Individual functional RGC types	117
Chromatic vs achromatic vision	118
Discussion.....	119
General.....	119
“Double cone-RGCs”?	120
A double cone pathway?	121
Chapter 7: Conclusion	135
Significance of findings	135
Limitations	136
Outlook	137
Literature	138

LIST OF FIGURES

Figure 1 Organization of the vertebrate retina.....	19
Figure 2 The basis of chicken colour vision. Redrawn and modified from (Kelber, 2019).	22
Figure 3 Overview over bipolar-, horizontal-, and ganglion cell morphology.	32
Figure 4 Delivery of light stimuli on the MEA setup.	38
Figure 5 LEDs used in relation to chicken opsins.	39
Figure 6 MEA recording of the chicken retina..	53
Figure 7: Overview over recordings used for this study	55
Figure 8: Quality differences between recordings; waves of spreading depression.....	57
Figure 9 Spike sorting pathway and results	58
Figure 10: ON OFF dominance by species.....	67
Figure 11: RGC responses to white and chromatic ON and OFF steps.	71
Figure 12: Examples of single cell responses to the “white” step stimulus.....	72
Figure 13: Examples of single cell responses to chromatic stimuli.....	73
Figure 14: Comparisons of ON and OFF response amplitudes.	75
Figure 15: Full Field Colour Noise	77
Figure 16 Full Field Colour Noise: general kernel properties.	79
Figure 17 Chirp Responses Overview.....	81
Figure 18 Chirp responses of single cells.	82
Figure 19 Basic clustering statistics.	99
Figure 20: General response properties of the 10 biggest clusters.....	101
Figure 21 Overview over responses of the ten functional RGC types with the most cells (sorted by cell number, rows) and four additional handpicked functional RGC types.	104
Figure 22 Overview over response properties of all clusters (rows).	108
Figure 23: Condensation of 100 clusters into 27.	110
Figure 24 Modelling of photoreceptor inputs of functional RGC types.....	112
Figure 25 Major chromatic opponency axes in chicken RGCs	113
Figure 26 Response shapes and population time to first spike depend on stimulus wavelength and contrast.	125
Figure 27 ON responses at different wavelength and contrast levels follow different trajectories in PCA space in contrast to OFF responses.	127
Figure 28 Comparison of population responses response shapes at different wavelengths and stimulus contrast levels and between ON and OFF.	129
Figure 29 Response shape differences of single functional RGC types evaluated in PC space.	131
Figure 30 Time to first spike differences between different functional RGC types.....	133
Figure 31 Comparison of chirp responses between different functional RGC types.....	134

LIST OF TABLES

Table 1: Photoreceptor topography in the chicken retina as found in the literature.	23
Table 2: Ringer solution ingredients.	35
Table 3 Stimuli used for this study and their properties	40
Table 4 Most common types of chromatic opponencies and their modelled inputs as displayed by functional RGC types.	96

ACKNOWLEDGMENTS

This PhD has been an extremely instructive time for me, and this is almost entirely due to all the people who have shared (parts of) the journey with me. I am greatly thankful to all these people and to some people specifically. Foremost, I would like to thank Tom Baden and Daniel Osorio for entrusting me with the launching of a completely new experimental setup and analysis pipeline in the lab and for all the advice they have given me along the way. I have learned so much from you.

This thesis would have not been possible without the help of my thesis committee: I thank Leon Lagnado, Jeremy Niven, and Chris Buckley for their input.

I thank the University of Sussex for providing me with a research grant and the Rank prize trust for supporting me financially during the difficult Covid years.

Learning science is not only a story about supervision, but also collegueship. I have learned everything about optical stimulators and open hardware from Maxime Zimmerman and André Maia Chagas. Thank you, guys, that you were patient with me while I was short circuiting one Arduino at a time until I learned to do better. Thanks Max, for teaching me how to 3D print my own ear.

I thank Philipp Bartel for introducing me to Python, endless discussions about neuroscience, metaphysics, ethics, Kant, Aristoteles, and the futility of human existence.

Special thanks to Takeshi Yoshimatsu for introducing me to the world of retina dissections and to Natasha P-Stantcheva for ordering thousands of parts for the setup.

Thanks to George Kafetzis for testing all my scripts, the help with the chirp analysis, lots of good discussions in the lab and all the Sunday roasts/breakfasts that we have shared.

Thanks to Paul A. Roberts for developing a clustering algorithm fitting my dataset.

I'd like to thank my family for all the support they have given me over the years, especially my mum Monika and my grandma Annelies. I wish to thank Simon for staying a close friend despite my "escape" to the other side of the channel.

Finally, I wish to thank Francesca for her loving support over these years. At first, I wasn't sure about sea swims in 15° C water, but they surely have helped me keeping a cool head over the years. Thank you for all the different perspectives on life you have given me, and for never giving up showing me what really matters in life (it's not action potentials).

ABBREVIATIONS AND TERMS

“White” steps	Steps that consist of all LEDs and are perceived as “white” by the chicken
AC	Amacrine cell
Achromatic cells	Cells that do not show chromatic opponency
BC	Bipolar cell
BIC	Bayesian information criterium
Biggest RGC type	RGC type containing the highest number of cells
Bin	A single bin of the PSTH
Biphasic kernel	Kernels that show deflection from baseline that has two peaks (ON and OFF or vice versa)
Blue (LED; Kernel)	420 nm LED, Kernel derived from 420 nm stimulation
C(1,2,3 etc.)	Cluster = RGC type
Chirp	Frequency chirp, ON OFF stimulus with exponentially increasing sinusoidal frequency
Chromatic opponency	Opponency in the responses that is dependent on the wavelength of stimulation.
Chromatic stimuli	Stimuli that test responses at different wavelengths
Cluster	A group of data points that are more similar than data points in other groups
Clustering	The task of dividing data points into several groups such that data points in the same groups are more similar to other data points in the same group than those in other groups
Colour	Here used like “Chromatic information”
Complex chromatic opponency	Colour opponent responses that in addition display wavelength dependent integration time differences
Cone	Cone photoreceptor
Confidence interval	Represents the long-run proportion of correspondingly computed intervals that end up containing the true value of the parameter
Contrast	Weber contrast $\frac{I-I_h}{I_h}$ I=stimulus, I _h = stimulus history
CStep	Contrast Step
Cyan (LED, Kernel)	480 nm LED, Kernel derived from 480 nm stimulation
FFNoise	Chromatic full field binary noise
First order kernels	Linear kernels

First Spike Synchronization	The tightness of the kernel density estimation of first spikes. Tighter distributions are more synchronized.
GABA	Gamma-aminobutyric acid
Green (LED, Kernel)	505 nm LED, Kernel derived from 505 nm stimulation
HC	Horizontal cell
Hz	Frequency in Hertz
INL	Inner nuclear layer
Integration time	Time between the stimulus and the measurement of a triggered spike
IPL	Inner plexiform layer
Kernel amplitude	The max number of spikes that got triggered by a stimulus at given time before a spike
L cone	Long wavelength sensitive cone
LED	Light-emitting diode
Light spectrum	Usually the spectrum of visible light, here also used as the combined spectrum of all used LEDs (from 360 nm to 630 nm)
Luminance	Luminous intensity per unit area of light travelling in each direction
LWS	Long wavelength sensitive
LWS cone	Single cone expressing LWS opsin
M cone	Medium wavelength sensitive cone
Monophasic kernel	Kernel that shows a deflection from baseline that has one peak (ON or OFF)
ms	Milliseconds
mV	Millivolts
MWS	Medium wavelength sensitive
MWS cone	Single cone expressing RH2 opsin
nm	Nanometre
OFF cells	Cells that only respond to OFF steps
OFF step	Light decrement stimulus
ON cells	Cells that only respond to ON steps
ON step	Light increment stimulus
ONL	Outer nuclear layer
ON-OFF cells	Cells that respond to ON and OFF steps
OPL	Outer plexiform layer
PC	Principal component
Phase locked responses	Responses that follow the ON and OFF phases of the chirp with consequent increases and decreases in spike rate.
Photoisomerization	The process of photon absorption by the photoreceptor's opsin
Population first spike	The peak of the kernel density estimation of first spikes of a cell population
PSTH	Peristimulus time histogram

Red (LED, Kernel)	630 nm LED, Kernel derived from 630 nm stimulation
Response amplitude	The increase in spike rate above baseline
Response Kernel	Summary of the average stimulus history and integration time that triggered a spike
Response kinetics	Sustained vs transient responses, response integration time
Response shape	The combination of response amplitude and response delay.
Resulting vector strength	Given a set of vectors, the resulting vector strength is the mean direction of the set of vectors and the resulting mean strength of those vectors
RGC	Retinal ganglion cell
RGC Population	All RGCs that were measured
RGC types	Types of RGCs that are either functionally or genetically distinct
RPE	Retinal pigment epithelium
s	seconds
S cone	Short wavelength sensitive cone
Spectral tuning curve	The amplitudes of chromatic stimulus responses as a function of wavelength of stimulation.
Spike	Neuronal action potential
Spike rate	Nr of spikes per second
Spike sorting	The identification of signals coming from the same neuron recorded by multiple electrodes of the MEA
Spks/sec	Spikes per second
SWS	Short wavelength sensitive
SWS1 cone	Single cone expressing the SWS1 opsin
SWS2 cone	Single cone expressing the SWS2 opsin
Time to first spikes	The time delay between stimulus onset and onset of a cell's response
UV	Ultraviolet
μm	Micrometre

CHAPTER 1: INTRODUCTION

*So wie das letzte Grün in Farbentiegeln
sind diese Blätter, trocken, stumpf und rauh,
hinter den Blütendolden, die ein Blau
nicht auf sich tragen, nur von ferne spiegeln.*

*Sie spiegeln es verweint und ungenau,
als wollten sie es wiederum verlieren,
und wie in alten blauen Briefpapieren
ist Gelb in ihnen, Violett und Grau;*

*Verwaschenes wie an einer Kinderschürze,
Nichtmehrgetragenes, dem nichts mehr
geschieht:
wie fühlt man eines kleinen Lebens Kürze.*

*Doch plötzlich scheint das Blau sich zu
verneuen
in einer von den Dolden, und man sieht
ein rührend Blaues sich vor Grünem freuen.*

Blaue Hortensie, Rainer Maria Rilke

*An empty paint can's residue of green:
These leaves of dry and flaky faded hue
Beneath the blossoms, bristling the blue
They wear in borrowed coats, a reflected
sheen.*

*Mirroring colour, flickering and teary,
As if they'd rather it just went away,
Blue, faded leaves of brittle stationery
Now stained with yellow, violet, and grey.*

*An overwashed, discoloured childhood
apron,
No longer worn. Kept, not for any use.
An infant life, now fades towards cessation.*

*But suddenly, a nascent blue is seen
In yet another blossom, now one views
The tranquil blue, delighting in the green.*

Blue Hydrangea, translation by Kai Frieze

VISION

Light carries information about visual properties of objects in the physical world. Specialized photosensitive organs, eyes, have evolved multiple times for visual guidance of behaviour (Gehring and Ikeo, 1999; Lamb et al., 2007; Nilsson, 2013; Nilsson and Arendt, 2008). Distinct habitats have specific visual characteristics that require well-adapted eyes. Eyes may therefore differ from species to species, but according to the current visual ecology of a species and its evolutionary history (Cronin, 2014).

Unlike a camera, which represents optical signals passively pixel by pixel, eyes process visual information by enactment (Noë, 2006). This process starts at the instant a photon is detected by retinal photoreceptors, and by the time information is transmitted to the brain, it is heavily compressed (Meister, 1996; Meister and Berry, 1999). Understanding this compression has been the aim of thousands of studies in recent years.

Because humans are vertebrates many studies have investigated visual processing in vertebrates (Baden, 2020). Vertebrate vision first evolved during the Cambrian explosion over 500 million years ago (Lamb, 2019; Lamb et al., 2007). The *Bauplan* of the ancestral vertebrate eye serves as the basic framework of all modern forms, despite evolutionary modifications to match ecological needs (Baden, 2020; Bowmaker, 2008; Yokoyama, 2002).

THE VERTEBRATE RETINA

The vertebrate eye consists of an eyecup containing a lens at the distal end and the inverted retina, which is a highly organized, layered structure of five canonical retinal cell types: photoreceptors, horizontal cells, bipolar cells, amacrine cells and retinal ganglion cells (Lamb et al., 2007; Masland, 2012, 2001), (**Figure 1**). Each type populates one of three nuclear layers and projects axons and dendrites into two synaptic (plexiform) layers. Photoreceptors populate the outer nuclear layer (ONL) and contain light sensitive visual pigments called opsins. They form connections with bipolar cells and horizontal cells in the outer plexiform layer (OPL). Cell bodies of bipolar cells, amacrine cells and horizontal cells are in the inner nuclear layer (INL). Bipolar cells transmit their signals to retinal ganglion cells (RGC) by synapses in the inner plexiform layer (IPL). The ganglion cell layer (GCL) consists of RGCs which collect visual information and transmit it to the brain via the optic nerve.

Modification of photoreceptor inputs is a key aspect in the evolution of the vertebrate retina, leading to modification in the organization and diversity of downstream cell types (Baden, 2020; Baden and Osorio, 2019). The initial vertebrate retina likely consisted of two different types of photoreceptors (Lamb, 2019, 2016). Rods containing the photopigment RH1, have a higher light

sensitivity and primarily serve vision in dark conditions (scotopic vision), whereas cones are sensitive to daylight luminance levels (photopic vision). Each type can be further divided into subtypes based on spectral tuning, which is given by the probability of a photon initiating the light response as a function of wavelength (Baden and Osorio, 2019). Photoreceptor spectral tuning depends primarily on the opsin. SWS1, SWS2, MWS and LWS cones express SWS1, SWS2, RH2, LWS opsin respectively. This is where colour vision arises. The outputs of (rod and) cone subtypes with different spectral tuning are compared on the level of horizontal, bipolar and ganglion cells which ultimately enables the perception of chromatically distinct stimuli.

THE STRUCTURAL DIVERSITY OF VERTEBRATE RETINAS

Photoreceptors consume high amounts of energy by maintaining the dark current (the continuous depolarization of the photoreceptors membrane potential in dark conditions) (Country, 2017). This represents a high evolutionary pressure (Niven and Laughlin, 2008) leading to a “use it or lose it” principle, whereby unused photoreceptor subtypes are lost under natural selection. This has happened during vertebrate evolution on several occasions (Baden, 2020; Baden and Osorio, 2019): Mammals have lost SWS2 and MWS cones, while Sharks have lost all but MWS cones. Similarly, the ability to better differentiate chromatic distinct stimuli can be selectively advantageous, and vertebrates have evolved photoreceptor types with new spectral tuning multiple times. For example, Primates and Marsupials gained a long wavelength sensitive opsin based on the LWS opsin. Amphibians evolved an additional rod type allowing colour vision in scotopic conditions. Some vertebrates (including birds) gained an additional double cone expressing LWS opsin, whose exact function remains unknown.

Changing the number of input channels can affect the organization and function of downstream neurons of the retina. Despite the common framework, vertebrates can differ strongly in the number of retinal cell types (Baden, 2020). A challenge faced by any attempt to describe the typical vertebrate retina and its processing capacities, is the limited understanding of non-mammalian groups (Baden, 2020). Mammals serve as a good model organism to study human vision, but they are a suboptimal model of typical vertebrate vision. This is because mammals have been nocturnal for a long period of their evolutionary history (Heesy and Hall, 2010), when simplification of inputs was selectively advantageous, which resulted in the loss of two different types of cones (carrying SWS2 and RH2 opsins). Thus most contemporary diurnal mammals carry only two types of cones: SWS1 cones and LWS cones (Baden and Osorio, 2019).

In contrast, contemporary bony fish (teleost) may well have a retina that closely resembles the original vertebrate framework, and in recent years the zebrafish has emerged as a model

organism for vertebrate vision (Baden, 2021). Zebrafish express all the original four types of cone opsins and rods and have specialist areas within their retinas for prey capture in their specific habitat. Accordingly, chromatic information provided by all four cone types is processed and the SWS1 cone specifically utilized for detection of prey.

The first vertebrates were fish-like and aquatic. Hence, similarities in retinal structure between modern day bony fish and early vertebrates are expected. It is more remarkable that fish and tetrapods share so many key principles of retinal processing.

VISUAL PROCESSING IN THE VERTEBRATE RETINA

During visual processing, input signals quickly need to be filtered for important information, leading to two common principles in neuronal sensory processing, namely parallel retinotopic processing and convergence of information (Wässle, 2004). Retinotopic processing means that the retina consists of neighbouring, functionally similar units of neuronal circuits, which process visual information from neighbouring parts in the visual field. Convergence means, that within these units, many photoreceptors project to fewer bipolar cells which project on even fewer RGCs (**Figure 1 a**). The strength of convergence may differ across the retina, depending on the situation (day vs night), and on how much weight is given to the information coming from a single photoreceptor (Querubin et al., 2009; Volgyi, 2004). Together these principles directly lead to the concept of receptive fields, which in our case corresponds to the region of the retina that triggers a response within a retinal neuron (Hubel and Wiesel, 1959).

The first receptive field in the visual pathway is the spatial and spectral range over which a photoreceptor can detect light (Warrant and Nilsson, 1998), (**Figure 1 a**). During phototransduction, the energy of the photon is converted into a graded potential that is transmitted chemically via synapses to bipolar cells in the OPL (Yau and Hardie, 2009) under modulation of horizontal cells (Behrens et al., 2019; Chapot et al., 2017; Crook et al., 2011). Each bipolar cell receives signals from multiple photoreceptors (Behrens et al., 2016; Euler et al., 2014; Nelson and Connaughton, 2012). This establishes the receptive field of bipolar cells. Bipolar cells commonly show centre surround inhibition whereby the light stimulation of photoreceptors within the centre of the receptive field triggers responses in opposed polarity compared to light stimulation of surrounding photoreceptors. Optical stimulation of the receptive field centre can either lead to excitatory (ON bipolar) or inhibitory (OFF bipolar) responses, depending on which kind of ligand gated ion channels are expressed (DeVries, 2000). If both, centre, and surround are stimulated, the antagonistic inhibitory and excitatory signals reduce the neural response (Victor, 2005). Bipolar cells thus integrate information from multiple

photoreceptors, and by comparison of centre and surround inputs over a given integration time window, filter this information based on spatial and temporal properties.

At the next stage of the visual pathway multiple bipolar cells transmit information via chemical synapses onto RGCs, with modulation by amacrine cells (Pang et al., 2002)(Van Wyk et al., 2009). Since they are located further downstream in the circuit, RGC receptive fields can encode more complex stimulus information, including visual motion, orientation, or chromatic information (Baden et al., 2016; Goetz et al., 2021; Jouty et al., 2018).

By the time the visual signal has reached RGCs, it is compressed through the above-mentioned processes, and thus carries specific, filtered information about the stimulus. Here we return to the concept of functional units. RGC must transmit all stimulus information to the brain. Their signal bandwidth however is limited (Meister, 1996; Meister and Berry, 1999). RGCs are spiking neurons, hence, all information is transmitted to the brain encoded in spike trains – sequences of action potentials generated at the RGC's axon hillock. Because visual stimuli are rich in information, the retina has different types of RGC's that encode different kinds of visual information. One RGC type might encode contrast in its receptive field while another encodes chromatic information and so on. Because of this, receptive fields of RGC types often overlap, while individual types tile the retina covering all visual space(Field and Chichilnisky, 2007). This organization is extensively studied in primates, and it is now possible to reconstruct the contrast information of the entire visual scene by decoding the information content of spike trains of contrast coding RGC types (Brackbill et al., 2020).

CONTRAST VISION

On the most fundamental level, vision is the extraction of information contained in the light that reaches the retina. What information does light contain? On the most basic level the absence or presence of light is information. Consider a bacterium in which a specific cascade of genes encoding the photosynthesis apparatus can be activated or not. A simple binary light detector would do the job. Vertebrate photoreceptors are light detectors, but rather than being either switched on or off, they extract the information about light intensities as well. Because the eye allows the projection of an image of the visual world onto its retina, spatial and temporal information about differences of light intensity can be extracted. This allows for the most basic kind of vision: contrast vision. (Amesbury and Schallhorn, 2003). Because of adaptation, Weber Fechner law applies which states that the threshold for detection of a stimulus is proportional to the stimulus intensity (Johnson et al., 2002). In case of vision, background luminance level mostly determines the adaptive state of the eye. Adaptation allows stimulus detection over light

intensities spanning over multiple order of magnitude. Contrast responses encode most of the important features, such as object shapes and movement.

Contrast vision is established in the OPL, where photoreceptor outputs are integrated via horizontal cells, and transmitted to bipolar cells. Horizontal cells compare activation states of multiple connected photoreceptors and provide feed-forward excitation and lateral inhibition (Behrens et al., 2019, 2019; Chapot et al., 2017; Crook et al., 2011). Consider a light dark edge image on the retina: on the light side, photoreceptor responses are amplified by feed forward excitation while cone responses on the darker side are suppressed further by lateral inhibition. In combination the spatial contrast sensitivity is dynamically increased (Amesbury and Schallhorn, 2003).

Bipolar cells implement contrast coding through receptive fields with centre surround inhibition. As a result, bipolar cells with receptive fields located on the dark light edge will respond more strongly than bipolar cells further away from the edge receiving uniform inputs across the receptive field (Amesbury and Schallhorn, 2003). In summary, receptive field properties specifically serve contrast vision, and thus extract the most important information from a visual scene efficiently.

COLOUR VISION

Light reaching the retina contains another dimension of information. As an electromagnetic wave, light has a specific wavelength or frequency. Vertebrate photoreceptors contain opsins that have different spectral tuning functions, which means they are sensitive to different wavelengths of light (Baden and Osorio, 2019). The ability to differentiate spectral information of a stimulus independent from information about stimulus light intensity is commonly referred to as colour vision. Activation of each type of photoreceptor is a combined function of wavelength and light intensity. Thus, a single type of photoreceptor is not sufficient for colour vision. By comparing the responses of a least two types of photoreceptors, the information about stimulus intensity can be distinguished from information about chromatic stimulus content (Walls, 1942). It might appear that the more spectrally distinct types of receptors can sample the available light, the better is stimulus differentiation based on chromatic content. However, receptors are not infinitely small and packing the retina with too many types of photoreceptors may cause a break down in the above-described contrast vision ability and effect visual acuity. Furthermore, most natural reflectance spectra vary smoothly over wavelength, which would leave ever more types of receptors with little additional spectral detail to extract (Osorio and Vorobyev, 2008). Which number of receptor types is ideal? Principal component

(PC) analysis can help understanding the information content available in a natural scene. It was found that the first PC, accounting for achromatic stimulus information explains 90% of the variance in the data (Ruderman et al., 1998). (Maloney, 1986) found that three PCs can explain 98% of the available variance in natural spectra over the human visible spectrum. (van Hateren, 1993) asked how receptor noise would affect spectral coding and concluded that three or two spectrally distinct receptor types maximize spectral information coded by noisy photoreceptors. Based on these findings, a high number of spectrally different receptor types does not seem beneficial. In fact, most vertebrates have at least two and maximally four spectrally distinct input channels. Dichromacy is typical in mammals with the exceptions of primates and some marsupials which are trichromats. Much of our understanding how colour vision is established at the retinal level comes from extensive studies on primates.

COLOUR VISION ON THE LEVEL OF THE RETINA

Colour vision uses many of the basic visual processing principles of contrast vision as described above. Consider the primate retina: it displays a MWS cone sensitive to medium wavelength and a LWS cone with a red shifted spectral sensitivity. As for contrast vision, LWS and MWS cone outputs are laterally integrated in the OPL under the mediation of horizontal cells, which provide feedback and lateral inhibition. At the level of ganglion cells simple colour opponency (red vs green) is established (Kolb and Marshak, 2003): MWS cones constitute receptive field centres and LWS cones receptive field surrounds or vice versa. As for contrast vision, this leads to an enhancement of colour contrast at the level of bipolar cells. In the periphery, one additional input channel, SWS2, provides additional information about short wavelengths stimulus content and its outputs are laterally integrated with MWS and LWS cone signals establishing a second opponency axis (blue vs yellow). Primate RGCs have four chromatic axes : SWS2 - MWS+LWS, MWS - LWS, LWS+MWS-S and LWS-MWS (Patterson et al., 2019).

TETRACHROMACY

Far less is known about the signal integration in tetrachromatic visual systems. Recently, studies have begun to uncover the colour vision of zebrafish. Here, integration of signals coming from different cone types begins in the OPL under HC modulation. Lateral inhibition establishes an opponency axis between MWS cone outputs and SWS2 cone outputs, while LWS cone responses and UV cone responses remain mostly non-opponent. Zebrafish use LWS cone inputs mostly for achromatic vision and UV cone inputs specifically guide prey capture behaviour (Baden, 2021; Bartel et al., 2021). In addition, Zebrafish eyes have strong retinal specialization, consisting of a "strike – zone" with high visual acuity for prey capture (Zimmermann et al., 2018). Overall zebrafish might be considered trichromats with an additional specialised UV channel.

Little is known about other tetrachromatic vertebrate species. Turtles have a least 12 types of ganglion cells with chromatic opponency, including a SWS1 vs SWS2 cell (Rocha et al., 2008; Ventura, 2001). Little is known about how these opponencies are established prior to RGC outputs. The functional realization of bird colour vision is unknown.

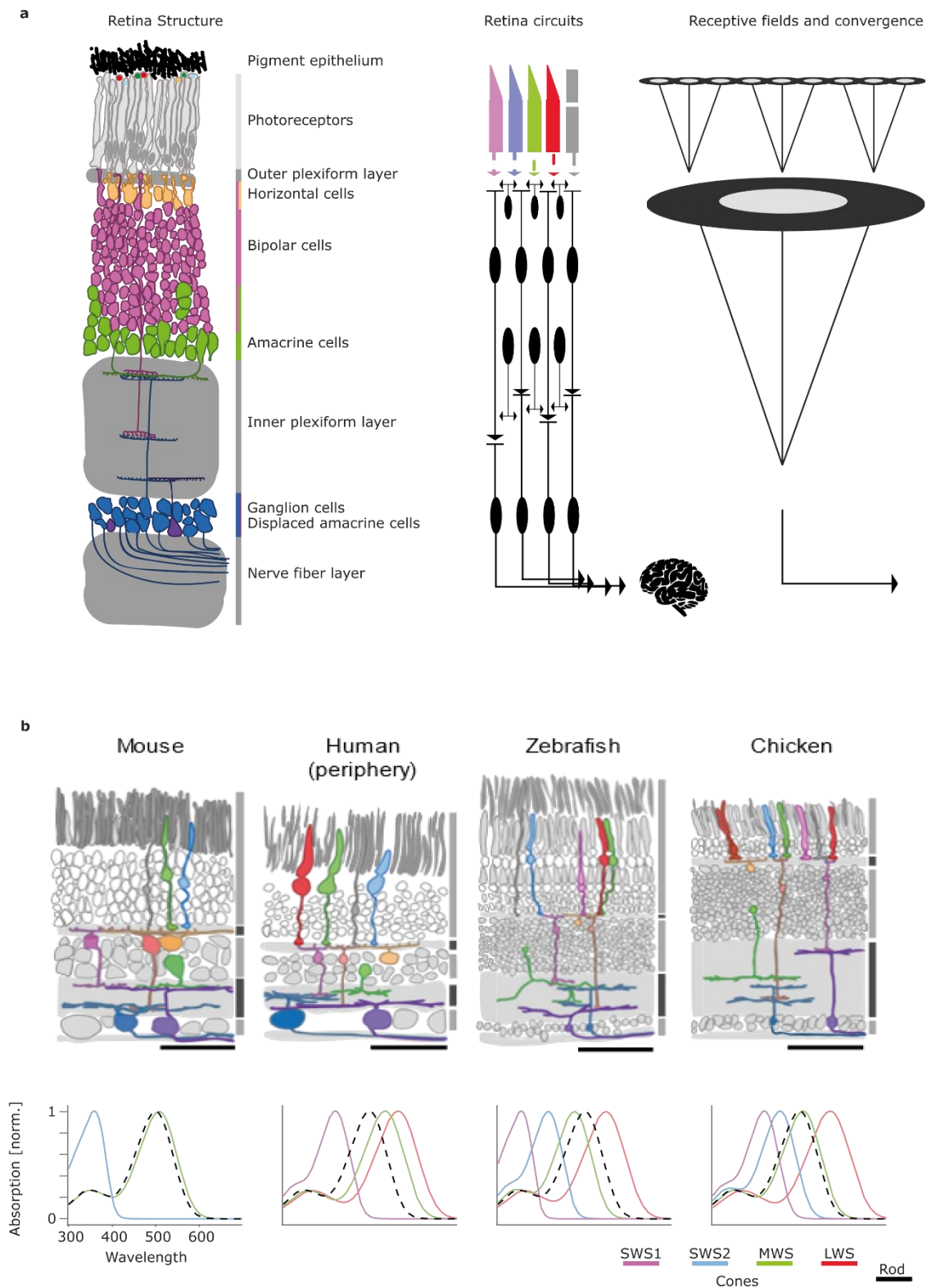


Figure 1 Organization of the vertebrate retina. a. The layered structure of the retina formed by distinct cell types organized into parallel functional units, that establish receptive fields by signal convergence. **b.** Diversity of the retinal structure across different vertebrate species. A main driver of diversity is the differential expression of spectrally distinct opsin families. (Retinal cross sections by Tom Baden)

AVIAN VISION

Observing an eagle majestically gliding over a field, it might be hard to believe that these creatures share an ancestry with fish, but on the level of the retina, the similarities are striking. Birds have retained all original four vertebrate opsins and gained additional structures, which give them excellent vision (Hart, 2001). Bird-typical behaviours like flight, bill control or predator detection require different types of visual guidance, which leads to questions about retinal specialisation (Martin, 2017). Furthermore, it raises the question of how the blueprint of the vertebrate retina has been elaborated, and the extent to which structural and functional similarities are shared with mammalian retinas.

Studying these questions is tricky in part because there is no established avian model organism. Many birds are endangered which prevents their use as models.

Consequently, most knowledge of avian vision comes from extensive anatomical but limited functional studies of the chicken retina. Genetic insights originate from the use of the chicken retina as model for eye disease and development (Wisely et al., 2017). Chickens have a morphologically dense retina populated by neurons with complex branching patterns establishing multistratified plexiform layers, which presumably have different functions. In the following I will give an overview of the literature on the chicken retina, along with significant studies of other birds. The overview is based on (Seifert et al., 2020), updated with some most recent findings.

THE RED JUNGLEFOWL

Subspecies of Red jungle fowl (*Gallus gallus*) were domesticated as chickens independently multiple times in their natural habitat in southern Asia (Eriksson et al., 2008; Fumihito et al., 1994; Kanginakudru et al., 2008; Storey et al., 2012). Today, several, genetically distinct breeds of chicken are used as poultry for egg and meat production (Tadano et al., 2014). It may be that fowl with “poor” visual capabilities were positively selected during domestication (Wang et al., 2016). Nevertheless, chickens rely on visually guided behaviour and their eyes, although of bird-average size, account for a large proportion of their cranial volume compared to mammals.

THE STRUCTURE OF THE CHICKEN RETINA

The chicken retina has all the previously described layers typical in vertebrates. Compared to mammalian retinas the chicken shows more densely packed cell layers, but unlike primates lacks a fovea (Morris, 1982). This is somewhat atypical for a bird, as many species like birds of prey feature two foveae (Mitkus et al., 2017).

PHOTORECEPTORS

Chicken photoreceptors are probably best studied among birds. Photoreceptor cell bodies lie in the ONL, and their outer segments face outwards into the retinal pigment epithelium (RPE). On their proximal side, the pedicle of the receptor axons forms connections with bipolar and horizontal cells in specific layers in the OPL. Many avian retinas, including pigeon (Querubin et al., 2009) and Australian passerines (Wells-Gray et al., 2016) show non-uniform photoreceptor density across the retina reflecting ecological adaptation. The chicken is no exception: the rod free area centralis features about 20,000 photoreceptors per mm^2 while the density at the periphery decreases linearly with eccentricity to about 8000 cells per mm^2 (da Silva and Cepko, 2017; Morris, 1982; Weller et al., 2009).

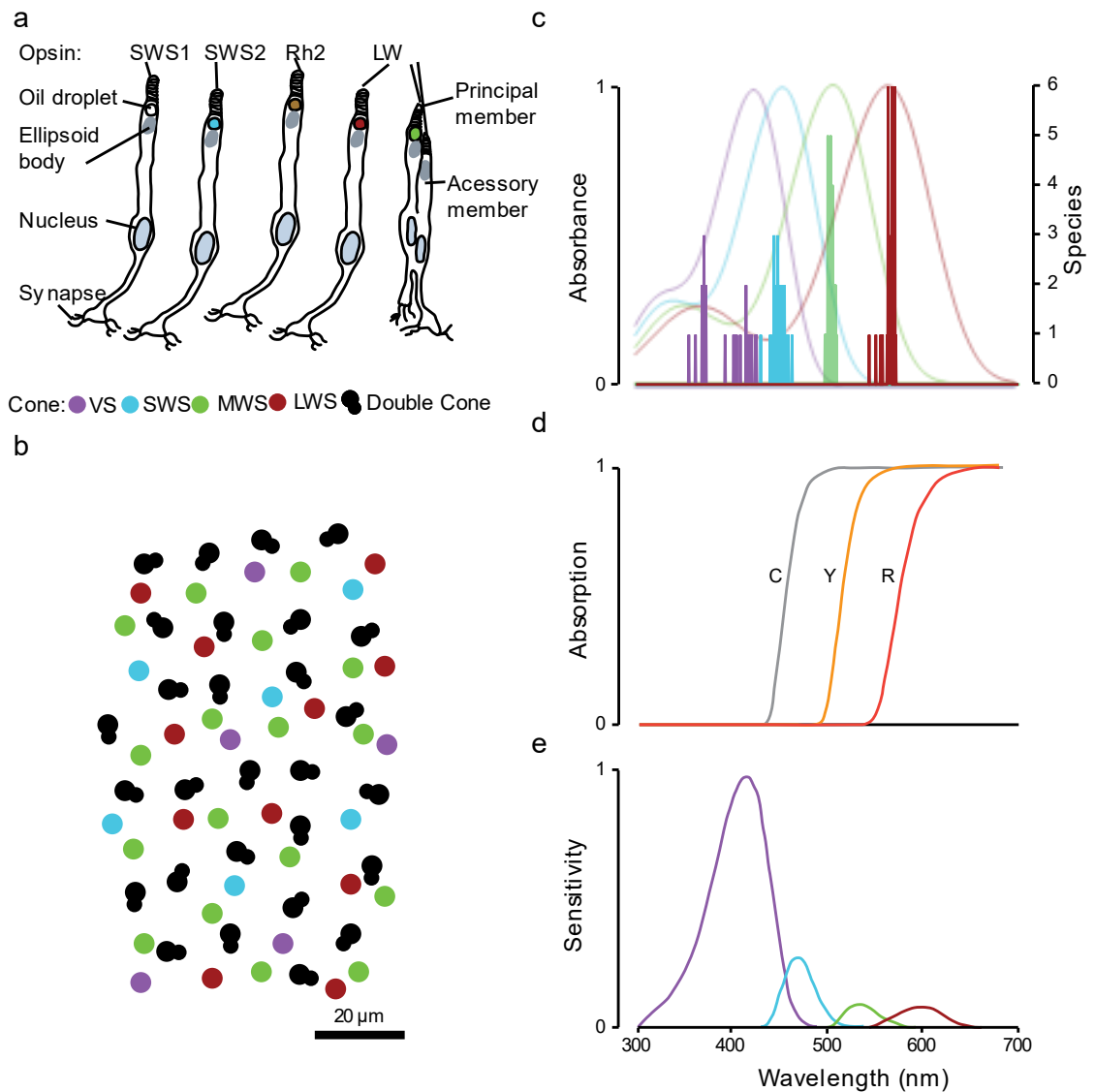


Figure 2 The basis of chicken colour vision. Redrawn and modified from (Kelber, 2019). a. Chicken have five different types of cones and a rod photoreceptor. Cones have oil droplets and ellipsoid bodies which modify the effective opsin spectra. **b.** Cone mosaic in the retina as described by (Kram et al., 2010). Different cone types form independent mosaics with different sized exclusion zones. **c.** Absorption spectra of chicken opsins calculated based on λ_{max} values summarized in (Hart, 2001) and using the opsin template from (Govardovskii et al., 2000). In comparison, the histogram shows λ_{max} values for different other birds. Bin size of the histogram = 0.5nm. **d.** Absorption of the three pigmented types of colour oil droplets found in the chicken as described by (Olsson et al., 2015). The pigments effectively act a long pass filters. **e.** Simulated cone sensitivities based on modelling the light path through the ellipsoid body, oil droplet and outer segments (Wilby et al., 2015; Wilby and Roberts, 2017). The VS cone is the most sensitive by far, the effect of the oil droplet narrows the spectra which show little overlap with each other.

TYPES OF PHOTORECEPTORS

The chicken retina contains all above introduced original vertebrate cone types plus rods and double cones, a set which is typical for birds (Bowmaker and Knowles, 1977; Hart, 2001; Okano et al., 1992). While a general trend can be observed for rods, with density increasing towards the periphery, relative cone (and double cone) ratios vary with eccentricity and between studies, (**Table 1**). This is likely due to examination of different areas of the retina and inter-animal differences. For example, it was suggested that the ratio of L and M cones is determined genetically. It was also shown that L cone densities and the depth of the vitreous chamber of the eye are positively correlated (Gisbert and Schaeffel, 2018). Despite possibly different proportions, each photoreceptor type forms a loose hexagonal mosaic across the retina, likely originating due to lateral inhibition of similar cone types during development. The exclusion differences vary depending on the cone type. In the periphery, double cones form the smallest mosaics and SWS1 cones the biggest (Kram et al., 2010).

Table 1: Photoreceptor topography in the chicken retina as found in the literature. The relative proportion of different types of photoreceptors as described in different studies are compared. The location refers to the location in the retina from which the retinal probes for the respective studies were taken. Values were rounded to nearest integers. (Kram. et. al only counted cones).

Reference	Location	Single cones in %	Double cones in %	Rods in %
(Kram et al., 2010)	Periphery	59	41	
(Morris, 1970)	Central	54	32	14
	Periphery	37	30	33
(López-López et al., 2008)	Central	38	44	18
(Meyer and May, 1973)	Temporal (Segment 3)	23	45	32
	Periphery	20	40	40

SINGLE CONES

The four single cone types found in the chicken express the vertebrate typical opsins SWS1, SWS2, RH2 and LWS (Bowmaker, 2008; Hart, 2001; Okano et al., 1992; Yokoyama, 2008, 2002). The absorption spectra maxima are at 419 nm, 455 nm, 508 nm and 570 nm respectively (Bowmaker and Knowles, 1977; Okano et al., 1989). The nomenclature of the single cone types is based on the expressed opsin, with one exception: MWS cones express RH2. The four different single cone types enable vision of light between 370 nm – 700 nm, and probably give chicken tetrachromatic vision (Kelber, 2019; Olsson et al., 2015; Osorio et al., 1999). Birds can be

classified as UV sensitive or VS sensitive birds, depending on whether the peak sensitivity of the SWS1 opsin lays in the UV range. This is the case for the common starling and the common blackbird, but not for the chicken. In UV sensitive birds, the SWS 2 opsin is UV shifted compared to VS sensitive birds as well, but remaining opsins have similar peak absorption sensitivities (Hart, 2001).

DOUBLE CONES

Birds and other reptiles gained double cones during evolution, which means the addition of a fifth photopic input channel. Double cones consist of gap junction coupled principle member and accessory member both express the opsin LWS (Smith et al., 1985). In fish, a structure referred to as “double cone” consisting of two electrically insulated attached single cones expressing different opsins exists and should not be confused with avian double cones (Meier et al., 2018; Pignatelli et al., 2010). Due to the lack of electrophysiological evidence, the function of the double cone is debated. A prominent hypothesis suggests their involvement in luminance pathways, but not chromatic processing (Jones and Osorio, 2004; Olsson et al., 2015; Sun and Frost, 1997; v. Campenhausen and Kirschfeld, 1998). A recent study questions this hypothesis, showing connections between primary and accessory member with bipolar cells that receive inputs from other single cones. However, two bipolar cell types are suggested to receive sole input from double cone primary members and rods, which is consistent with specific involvement of the double cone in luminance processing (Günther et al., 2021). Importantly however, raptor fovea lacks double cone , which indicates that single cones are sufficient for luminance vision (Mitkus et al., 2017).

RODS

Few studies have investigated scotopic vision and the function of rods in chicken, but they are known to contain the photopigment RH1 and serve vision in dim light (Bowmaker and Knowles, 1977; Schaeffel et al., 1991). As mentioned above, the rod density in the chicken retina increases towards the periphery but remains well below that of common mammals.

OPTICAL PROPERTIES OF CHICKEN PHOTORECEPTORS

Photoreceptors are comprised of inner and outer segments, the latter containing the photosensitive opsins. They are about 1.5 μm in diameter and 30 μm in length. Light is guided through the inner segments and absolute, angular, and spectral sensitivity is altered by refractive index differences within the cell and with the external medium (Westheimer, 2008; Wilby et al., 2015). Between the inner and outer segments lie two organelles with high refractive index, the ellipsoid body, and an oil droplet, which affect spectral sensitivities. The ellipsoid body contains an abundance of mitochondria, which increase the refractive index (Wilby et al., 2015;

Wilby and Roberts, 2017). Oil droplets can have two different functions: they either act as mini lenses focusing (and guiding) light onto the outer segment (Stavenga and Wilts, 2014) or as long pass filter, narrowing spectral sensitivities (Wilby et al., 2015; Wilby and Roberts, 2017). The spectral properties of the oil droplet are largely determined by their pigment. In chicken, VS cones have unpigmented T-type oil droplets with no long pass filter properties, while other cones contain oil droplets with carotenoid pigmentation, which act as long pass filters (Wilby and Roberts, 2017). Different constitutions of pigmentations are classified as C-type (SWS cone), Y-type (MWS cone), R-type (LWS cone) and P-type (double cone) (Toomey et al., 2015). There is some debate about the type in the double cone, which may contain different types of oil droplets (López-López et al., 2008). In addition, some studies report P-type oil droplets for both members of the double cone, while others find no oil droplets in accessory members. Due to their strong filter properties, oil droplets allow identification of cone types using a light microscope without further staining.

The filter properties of oil droplets have been modelled by (Wilby and Roberts, 2017, 2017) who found that the transparent oil droplet found in SWS1 cones enhances the absolute sensitivity of receptor. In contrast, the pigmented oil droplets in other cone types narrow the spectral sensitivity at the cost of absolute sensitivity.

Although each cone type seems to express their specific oil droplet (but see (López-López et al., 2008; Toomey et al., 2015)), the pigment density may differ substantially between animals, different areas of the eye and depending on environmental conditions, reflecting a trade-off between spectral sensitivity tuning and absolute sensitivity of the receptor (Hart et al., 2006). Consequently, it may not be surprising that independent studies report considerable differences in visual properties of oil droplets. Furthermore, filter properties of C – and P- type oil droplets differ between ventral and dorsal retina. Oil droplets in the dorsal retina have significant higher cut-off wavelengths. In the pigeon, the retina can be divided into a dorsal red field and a ventral yellow field, reflecting a 10nm red shifted cut of wavelength of oil droplets in the dorsal hemisphere (Bowmaker, 1977).

Observations of locally specialized photoreceptor subtypes have been reported also in mice, primates, and zebrafish (Baden et al., 2013; Baudin et al., 2019; Sinha et al., 2017; Yoshimatsu et al., 2019). The chicken retina may offer further variety. Some studies divide single cones into straight and oblique subtypes, with the straight cone having a relatively short vertical axon, while the axon of the oblique cone projects more horizontally into the OPL (Mariani and Leure-Dupree, 1978). The proportion between straight an oblique cone in the area centralis was

reported to be 36.5 % and 1.5 % (relative to double cones and rods) (López-López et al., 2008). Subtypes are not fully established in the literature, and it remains unclear how observations made in different studies can be combined. For example, (Wai et al., 2006, 2002) differentiated single cones based on either short blade like outer segments or longer outer segments and rod like inner segments. In the same study, three different subtypes of double cones were described. This needs further investigation and could increase the number of input channels that must be considered for the chicken. In this work six different cone photoreceptor types leading to potentially seven different input channels are considered.

OPL PROJECTIONS

In chicken and pigeons photoreceptors project axons into three different strata in the OPL where the signal is transmitted to bipolar cells under modification by horizontal cells (Fischer et al., 2007; Gallego et al., 1975; López-López et al., 2008; Mariani and Leure-Dupree, 1978; Waldner et al., 2019). Each stratum receives projections from different photoreceptor types: the first stratum receives double cone and rod inputs, the second stratum LWS and MWS cone inputs and the third stratum VS and SWS cone inputs (Wahlin et al., 2010). A recent study (Günther et al., 2021) has shed some light on OPL connections between cone types and bipolar types. It was found that most bipolar cells receive input from all cone types at different weights. One bipolar cell type was reported to get sole inputs by SWS1 and SWS 2 cones. Two bipolar types were reported to get inputs exclusively from double cones and rods. Problematically, only one segment of the retina was examined, and the known specialization of different areas of the retina means that this finding may not reflect a general picture.

HORIZONTAL CELLS

Horizontal cells (HC) form horizontal feed forward connections in the OPL integrating input signals from multiple receptors and bipolar cells (Chapot et al., 2017; Thoreson and Mangel, 2012). Thus, they play an important role in the above-described convergence of information in the retina. Four different types of HC have been found in vertebrates; some species only have a subset (Boije et al., 2016). Golgi staining identified four types in the pigeon retina (Mariani, 1987) and similar morphological studies identified at least three types in the chicken (Tanabe, 2006), (**Figure 3**). Immunohistochemistry identified a further type confirming that chicken have four HC types (Fischer et al., 2007; Sun and Crossland, 2000; Wahlin et al., 2010). Due to different methods of identification, the literature lacks consistent nomenclature of all four types (Type 2 described by (Edqvist et al., 2008; Tanabe, 2006) appears to match type 3 and/or 4 of (Fischer et al., 2007; Mariani, 1987; Sun and Crossland, 2000) and vice versa). Here I follow the recent nomenclature of (Boije et al., 2016). Although about 50 % of chicken HCs are GABA positive,

GABAergic inhibitory signal transmission in the OPL is not yet confirmed (Araki and Kimura, 1991; Fischer et al., 2007; Kalloniatis and Fletcher, 1993; Sun and Crossland, 2000). In the mouse, bipolar cells lack ionotropic GABA receptors, but HCs express them, which suggests auto-reception: the inhibition of a neuron by self-released GABA (Chapot et al., 2017). In contrast to mammals, chicken GABA positive HCs are often positive for glycine, suggesting that GABA mediates rapid transmission to bipolar cells which is modulated by glycine (Sun and Crossland, 2000), but see (Thoreson and Mangel, 2012).

HC TYPE 1

This HC type features a narrow dendritic field of about 230 μm^2 and an axon of about 80 μm length projecting into the first stratum of the OPL. Interestingly, evidence suggests that the axon forms connections with double cones and rods (Tanabe, 2006) while the dendritic tree connects with all five types of cones in all strata of the OPL (Fischer et al., 2007; Mariani, 1987; Tanabe, 2006). At the principal member of the double cone HC1 synapses are GABA positive but not synapses at the accessory member (Araki and Kimura, 1991). The differential connections between accessory and principal members with HC 1 axons and dendrites might suggest that double cones give input to two different pathways. One connecting double cone and rod signals and a one connecting double cone and single cone inputs. HC 1 is like the sole HC type found in the mouse (Chapot et al., 2017). In zebrafish, the same type projects to all single cones except the UV cone (Li et al., 2009).

HC TYPE 2

The dendritic field of HC this type is about 700 μm large, the arborization is mostly flat (stellate) projecting mostly into the first stratum in the OPL but a few branches project into the second strata and form connections with MWS and LWS cones (Tanabe, 2006; Wahlin et al., 2010).

HC TYPE 3

This HC type has a candelabrum-shaped morphology comprising a 200 μm large dendritic field projecting into all three strata of the OPL. In the first stratum, it forms connections exclusively with the principal member of the double cone (Tanabe, 2006).

HC TYPE 4

This HC type has been described first in pigeon and here shows a large dendritic tree like HC type 3 (Mariani, 1987). Because of their morphological resemblance, HC type 4 has been confirmed only by immunohistochemistry (Fischer et al., 2007), but it remains unclear how similar or different its projections are compared to HC type 3 (Fischer et al., 2007; Sun and Crossland, 2000).

BIPOLAR CELLS

Bipolar cells (BC) transmit signals received by their dendrites in the OPL onto RGCs in distinct layers of the IPL. Signal transmission is modified by HCs in the OPL and amacrine cells (AC) in the IPL. Based on AC projection patterns the IPL has been divided into five distinct strata (Millar et al., 1985), but RGC projection patterns suggests eight strata (Naito and Chen, 2004a), which I will consider here. BCs are glutamatergic, and GABA negative (Kalloniatis and Fletcher, 1993; Nelson and Connaughton, 2012; Sun and Crossland, 2000).

Based on morphology at least eleven BC types have been identified in chicken, but the actual number is likely higher because initial classification considered only dendritic trees and not axonal trees (Quesada et al., 1988), (**Figure 3**). In common with teleost fish and amphibians, chicken BC dendrites are often bi – or tri – stratified (Nelson and Connaughton, 2012), whereas they are mono or bistratified in mammals (Behrens et al., 2016; Euler et al., 2014), (**Figure 3**). This suggests a functional diversity between BC type which remains to be investigated.

Bipolar cells have marked differences in dendritic field sizes ranging from 3 μm ($\approx 0.013^\circ$ of visual angle) to over 25 μm ($\approx 0.11^\circ$ of visual angle), with symmetric or asymmetric field shapes, which might be functionally important for motion vision. In the primate fovea, midget like bipolar cells with small dendritic fields transmit single photoreceptor inputs to RGCs allowing for single photoreceptor resolution (Kolb and Marshak, 2003). Chickens might have midget BC; the smallest BCs have a morphology consistent with single cone connectivity (Quesada et al., 1988) but specific midget like pathways are unknown in the chicken retina. Such a pathways might be limited to the area centralis which features the highest density of RGCs. Importantly, midget like cell types seen in primates seem have been evolved derived from non midget mammalian cells (Mollon, 1989). Therefore, an evolutionary equivalent in avian retinas might be unlikely.

The chicken retina features avian typical BCs. In the pigeon eight different types of BCs have been described based on morphology, including a midget like type (Mariani, 1987). In addition, the chicken retina likely consists of an interplexiform cell (Kalloniatis and Fletcher, 1993) which has also been described in the pigeon retina and other non-mammalian retinas. It forms medium field connections between the OPL and IPL but exact projections or function remain unknown (Mariani, 1987).

Interestingly, avian BCs contain a specific structure not found in mammals known as Landolt's club. This is a specialized dendrite reaching into the external limiting membrane of the retina (Quesada and Génis-Gálvez, 1985), and probably supports metabolic/nutritional needs as it connects BCs and Müller (glia) cells, and is also found in pigeons (Mariani, 1987). Importantly,

the avian retina lacks blood vessels and inner layers are likely somewhat anoxic. Landolt's club might be involved in nutrient transfer (Quesada et al., 1988).

AMACRINE CELLS

Amacrine cells realize the second level of horizontal connections in the retina. Common to vertebrate retinas, they form a distinct layer in the bottom half of the INL featuring larger cell bodies than most BCs (Fischer and Stell, 1999; McMains et al., 2011; Millar et al., 1987; Sun and Crossland, 2000; Waldner et al., 2019). Additionally, it was suggested that about 30 % -35 % of cells in the RGC layer are displaced ACs (Chen and Naito, 1999). This matches findings of about 40% of GABAergic cells in the RGC layer (Kalloniatis and Fletcher, 1993), a neurotransmitter often used by ACs (Masland, 2012). Other neurotransmitters commonly used by ACs across vertebrate species including the chicken are glycine, acetylcholine, substance P, serotonin, nitric oxide, and dopamine, further highlighting their functional diversity (Morgan, 1983). ACs project into the IPL where they modulate signal transmission between BCs and RGCs. Unsurprisingly they serve multiple functions of which most remain poorly understood. In the mouse at least 60 different types have been described based on genetic markers. It has been assumed that the number of ACs scales with the number of RGCs which would predict many AC types in the chicken retina (Masland, 2012). To date several different types have been described based on anatomical and immunohistochemical studies. In the following some interesting types will be described.

CHOLINERGIC ACS

At least three different cholinergic AC types have been described in the chicken retina. Type 1 and 2 are monostratified and project on BCs other ACs and RGCs. Type 3 is bistratified and projects into separate strata in the IPL forming connection with other ACs and RGCs (Millar et al., 1987). Most extensive AC types in the vertebrate retina are starburst ACs serving important functions in direction selective circuits (Masland, 2012) by gating dendritic spikes in direction selective RGCs (Brombas et al., 2017). Chicken AC type 1 is morphologically like mammalian starburst type-a while chicken AC type 2 resembles mammalian type-b. Type 3 shows morphology not found in mammals (Millar et al., 1987).

GLUCAGON ACS

Glucagon positive ACs have been found in the chicken retina but are absent from mouse retina (Mathis and Schaeffel, 2007). They serve a developmental function (emmetropization) signalling the stop of axial growth by glucagon release into the tissue (Feldkaemper and Schaeffel, 2002). This process is controlled by the transcription factor ZENK which is expressed in correlation with

the sign of imposed image defocus, increasing expression with positive defocus (Fischer et al., 1999).

EFFERENT AC SYSTEMS

A specific axon-bearing network of ACs using nitrogen as neurotransmitter can be found in the chicken retina (Fischer and Stell, 1999; Weller et al., 2009) including the area centralis (Weller et al., 2009). These cells are targeted by efferent projections originating in the isthmo-optic nucleus in the midbrain (Lindstrom et al., 2009). The function of this network is unknown but cooling down of the isthmo-optic nucleus was shown to reduce responsiveness of the retina but has no effect on receptive field properties (Pearlman and Hughes, 1976). Retinopetal axons are common among vertebrate species but are featured in relative abundance in the avian visual system (Miles, 1972; Repérant et al., 2006).

RETINAL GANGLION CELLS

Retinal ganglion cells receive dendritic inputs in the IPL and their combined axons form the optic nerve which transfers all visual information received by the retina to the brain. The density of RGCs varies strongly between vertebrate species from low in sharks to very high in avian retinas (Baden, 2020). Pigeon and starling have about 10,800 RGCs per mm² and 20,000 RGCs per mm² respectively in the fovea (Dolan and Fernández-Juricic, 2010; Querubin et al., 2009). In the chicken area centralis the density is comparably low at 13,500 mm² (Chen and Naito, 1999) comparable to the human parafovea (Quinn et al., 2019). In addition, the chicken retina features a second area of high visual acuity in the dorsal hemisphere (10,200 RGCs mm²). Two areas of high acuity are common for birds, with some raptors featuring two foveae (Mitkus et al., 2017). In ground foraging birds the two areas serve different behavioural needs: The area centralis/fovea allows good lateral/frontal vision while the dorsal are allows for high visual acuity in the pecking area (Evans and Evans, 1999). Despite lower peak densities of RGCs in the chicken compared to human, the total number of RGCs found in the chicken retina at 2.9 (Ehrlich, 1989) to 4.9 million (Naito and Chen, 2004a) is about twice as high compared to humans, despite a smaller ocular diameter. Comparing photoreceptor densities with RGC densities in the area centralis suggests a ratio of 1.5:1.

Like the density, the size of RGC somata and dendritic trees varies across the retina. Somata size increases from 40 µm in the areal centralis to about 560 µm in the periphery, linearly increasing with eccentricity. Similarly, the dendritic field size increases from 43 µm in the centre to about 504 µm (Naito and Chen, 2004b). Assuming correlation between receptive field sizes and dendritic tree sizes, this would predict receptive field sizes between 0.18° of visual angle to 2.2° of visual angle in the respective areas of the retina. Humans have a visual acuity of about 50

cycles per deg⁻¹. Behavioural studies suggest a visual acuity of 6.0 to 7.7 cycles per deg⁻¹. This difference is likely explained by the absence of fovea in the chicken retina. In primates, the midget pathways provide high visual acuity in the fovea. It remains unknown to which degree a similar pathway exists in the chicken. Other avian species show much higher visual acuity, 62.3 cycles per deg⁻¹ were reported for the Harris's hawk (Potier et al., 2018), surpassing human visual acuity.

The stratification patterns of chicken RGCs in the IPL are highly diverse and show mono-, bi-, multistratified patterns as well as diffused patterns which connect to almost all strata in the IPI, (**Figure 3**). In mammals, the IPL is commonly split into ON and OFF sensitive strata. In how far the same differentiation can be made in the chicken IPL remains unknown. Mono and bistratified RGC types are most common, and the stratification complexity appears to be inversely related to RGC density (Naito and Chen, 2004b).

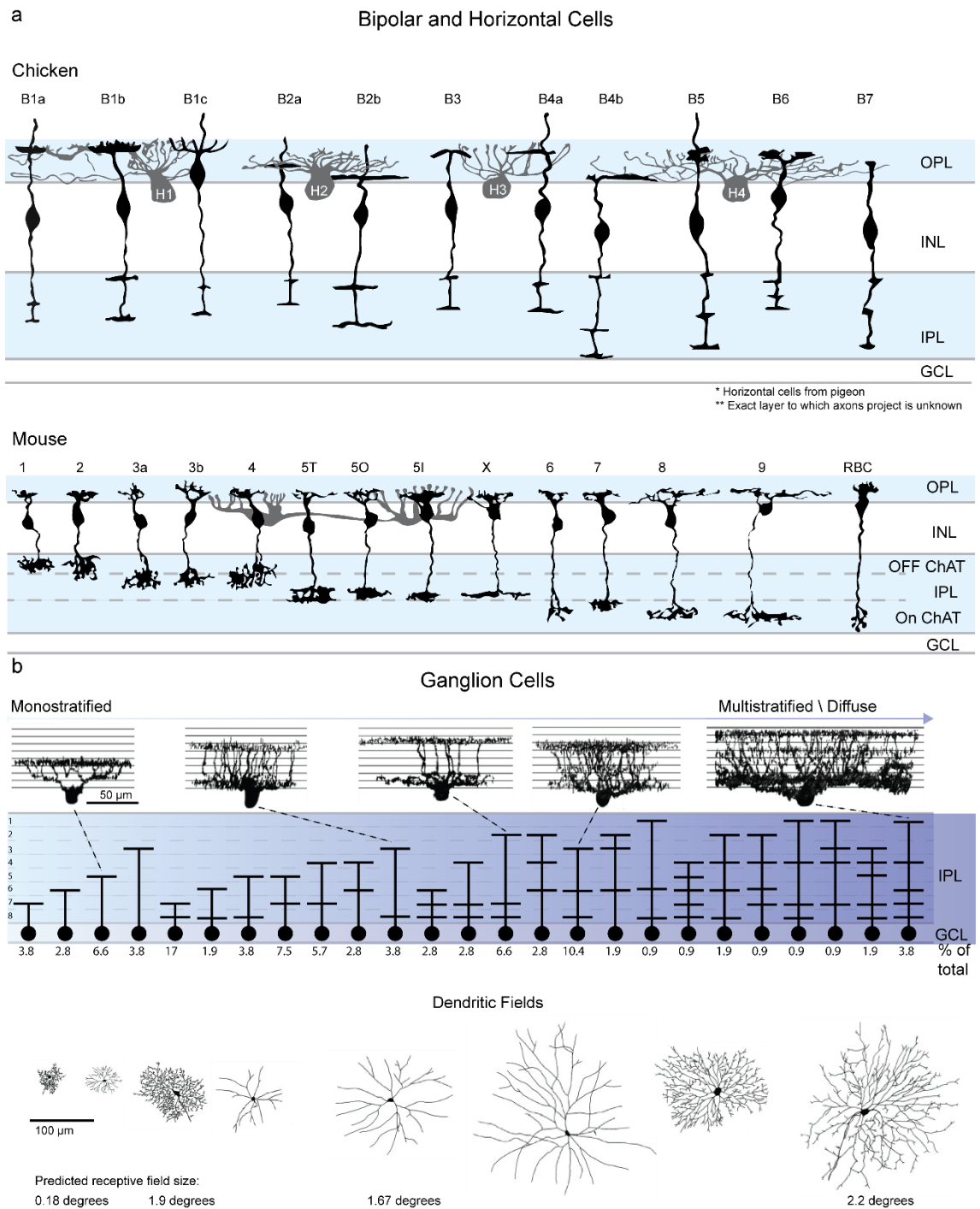


Figure 3 Overview over bipolar-, horizontal-, and ganglion cell morphology. a. BCs and HCs found in the chicken compared to those found in the mouse. Chicken BC are often bi- or tristratified which is uncommon in the mouse. The exact layers to which BC axons project in the chicken are unknown. BC drawings for the chicken were taken from (Quesada et al., 1988), HC drawings were taken from the pigeon (Mariani, 1987), but their morphology is comparable to those found in the chicken. Mouse BCs drawings were taken from (Behrens et al., 2016), HC drawing was taken from (Wang et al., 2003). Cell sizes are not to scale. **b.** Stratification patterns of RGC found in the chicken as described by (Naito and Chen, 2004a). Some example cell morphologies are shown, these are copied from (Naito and Chen, 2004a). Receptive field

sizes for these cells were approximated by calculating the angle in the visual field which the dendritic tree potentially sees.

RETINAL FUNCTION

The function and electrophysiology of chicken RGCs is poorly understood. Electroretinograms have been used to show that chicken retinas are able to integrate stimuli at a speed of about 100 Hz (Lisney et al., 2012), depending on luminance levels, which is above human flicker fusion frequency at 95 Hz (Mankowska et al., 2021).

Multielectrode array (MEA) studies of chicken RGCs are very limited. Early studies confirmed little more than RGC responsiveness to light stimulation (Chen, 2003). Further studies revealed some basic properties, including spatial resolution and contrast sensitivity (Diedrich and Schaeffel, 2009) in normal and defocused conditions, showing that chicken have low contrast sensitivity, which is common for birds. (Stett et al., 2000) used the chicken retina for electrical stimulation of RGCs and subsequently recorded responses.

Despite the unique structure of avian retinas and the likely huge functional diversity of its neurons, avian visual processing remains a black box. The chicken is an ideal model organism to give a complete picture of vertebrate vision, and to address some avian specific questions about visual processing:

1. How do terrestrial vertebrates with flight process visual information?
2. How is chromatic information encoded in a retina that has four spectral inputs?
3. What is the function of the double cone found in reptiles (including birds) but no other vertebrates?

THESIS AIMS

For a deep understanding of vertebrate visual ecology of detailed study of avian retinal physiology is overdue. The chicken has potential as a model organism because detailed knowledge about the morphology of its retina exists as outlined above. Here I seek to shine light on the black box that avian visual processing is by investigating how information is processed at the level of the output layer of the retina in RGCs. Since the chicken is not established as a genetic model organism non-invasive study by 2-photon imaging are impractical. Therefore, a MEA was used to record electrical signals from RGCs in vitro. Although MEA recordings have been performed on the chicken retina, a good recording protocol was lacking. The first aim of this thesis was the establishment of said protocol. I have modified the existing MEA protocols and established an enhanced protocol that allows for electrophysiological recordings over multiple hours under light stimulation. This protocol is presented in (*Chapter 2: Methods*).

Existing chicken MEA studies have failed to investigate one of the most interesting aspects about avian vision: chromatic processing. Using a custom build chromatic stimulator, my aim was to investigate wavelength dependent response characteristics of chicken RGCs, and the respective results are presented in (*Chapter 4: General RGC responses*).

For a full understanding of retinal outputs in the chicken, the identification of different types of RGCs is crucial. Modern classification relies either on expression of genetic markers or functional diversity of RGC responses. Aiming at identifying functionally diverse RGC types I have used a clustering algorithm developed by Paul Roberts to identify chicken RGC types based on their electrophysiological responses to a set of different light stimuli. The so found functional diversity is presented in (*Chapter 5: Functional RGC types, part 1*).

The number of receptor inputs seen in avian retinas raises questions about how chromatic information is processed in the chicken retina. In (*Chapter 5: Functional RGC types, part 2*) I show modelled input contributions of different cone types to the identified functional diverse RGC types.

Finally, the high number of input channels found in avian retinas raises the question about how the abundance of information is processed in downstream circuits. My results show that time might be an important dimension in RGC responses. I aimed to investigate this question and show in (*Chapter 6: Response Shapes*) how time coding might play an important role in chromatic and achromatic processing in the chicken retina.

This thesis aims at providing a solid initial framework for further investigations of avian retinal physiology. My data can be used to compare visual processing of birds with other vertebrates and contributes to our understanding of functional similarities and differences in vertebrate vision, this is discussed in (*Chapter 7: Conclusion*).

CHAPTER 2: METHODS

ANIMAL HANDLING

All procedures were performed in accordance with the UK Animals (Scientific Procedures) act 1968 and approved by the animal welfare committee of the University of Sussex. Male chicks, breed Shaver Brown, aged between 1- and 14-days post hatching were obtained from (Joice and Hill (part of Hendrix Genetics), Peterborough, UK) and kept in a specifically designed cage in the university's animal facility. Food (Chick Crumb) was provided ad libitum and elements for facilitating play behaviour were provided. Chicks were never kept in isolation for a prolonged time, the last two chicks were processed at the same day.

DARK ADAPTATION AND SACRIFICE

Chicks were dark adapted for at least 12 hours overnight. The night day cycle was set to 12h each from 10 am to 10pm. The respective chick used for experiments was transferred into a light sealed box in the morning and sacrificed in the dark. Chicks were sacrificed by cervical dislocation and follow up cutting of the aorta.

MEA EXPERIMENTS

DISSECTION

RINGER SOLUTION

Ringer solution for the experiment was based on a recipe previously used by (Stett et al., 2000) (osmolarity = 0.331 osmol):

Table 2: Ringer solution ingredients.

Ingredient	Concentration in $\frac{Mol}{L}$
NaCl	0.1
KCl	0.006
MgSO ₄	0.002
CaCl ₂	0.001
NHCO ₃	0.03
C ₆ H ₁₂ O ₆	0.05
NaH ₂ PO ₄	0.001

Two litres of ringer solution were freshly prepared for each experiment. The solution was bubbled with 95% O₂+CO₂% for at least one hour before experiments. Solution was heated to 37° C.

A second ringer solution containing 0.4 mM MgSO₄ was prepared for dissection.

ENUCLEATION

Eyes were enucleated by first cutting the eyelid around the cornea. A single anterior leading cut between eyes and beak was performed. Using curved forceps (FST 11652-10, FST Heidelberg, Germany), the eyes were then lifted, and the optic nerve was cut using scissors with a partially blunt tip (FST 14083-08). In the following the remaining muscle tissue around the eyes were removed and lifted from the skull. The eyes were cut two times proximal to the edge of the cornea using pointed scissors (FST 15017-10) and transferred into two bottles containing preheated, oxygenated ringer solution at 37° C. The bottles were light sealed. Eyes were transferred to the experimental site where the follow up dissection took place. (Transfer took about 3 minutes, dissection 15 min in total).

RETINA DISSECTION

The retina was dissected based on a protocol established by (Stett et al., 2000). In addition to that protocol, all steps were performed under infrared light using night vision goggles (PSV-14, ACT in Black, Luxembourg), and under a special dissection ringer solution. All steps were optimized to avoid triggering spreading waves of depression, see (*Chapter 3: Chicken retina MEA recordings*). The dissection protocol consisted of the following steps, which were performed in a petri dish in ringer solution unless otherwise stated:

1. Removal of the cornea from the eyeball with as few cuts as possible (FST 15017-10).
2. Cutting the eyeball alongside the dorsal – ventral axis. This was done in two cuts from opposite sites.
3. Removing the vitreous from the eyeball by pulling it up using forceps.
4. Cutting a ca. 4mm² large piece out of the central area of the dorsal hemisphere.
5. Transfer of this piece onto a filter paper, with the RGC facing the filter paper and the remaining sclera facing up.
6. The filter paper and tissue were then transferred onto a kitchen roll paper. During this step ringer solution was sucked away from the tissue which flattened the tissue and properly attached it to the filter paper. Method previously described by (Stett et al., 2000).
7. The remaining sclera, choroid and retinal pigment epithelium were removed from the retina by using forceps to “peel” those layers off the retina which remained attached to the filter paper.
8. The filter paper and retina were transferred back to the petri dish.
9. The retina was removed from the filter paper using forceps.

10. A smaller, about 2.5 mm² large piece was cut from the tissue. The retina would commonly get folded at a few places during step 6 due to flattening of what normally is a curved tissue. In this step, the part without folds was chosen. Folded parts of the retina were avoided at all costs even if this resulted in smaller sized than ideal preparation.
11. The retina was transferred to the MEA chamber using a spoon. The tissue was guided onto the spoon using forceps and was continuously guided while being on the spoon to avoid strong movement of the tissue during transfer.
12. In the MEA chamber the corners of the tissue were cut. This was done, to remove parts of the tissue that had been damaged by the forceps during tissue guiding steps.
13. The tissue was placed properly onto the electrode array with a fine painter's brush.
14. The MEA chamber was dried using kitchen roll to suck out the ringer solution. As soon as the tissue was exposed to the air new ringer solution was added directly on top of the tissue. This would normally attach the tissue to the MEA.
15. The MEA chamber was transferred to the MEA machine.
16. The tissue was left to further attach to the MEA for about 30 additional minutes.

PERFUSION

The tissue was perfused throughout the experiment using the according ringer solution. The MEA chamber was heated to 37° C and the perfusion solution was preheated inline to the same temperature.

LIGHT STIMULATION

Due to the nature of the MEA, RGCs were facing away from the light, the light hit the photoreceptors directly without passing the retina first. This means, that photoreceptors received light which was not filtered by oil droplets.

GENERAL SETUP

Light stimulation was delivered using a slightly modified version of a previously described protocol for 2photon setups (Franke et al., 2019). Six chromatically distinct LEDs were controlled by two fibre-coupled DLP LightCrafter 4500MKII (developed by Texas Instruments, Dallas, Texas manufactured by EKB, Bat Yam, Israel), (3 LEDs per projector), showing the same picture with different chromatic content. The projector images were recombined to one common image using a beam splitter. The final image was projected on the tissue using a mirror, (**Figure 4**).

LEDS

Six LEDs with different peak emission wavelengths were used. The LED powers were set so that stimulation using all six different LEDs simultaneously ("white" light) would result in higher photoisomerization rates in long wavelength sensitive opsins than in short wavelength sensitive

opsins. This was done to mirror the spectrum of natural light and to account for supposed increased gain of the short wavelength sensitive cones.

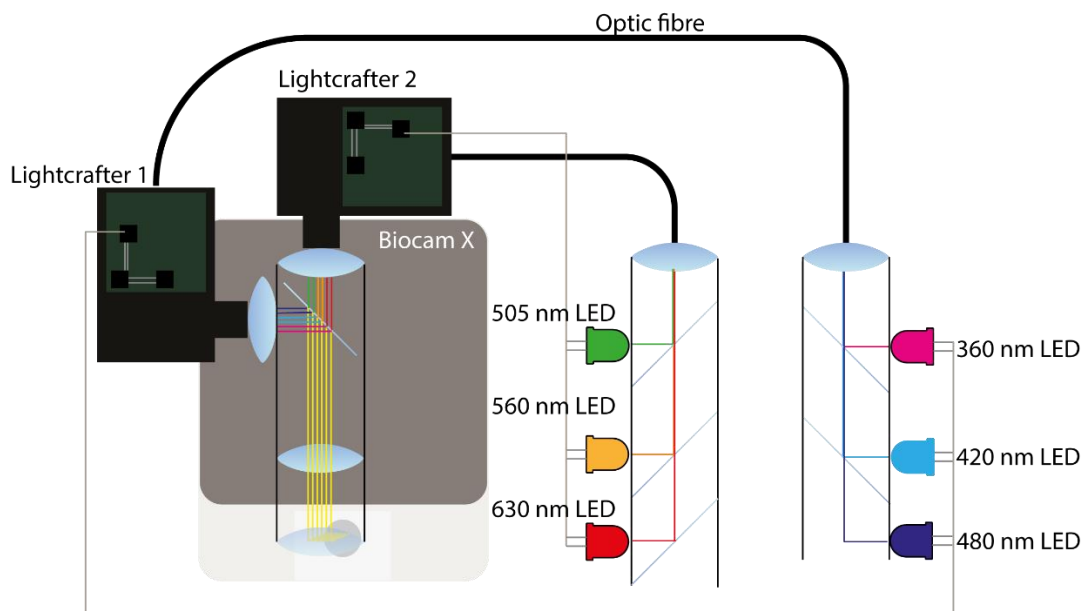
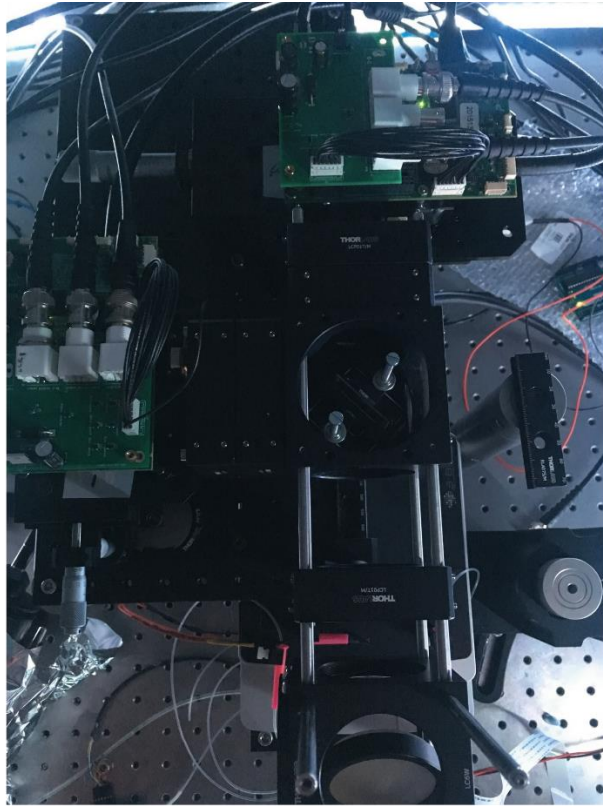


Figure 4 Delivery of light stimuli on the MEA setup. The light from six different LEDs is combined using beam splitters. Short wavelengths LEDs were controlled by Lightcrafter 1, long wavelengths LED by Lightcrafter 2. Both Lightcrafters projected the same image with different chromatic quality. The images were merged using another beam splitter. The size

of the image was controlled using a lens. Finally, the image was projected on the tissue by a mirror.

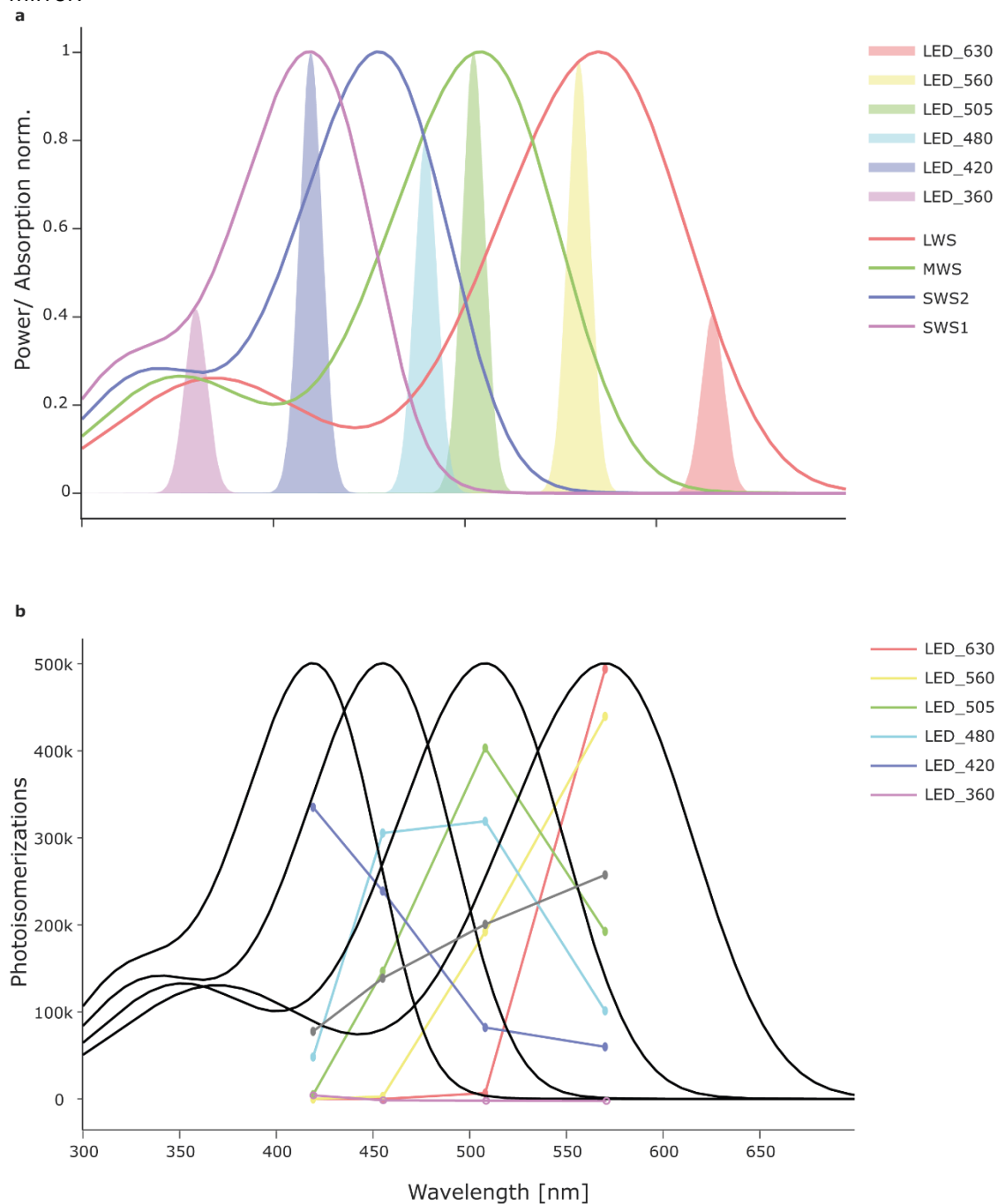


Figure 5 LEDs used in relation to chicken opsins. Six LEDs with different peak emission wavelengths were used for this study. **a.** LED positioning over the spectrum of visible light and in relation to absorption spectra of chicken opsins. **b.** The modelled photoisomerization rates for each LED and opsin combination. Opsin absorption based on (Govardovskii et al., 2000) The 360 nm LED was significantly weaker than other LEDs due to technical limitations.

STIMULI

All stimuli were coded in Python using the QDSpy package (@Thomas Euler, Tuebingen, Germany, <http://qdspe.eulerlab.de/>). The two LightCrafter were connected to a computer as additional displays. QDSpy was used to present the stimuli. The following stimuli were used:

Table 3 Stimuli used for this study and their properties

Stimulus nr(chronological)	Name	Trigger per repeat	Sequence	Repeats	Frequency in Hz	Time total in min
1	Chromatic full field flash	6	630nm, OFF, 560nm, OFF, 505nm, OFF, 480nm, OFF, 420nm, OFF, 360nm, OFF	5	2 s per flash	2
2	Full field colour noise	18000	Mix of 630 nm, 505 nm, 480 nm, 420 nm		20	15
5	Contrast Steps	10	100:OFF, 90:OFF...10:OFF	10	2 s per step	3.2
6	Chirp	4	OFF, 50% ON, frequency chirp,	3	≈0 - 30 Hz, exponential	5.15

FULL FIELD FLASH

Consisted of 2 s ON steps per LED followed by 2 s OFF to full dark.

FULL FIELD COLOUR NOISE

Four LEDs (630 nm, 505 nm, 480 nm, 420 nm) were switched ON or OFF (binary) at respective pseudorandom sequences at a frequency of 20 Hz.

CONTRAST STEPS

Consisted of 2 s “white” ON steps at decreasing Weber contrasts (100 – 10%) followed by 2 second lasting OFF to full dark

CHIRP

Consisted of 3 s step to 50% ON followed by exponentially increasing frequency chirp from about 0 Hz to 30 Hz within 30 s.

TRIGGER

The digital trigger signal was delivered via USB to an Arduino nano, (Arduino LLC, Italy) where it was converted into an AC signal which was sent to the MEA’s external analogue input.

RECORDINGS

MEA

MEA recordings were performed on a BIOCAM X platform produced by 3Brain AG, Wädenswil, Switzerland. The used chip was Arena HD-MEA. It consists of 4096 electrodes in a 2.67 mm² area. Each electrode is 21 μm² with a pitch of 42 μm. The chamber above the array is 7 mm deep and 25 mm in diameter.

SOFTWARE

The software for data acquisition was Brainwave 4. It was run on a bespoke computer provided as part for MEA by 3Brain. The integration time was set to medium, resulting in a sampling frequency of ca. 18 KHz

GENERAL DATA ANALYSIS

Data analysis was done by custom written Python (Python Software Foundation, Wilmington, Delaware, USA) which were executed in JupyterLab. For some analysis Matlab (MathWorks, Natick, Massachusetts) was used in addition.

SPIKE SORTING

Herding Spikes 2 (HS2) algorithm (Hilgen et al., 2017b) was used for spike sorting. HS2 uses a combination of spike location and spike shapes information and performs a mean shift clustering approach to separate spikes coming from different cells.

The following parameters were used:

```
'clustering_bandwidth': 8,  
'clustering_alpha': 5.5,  
'clustering_n_jobs': -1,  
'clustering_bin_seeding': True,  
'clustering_min_bin_freq': 16,  
'clustering_subset': None,  
'left_cutout_time': 0.3,  
'right_cutout_time': 1.8,  
'detect_threshold': 5,  
'probe_masked_channels': [],  
'probe_inner_radius': 70,  
'probe_neighbor_radius': 90,  
'probe_event_length': 0.26,  
'probe_peak_jitter': 0.2,  
'num_com_centers': 1,  
'maa': 12,  
'ahpthr': 11,  
'out_file_name': 'HS2_detected',  
'out_file_cluster': 'HS2_sorted.hdf5',  
'decay_filtering': False,  
'save_all': False,  
'amp_evaluation_time': 0.4,  
'spk_evaluation_time': 1.0,  
'pca_ncomponents': 2,  
'pca_whiten': True,  
'freq_min': 300.0,  
'freq_max': 6000.0,  
'filter': True,  
'pre_scale': True,  
'pre_scale_value': 20.0,  
'filter_duplicates': True
```

FIRST QUALITY CONTROL

After spike sorting, cells that spiked > 10 spikes or less than 1 spike per second on average over a period of one hour were excluded from any further analysis.

STIMULUS AND SPIKE ALIGNMENT

After spike sorting each spike was aligned with the trigger channel. Spiketrains were separated by stimulus and analysed accordingly.

SECOND QUALITY CONTROL

To determine the firing rate over time for each cell in response to each of the FFF, CStep and Chirp stimuli we mapped all spike times onto the time interval spanned by the first repeat of that stimulus and applied kernel density estimation (KDE) using the Matlab routine `ksdensity`. We used the default probability density function for the KDE, such that the area under the resulting curve is equal to one, thus normalising the spiking rate across cells and stimuli. The KDE was computed at 1000 equally spaced points and a smoothing bandwidth of 0.05 employed for all three stimuli.

Cells with low-quality responses to all four stimuli were identified and removed from the data set, cells with a high-quality response to at least one stimulus being retained in all cases. The quality of response to the FFF, CStep and Chirp stimuli was determined using the signal-to-noise ratio quality index: $QI = Var[\langle C \rangle_r]_t / \langle Var[C]_t \rangle_r$, where C is the T by R response matrix (time samples by stimulus repetitions), and $\langle \cdot \rangle_x$ and $Var[\cdot]_x$ denote the mean and variance respectively across the indicated dimension, $x \in \{r, t\}$ (see Baden et al., 2016). This quality index was applied to the KDE derived spiking rates, where KDE was applied to each repeat separately rather than mapping all spikes onto the first repeat as for the computation of the spiking rates used for clustering (described above). A quality threshold of 0.4 was chosen, below which FFF, CStep and Chirp responses were judged to be of poor quality. We calculated the standard deviation in the light intensity over time for each stimulus colour in the kernel (R, G, B and UV). The kernel quality of each cell was defined as the maximum standard deviation across the four colours. A kernel quality threshold of 2.5 was chosen, below which kernels were judged to be of poor quality. The raw data set was of size $n = 60,713$, spread across 17 separate experiments. Following quality control, the data set was of size: $n = 4248$ (7.00% (3 s.f.) of the original).

CLUSTERING

The clustering was performed by Paul A. Roberts, under consolidation with the author of this study.

Clustering was performed on the quality filtered dataset containing the functional responses of retinal ganglion cells (RGCs) to full field flash (FFF), contrast step (CStep) and chirp (Chirp) stimuli,

and colour kernels (spike-triggered averages, STAs) derived from a colour noise (FFFNoise) stimulus.

We used principal component analysis (PCA) to reduce the dimensions of the problem prior to clustering. PCA was performed using the Matlab routine `pca` (default settings). We applied PCA separately to each of the ten segments of the CStep stimulus (100%,90%,...10% contrast segments), to each of the step, frequency chirp and contrast chirp segments of the Chirp stimulus and to each of the FFF colours and FFFNoise kernel colours. We retained the minimum number of principal components necessary to explain $\geq 50\%$ of the variance. The resulting 23 'scores' matrices were then concatenated into a single matrix ready for clustering. The following numbers of principal components were used – FFF: 24 components in total (3 '630 nm' components, 3 '560 nm' components, 4 '505 nm' components, 5 '480 nm' components, 2 '430 nm' components and seven '360 nm' components); CStep: 61 components in total ([4,4,5,6,6,7,7,7,8] [100,90,80,70,60,50,40,30,20,10]% contrast components); Chirp: 47 components in total (5 step components, seven frequency components and 35 contrast components); FFFNoise: eight components in total (2 R components, 2 G components, 2 B components and 2 UV components), giving a grand total of 140 PCA components.

We clustered the combined 'scores' matrix using Gaussian Mixture Model (GMM) clustering, performed using the Matlab routine `fitgmdist`. We clustered the data into clusters of sizes 1,2,...,100, using i) shared-diagonal, ii) unshared-diagonal, iii) shared-full and iv) unshared-full covariance matrices, such that $(100 \times 4 =)$ 400 different clustering options were explored in total. For each clustering option 20 replicates were calculated (each with a different set of initial values) and the replicate with the largest loglikelihood chosen. A regularisation value of 10^{-5} was chosen to ensure that the estimated covariance matrices were positive definite, while the maximum number of iterations was set at 10^4 . All other `fitgmdist` settings were set to their default values.

The optimum clustering was judged to be that which minimised the Bayesian information criterion (BIC), which balances the explanatory power of the model (loglikelihood) with model complexity (number of parameters).

Using the above procedure, we obtained 23 clusters (One cluster with < 10 members was removed), with unshared diagonal covariance matrices providing the optimal solution.

Since multiple of the initially returned 23 clusters showed great variance in respective cell responses, we set the number of clusters to 100 and repeated the clustering. The so initially

returned 100 different clusters were recombined by hand to 35 clusters (*Chapter 5: Functional RGC types*).

SPIKE TRIGGERED AVERAGE

FFNoise kernels (STAs) were computed by collecting the stimulus segments preceding each spike to form a spike-triggered ensemble (STE) and taking the mean of this ensemble. We then subtracted the mean raw stimulus, calculated as the mean of all possible stimulus segments. Stimulus segments were calculated over the one second interval preceding each spike (-1 s to 0 s inclusive) at 51 evenly spaced time points (0.02 s intervals). Thus, the segments were calculated at a finer temporal resolution than the stimulus (20 Hz = 0.05 s intervals) resulting in smoother and more detailed STAs (since a spike may occur at any time within a given stimulus window, a higher temporal resolution results in different stimulus segments depending upon the spike's location within that window). For the mean raw stimulus, the mean was taken over all stimulus segments during the interval over which the stimulus was played, segment initiation times ranging from the earliest to the latest possible time that will allow a full stimulus segment, in intervals of 0.02 s. The FFFNoise kernels were further normalised, by subtracting the mean and dividing by the standard deviation of the STA in the [-2,-1] s interval preceding each spike, where this STA is calculated in the same way as the original FFFNoise kernels. This allows us to determine FFFNoise kernel quality (see below) in those cases where the spike count is low.

PSTH

For quantification and visualization of cell responses, peri stimulus histograms were calculated. Bin size of the histogram was set to 0.05 s for chromatic full field flashes and contrast steps. Chirp PSTH bin size was set to 0.01. to allow for higher resolution at high chirp frequencies.

SPECIFIC DATA ANALYSIS

ON OFF ANALYSIS

Single cell On and OFF response amplitudes were calculated as peaks of the PSTH. ON OFF index was calculated as $ONOFF_i = \frac{ON-OFF}{ON+OFF}$ resulting in weights between 1 (only ON) and -1 (only OFF responses). The threshold for sole ON cells was set to 0.9, for sole OFF cells to -0.9.

Population response ON OFF weights were calculated as:

$$ONOFF_w = \frac{ON\ step\ amplitude}{OFF\ step\ amplitude}.$$

ON and OFF step amplitude were the max PSTH for the whole cell population at a given contrast level.

TUNING CURVES

Tuning curves were calculated as the mean response amplitudes evaluated during ON OFF analysis, depending on wavelength of stimulation.

IDENTIFICATION OF KERNEL TYPES

Different kernel types in the population (**Figure 15**) were identified by identifying positive and negative kernel peaks in each chromatically distinct STA. Based on the relative position and orientation of the peaks (negative, positive, first, last) kernel shapes and polarization were identified per cell. Chromatic opponency was identified by comparing kernel polarization and timings between different colours.

This analysis also returned the time to peak, width, and amplitude of each kernel.

CHIRP ANALYSIS

Chirp analysis is based on an analysis pipeline established by George Kafetzis. To quantify how well a neuron follows the frequency of the stimulus, we compute the vector strength, a metric comparing the timing of the spikes with the phase of the periodic stimulus that they occur at. This stimulus-encoding strategy is termed phase-locking and its vector strength ranges between 0 (neuron responds independently of the stimulus) and 1 (each spike perfectly synchronized at the same stimulus phase).

95% confidence interval was calculated based on the variation of the vector strength of a thousand neurons firing with Poisson statistics and constrained to have the cluster-specific mean firing rate for each average frequency. For generating the artificial population of neurons, the PySpike package was used: <https://github.com/mariomulansky/PySpike>. Error bars indicate ± 1.5 median absolute deviation.

PHOTORECEPTOR MODELLING

Photoisomerization per LED and opsin was calculated from opsin templates (Govardovskii et al., 2000) and measured LED powers. Model tuning curves assume a linear correlation between photoisomerization and cell response using different input weights for each opsin (weights range = 3, -3).

For each RGC type, input weights were changed pseudo randomly 100,000 times at a resolution of 0.01. The best fit was calculated by subtracting the experimental obtained tuning curve for a given RGC type from the modelled tuning curve. Eventually, the modelled tuning curve with the best match to the experimental obtained tuning curves was obtained and the photoreceptor weights were saved.

FIRST SPIKE ANALYSIS

The first spike of a response was defined as the time at which the spike synchronicity (Mulansky and Kreuz, 2016), calculated across stimulus repeats reaches levels 5% above background spike synchronicity. This was done to distinguish spikes belonging to the background noise from actual stimulus responses.

KERNEL DENSITY ESTIMATION

To show the population response (of all cells or all cells of a RGC type) kernel density estimations were calculated based on all times to first spike in the population. Kernel density estimation was calculated using Sklearn python package and assuming a gaussian kernel. The kernel bandwidth was set to 0.01.

PRINCIPAL COMPONENT ANALYSIS

PC 1 and PC 2 were extracted based on PSTH response traces obtained from chromatic and “white” full field stimulation. For the whole population a time window of 0.2 s was used. For individual RGC types, the window was extended to 0.6 s to allow comparison between RGC types showing fast or slow responses.

STATISTICS

The intension of this study was to provide a detailed overlook over basic response properties in chicken RGCs. In accordance, this study relies heavily on descriptive statistics to describe trends in the data to establish an overview. Less emphasis was given to inferential statistics and hypothesis testing.

CHAPTER 3: CHICKEN RETINA MEA RECORDINGS

SUMMARY

Multielectrode arrays (MEAs) which can measure the electrical potentials of thousands of neurons in a tissue in parallel at a high temporal resolution, have been used in the past to study RGCs in the retina. So far Chicken MEA recordings have yielded limited insights into information processing of RGCs. It has been difficult to keep the chicken retina in a healthy condition *ex vivo*. This chapter presents an updated experimental protocol for chicken MEA recordings that enables for stable recordings over multiple hours. Using this protocol, multiple experiments with chicken retina were performed simultaneously recording electrical signals from hundreds of different RGCs. Based on this protocol, future studies on the chicken retina will be possible, making the chicken an optimal model organism to study avian vision.

INTRODUCTION

MEA INTRODUCTION

Neurons transfer signals by action potentials (spikes), electrical signals that can be measured intracellular or extracellular using electrodes (Verkhatsky et al., 2006). These signals are small and thus must be amplified for further analysis. In the past, electrophysiological studies have helped to understand fundamental functions of neurons within neuronal circuits (Hamill et al., 1981; Hodgkin and Huxley, 1952; Hubel and Wiesel, 1959; Werblin and Dowling, 1969). While these studies have delivered substantial insights into function of single neurons, examining the function of a complete neuronal circuit is limited by low throughput. Neurons in the circuit must be recorded one at a time which can be tedious (example studies: (Lefebvre et al., 2018; Rocha et al., 2008)). Multielectrode arrays (MEA) overcome low throughput limitations. MEA consists of tens of thousands of individual electrodes arranged in a grid, which can record electrical signals from a tissue attached to them (Reinhard et al., 2014). Because of this, they generate large datasets for analysis, which is computationally demanding. The increased capacity of modern computers allows fast data analysis of larger datasets and makes MEAs a very powerful tool for studying neuronal circuits. MEAs are commonly used to study brain slices or retinas, which have a “flat” neuronal organization by default, which simplifies electrode attachment.

One key challenge of MEA recording is the post recording analysis of the data. Since individual electrodes on the MEA are in proximity, individual neurons are recorded by multiple electrodes. Signals coming from the same origin recorded by multiple electrodes must be recombined and traced back to their origin. This process is often referred to as spike sorting (Barnett et al., 2016; Hilgen et al., 2017b; Yger et al., 2018). Through spike sorting, it is possible to identify single neurons from the electrical signals recorded by all electrodes on the MEA. This allows for simultaneous recording of hundreds of neurons without losing the option of analysing responses of individual neurons.

The retina has been studied extensively in recent years using MEAs (example retina studies: (Chen, 2003; Field et al., 2010, 2010; Hilgen et al., 2017b, 2022; Jones et al., 2015; Jouty et al., 2018; Portelli et al., 2016; Reinhard et al., 2014; Stett et al., 2000)). MEA recording are established for key model organisms like mouse and macaque, but also human retinas (Field et al., 2010; Hilgen et al., 2017b; Reinhard and Münch, 2021). Since RGCs form a layer, it is “easy” to record the electrical activity of individual RGCs using MEAs. Retinas are highly complex and highly parallelized neuronal circuits, MEAs are a powerful tool to examine them.

MEA STUDIES ON CHICKEN RETINA

Chicken retinas have been studied before using MEA (Chen, 2003; Diedrich and Schaeffel, 2009; Stett et al., 2000). These studies have been limited for three reasons:

1. The MEAs used had a low electrode density. The chicken retina has a high density of RGC (general introduction). Therefore, MEAs with sparsely arranged electrodes may overlook key aspects of electrophysiological properties. Spike sorting is challenging if the number of electrodes is limited.
2. Studies used a very limited set of optical stimuli. Avian retinas are highly complex and chromatic processing plays a key role in the processing of visual information. Any study that aims to gain insights into the electrophysiology of avian retinal circuits must account for this.
3. Avian body temperature and metabolism is high. Chicken has a normal body temperature of 42 °C. Extracting a retina out of these conditions and keeping it stable for a prolonged duration is challenging and likely limited insights (this was explicitly described in the Ph.D. thesis of (Graef, 2017), German). This hurdle must be overcome to allow long lasting recordings.

In summary, insights into avian retinal electrophysiology are sparse. This chapter will present the challenges faced by that MEA recording from avian retinas and explain how long lasting MEA recording were established by updating previous recording protocols.

RESULTS

MEA recordings of the chicken retina have proven to be more complicated than anticipated and experiment failed consistently during the early phases of this study. The following describes detailed insights that were learned from these initial setbacks and presents an enhanced protocol that overcomes previous limitations.

SPREADING WAVES OF DEPRESSION

Most problems encountered regarding degeneration of retinal tissue during the experiments probably originated from spreading waves of depression. This is an incompletely understood phenomenon in brain and retina (Bennett et al., 2008, 2008; Martins-Ferreira et al., 2000; Nedergaard et al., 1995; Shatillo et al., 2015; Torrente et al., 2014). The spreading waves are a front of increased neuronal activity that travels through the tissue causing strong depolarization of neurons. After the wave front has passed, neurons remain unable to initiate action potentials for many seconds or even minutes. While this is fundamentally an electrical phenomenon, its consequences can be observed visually, **Figure 8 b**. The wavefront turns the tissue bluer.

Unfortunately, spreading waves of depression are triggered very easily in the chicken retina, which has been used to study this phenomenon in the past (Martins-Ferreira et al., 2000). In chicken retina, spreading waves of depression can be triggered by poking the retina using forceps. During my experiments conducted, it became clear that triggering too many spreading waves of depression in short succession during the dissection probably damages the tissue and makes recordings impossible. Retinas often were in poor condition by the time experiments started, which would trigger further spreading waves of depression spontaneously leading to a progressive “circle of death”. Previous recordings of chicken RGCs probably suffered from similar problems, which would explain the - otherwise surprising - lack of findings from previous studies. After carefully study of the available literature, the dissection protocol was changed in a few but important details to prevent spreading waves and tissue degeneration.

DISSECTION PROTOCOL

Chicken retinas were dissected based on a previously established protocol (Stett et al., 2000), see **Figure 6**: 1. Enucleation of the eye. 2. Opening the eye around the cornea. 3. Cutting the eye in two halves along the dorso-ventral axis. 4. Cutting a smaller rectangular piece of the dorsal retina. 5. Removing the RPE using filter paper. 6 Cutting the tissue into a size that fits the MEA.

To prevent the triggering of spreading waves of depression the following changes were made to the dissection protocol:

1. After enucleation, eyes were immediately placed in preheated water (37 C) .
2. All further dissection steps were performed in a ringer solution that had increased levels of Mg^{2+} 4 mMol. This was done to block triggering and transmission of spreading waves of depression during the dissection, as previously described. (Martins-Ferreira et al., 2000).
3. Further dissection was performed exclusively under infra-red (IR) light using night vision goggles to avoid visual stimulation of the retina.
4. The tissue was touched as infrequently as possible, and as few cuts as possible were made. Dissection time was increased to allow breaks between each touch or cut of the retina.
5. Before attaching the retina on the MEA, all previously touched areas of the retina were removed. The tissue was then placed on the MEA using a fine brush. This was done, because previously touched areas of the retina seemed to be more likely to become the origin of randomly triggering spreading waves of depression during MEA experiments.
6. For the recording, Mg^{2+} concentration was returned to 2 mMol.

One additional change was made to the visual stimulus protocol. Sometimes, spreading waves of depression were triggered after prolonged exposure of the retina to “white” light and consequent steps back to full dark (for example after full field noise stimulation) (**Figure 8 a, b**). To prevent the triggering of waves in this way, all steps to full black after prolonged light stimulation were done in a series of steps of decreasing intensity. This prevented stimulus triggered waves of spreading depression.

These changes to the dissection protocol, substantially improved recording quality. Eventually, it was possible to record from the chicken retina for multiple hours without triggering a single spreading wave of depression (**Figure 8 c**).

RECORDINGS

Seventeen recordings were performed for this study. Recordings varied in quality, with some recordings having many active MEA channels and other few (**Figure 7 a, b**). This was probably due to how well the tissue attached to the MEA. In many experiments, one side of the MEA received stronger signals than the other, indicating that the retina was “resting” on one of its “edges” preventing the other edge from attaching properly (**Figure 7 b**). Attachment of the retina increased over time, resulting in increased overall number of spikes recorded **Figure 8 a&c**. Additionally, areas of the retina that had RPE attached seemed to generate better responses for a prolonged duration, possibly because of sustained photoreceptor health, (**Figure 7 b**).

SPIKE SORTING

Chicken RGCs often responded with bursts of spike activity to visual stimulation (**Figure 9 a**). Because of that and because recordings were performed for multiple hours, during a single experiment up to 20 million spikes could be recorded (**Figure 9 b, c**). As a result, spike sorting could take multiple days. The initial spike sorting commonly would return between 5000 and 20,000 clusters (potential cells) (**Figure 9 c, d**). This set of cells was filtered for responsive cells by calculating a response quality index (methods) for each cell and each stimulus. Cells that passed the quality threshold for at least one stimulus were considered for analysis. Stimuli were played multiple times during the recording to account for progressive improvement of tissue attachment to the MEA. Consequently, stimuli with the most responsive cells were considered for analysis.

The best recording had about 600 responsive cells, while the worst had 27 responsive cells, most common were recordings with in between 200 and 400 responsive cells (**Figure 7 a**).

DISCUSSION

DISSECTION

Establishing a suitable dissection and stimulation protocol was more complicated than expected. Two thirds of this study were spent on trial-and-error approaches to adjusting various details of the dissection protocol before retinas remained stable for a prolonged duration. The main obstacle was prevention of the initiation of spreading waves of depression during the dissection. Although described in detail (Martins-Ferreira et al., 2000), the fact that these waves are easily triggered in chicken retinas seems to be little known. I have had personal communication with researchers from other research projects which aim to investigate the chicken retina who described similar problems. Eventually I aimed to block waves during the dissection, when they are easily triggered by each contact between forceps and retina. Magnesium is known to block the initiation of spreading waves of depression (Martins-Ferreira et al., 2000). Thus, I established a protocol that raised magnesium concentration during the dissection and returning it normal levels during the recording. It is unlikely that increased Mg^{2+} concentration caused irreversible changes since the retina remained responsive for multiple hours after this treatment.

RECORDINGS

The final dataset consists of data collected within a period of two weeks of daily experiments from a single batch of chicks. After the dissection protocol had been established, the main factor affecting recording quality was the attachment of the tissue to the MEA. Other MEA studies commonly use weights to attach the retina to the MEA surface, for example (Hilgen et al., 2017b; Jouty et al., 2018). However, every poke of the retina can trigger spreading waves of depression, thus using a weight was not a viable option. Even so, the new protocol led to consistently successful recordings (albeit at altering quality).

TEMPERATURE

Temperature is crucial for neuron function on several levels and a change in temperature can have short term and long-term effects. The natural body temperature of chicken is 42.5° C (Randall and Hiestand, 1939) while the temperature used for experiments was set to 37° C. The reason for using a lower temperature was the limitation of the experimental setup. The MEA was likely built with human like tissue in mind and thus supported a temperature range between 30° C and 40° C. The temperature was set to 37° C as this proofed to be the most stable temperature that could be reached with this setup.

Lower temperature in a neuron leads to an increase in the resting potential, a lower depolarization during an action potential and a slower time course of an action potential (Klee et al., 1974). Studies suggest that the resting potential changes by about 1mV with every degree

in temperature change (Klee et al., 1974; Nakanishi and Norris, 1970). This would suggest that the resting potential of the here measured RGCs was about 5mV higher than in natural conditions. While we don't believe this will have dramatic effects on the results presented here, temperature effects on chicken RGCs should be studied in more detail. An easy to perform experiment would be to repeat the here presented experiments at a slightly higher or lower temperature and examine how this effects spike rates, spike durations and integration times.

SPIKE SORTING

Few spike sorting algorithms are capable of sorting datasets as big as generated in this study. Broadly used are Spiking Circus (Yger et al., 2018) and Herding Spikes 2. Herding Spikes 2 was specifically designed for the 3Brain MEA used in this study (Hilgen et al., 2017b) and hence was chosen for spike sorting in this study. Optimizing spike sorting parameters is complex and possibly has no ideal solution if no ground truth data exists as it was the case in this study. The same is true for comparison of results obtained using different sorting algorithms: Without ground truth data one cannot say which sorter may perform better or worse. In addition, changing sorting parameters often has unpredictable effects on sorting results. Instead of optimizing spike sorting, I decided to rely on multiple recordings and filtering of cells by response quality. It is possible that this introduced a bias towards easily detectable cells (for example bigger cells). Since this is an early study of chicken RGCs, this was considered an "acceptable" limitation.

In summary, the new recording protocol allows recording from chicken RGC using MEAs for many hours and are the foundation for further electrophysiological studies.

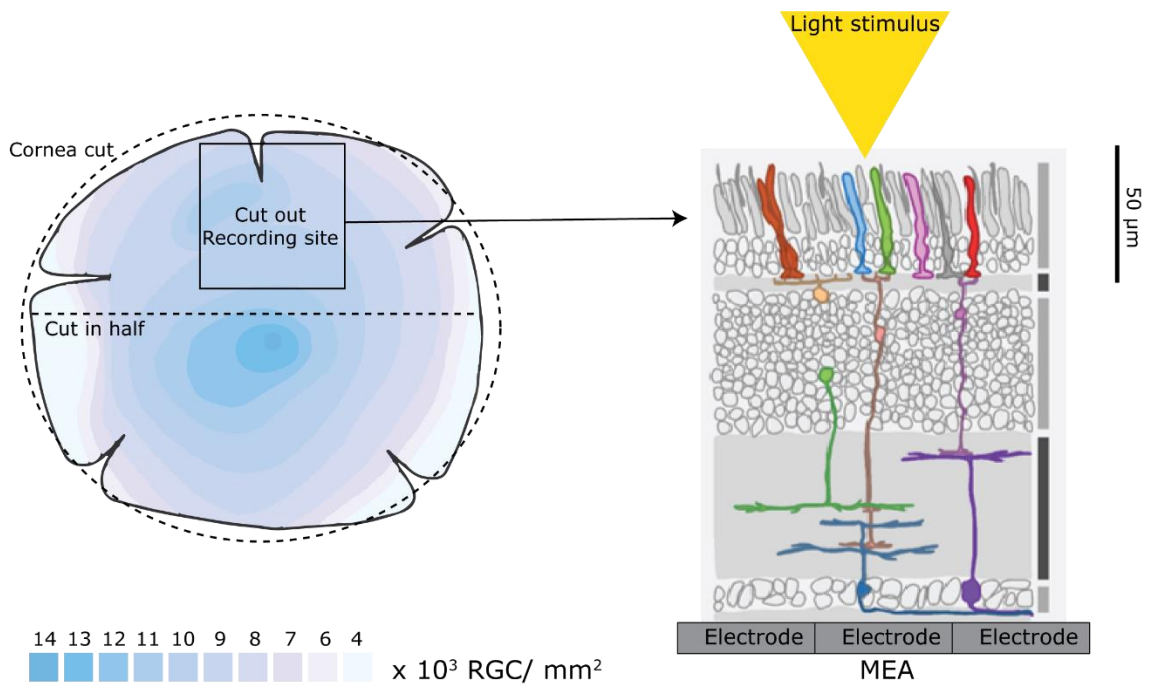


Figure 6 MEA recording of the chicken retina. A square area of about 4 mm² was dissected from the dorsal part of the retina and placed with the ganglion cell layer onto the MEA electrodes. Light stimulation was provided from the “wrong” side, directly hitting photoreceptors.

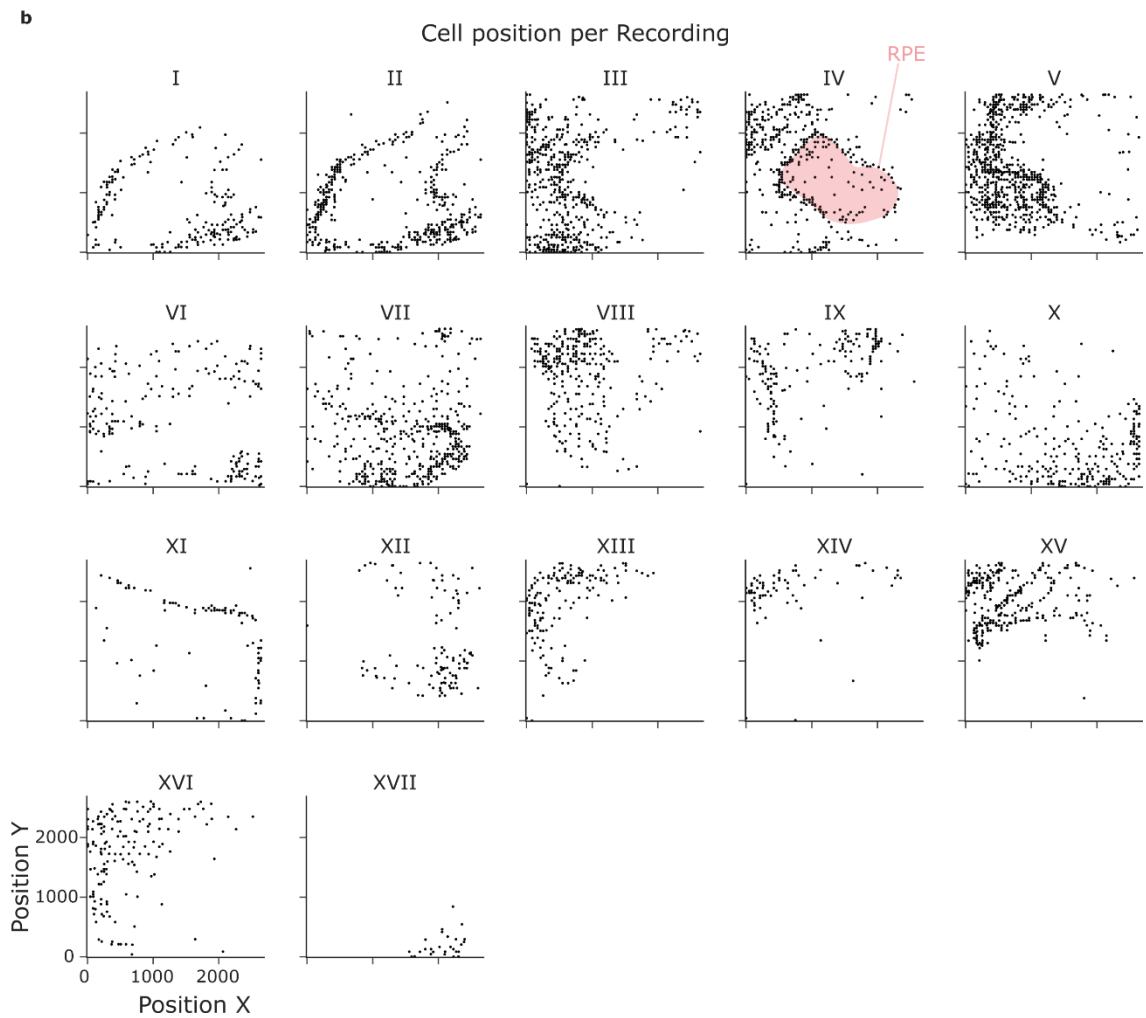
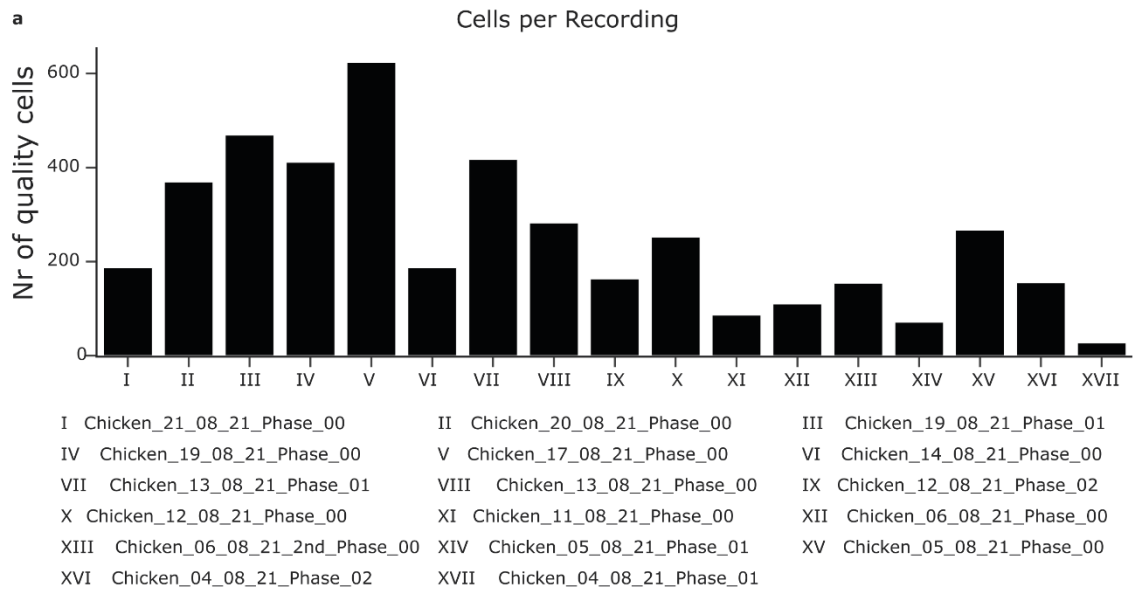
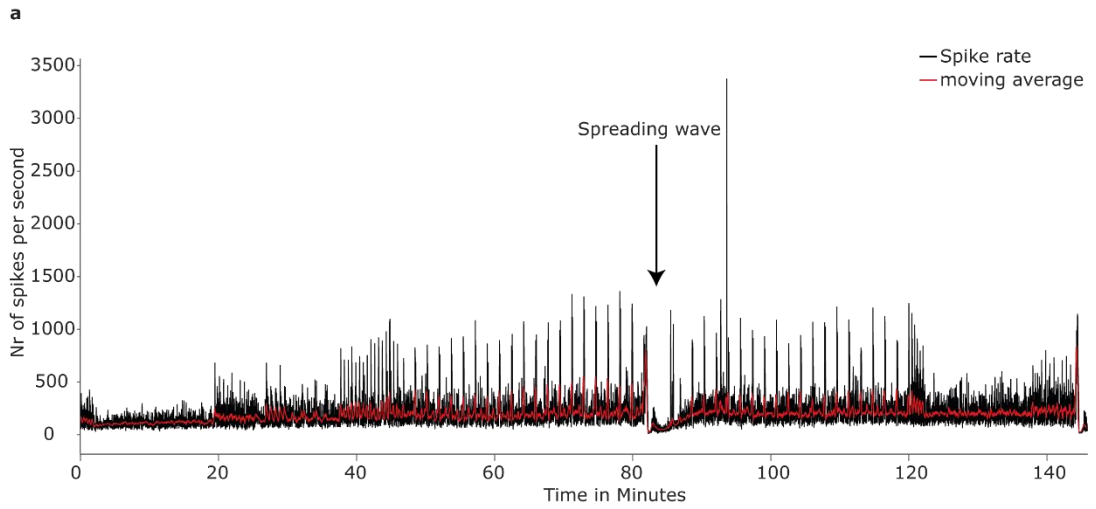


Figure 7: Overview over recordings used for this study

a. Seventeen recordings were made. The number of cells that passed the quality test are shown for each recording. All recordings were performed during a 2-week period. Experiments as indicated under the bar plot.

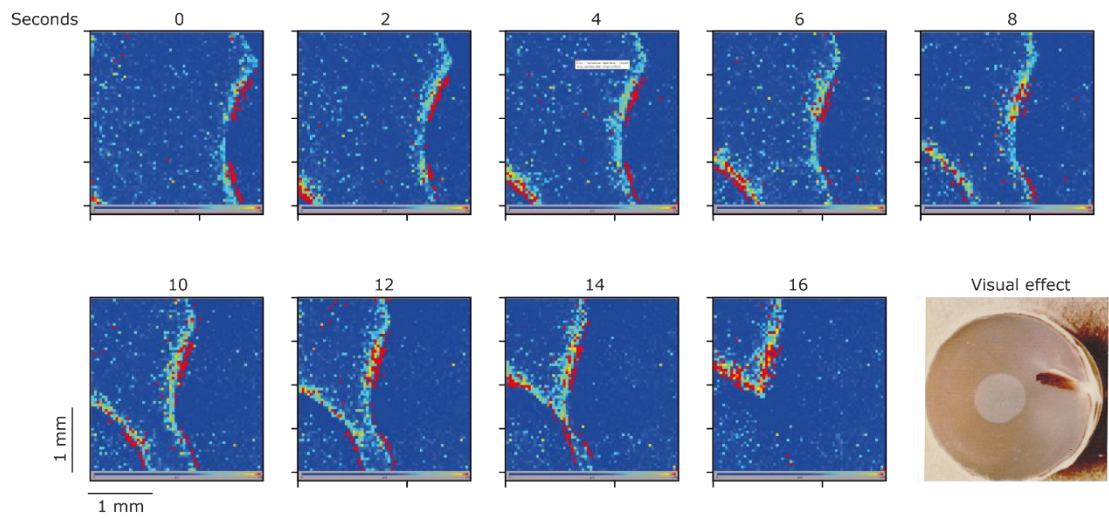
b. Location of the responsive cells on the MEA chip. Few recordings show responsive cells over the whole area of the MEA. Often the retina would attach only to one side of the MEA chip. Surroundings of RPE-remains covered parts of the retina would often yield better responding cells.

Mediocre Recording



b

Spreading wave



c

Good recording

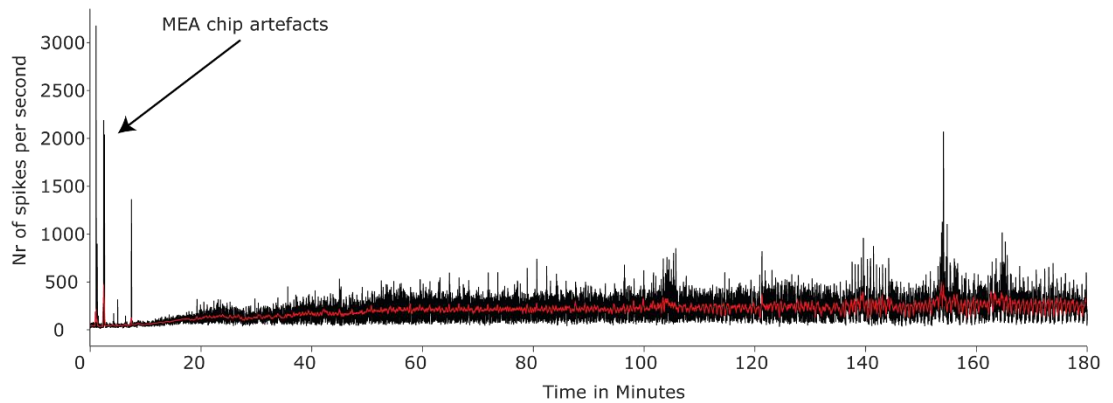


Figure 8: Quality differences between recordings; waves of spreading depression

a. Summed spike rate of all cells in the recording over time. The spike rate increased slightly over time (likely due to better attachment of the tissue) and peaked during stimulus presentations. The retina remained responsive for about 80 minutes after beginning of the recording. A spreading wave of depression as shown in **b** resulted in a loss of spiking activity for about 5-10 minutes before the spiking activity returned to normal.

b. Time course of a wave of spreading depression during MEA recordings. Shown are the activity of all 64x64 MEA channels at different time points during the wave event (Colourmap: Blue = Low electric activity, red = high electric activity). The wave started on the right side and the bottom left side of the MEA and spread in the direction of the top left. The wave travelled about 3 mm over 20 s. Electrical activity was reduced behind the wavefront. As comparison, the optical manifestation of a spreading wave is shown in the bottom right square. Image taken from (Martins-Ferreira et al., 2000).

c. Same as figure a. The best recording performed during the study. The retina remained responsive for 3 hours when the experiment was stopped. No spreading wave of depression was triggered. Spikes of heightened activity (arrow) are electrical artefacts of the MEA.

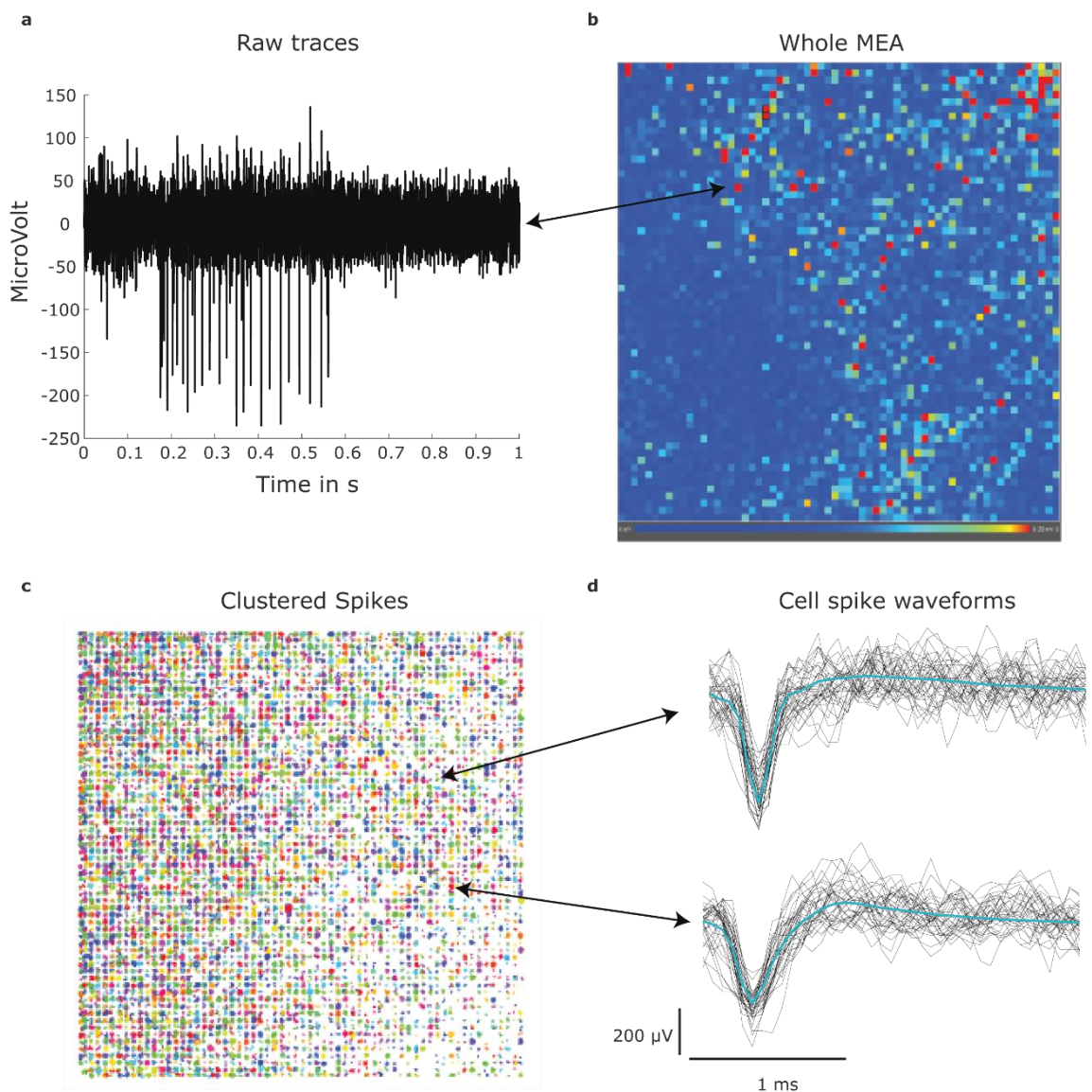


Figure 9 Spike sorting pathway and results

a. Raw traces from a single electrode of the MEA showing a bursting chicken RGC in response to light stimulation.

b. Overview of electrical activity of the whole MEA when the raw trace in **a** was taken. Multiple hot spots of activity are visible. Colourmap same as in **Figure 8**.

c. Clustered spikes returned from the spike sorting algorithm. Shown are 100,000 example spikes. Colours = clusters. Spikes indicated as clouds of dots. Because chicken RGCs are small, single cells were often recorded only by few or single electrodes.

d. Spike waveforms of single clusters (shown in **c**). Spikes differ in amplitude and shape of the waveform. The shape of the waveform was used as one way to distinct individual neurons during spike sorting.

CHAPTER 4: GENERAL RGC RESPONSES

SHORT SUMMARY

This chapter describes response characteristics common to most chicken retinal ganglion cells (RGCs) based on full-field stimuli: Achromatic “white” steps at changing contrast, chromatic steps at different wavelengths, chromatic noise, and a frequency chirp.

First, the majority of RGCs responded both to the onset and the offset of a ‘white’ step of light, rendering them ON-OFF cells. Substantially smaller populations of cells responded only to one polarity. Second, ON - responses were generally sustained, while OFF responses were transient. Third, RGCs generally encoded contrast in a linear fashion.

By comparison, responses to chromatic stimuli were more complex. First, the amplitudes of OFF responses roughly scaled with the spectral distance from the LWS opsin peak sensitivity. Second, ON-response amplitudes were diverse, 630 nm and 420 nm drove the strongest responses, and 480 nm stimuli the weakest. Third, most RGCs showed strong and often dynamically complex forms of colour opponency when probed with full field chromatic noise. Moreover, the integration times were systematically wavelength dependent, with long-wavelength stimuli driving fastest responses.

Finally, frequency chirp stimulation revealed that some RGCs phase-locked until up to 30 Hz, but most cut-off well below 3 Hz.

Taken together, these findings suggest complex chromatic, and temporal coding strategies in chicken RGCs. More than half of RGCs showed colour opponency, which highlights the importance of chromatic information in avian visual processing.

INTRODUCTION

Birds have six different types of photoreceptors (LWS-, MWS-, SWS2-, and SWS1 cone + double cone + rods) (Hart, 2001) and their retinas are highly specialized for “colour” vision on a morphological level (*Chapter 1: Introduction*). The four single cones express four different opsins, each with a different peak sensitivity: SWS1, 419nm; SWS2, 455 nm; MWS, 508 nm; LWS, 570 nm (Hart, 2001). Visual information is processed within the receptor, and by horizontal, bipolar and amacrine cells (Baden and Osorio, 2019) before it reaches RGCs, whose axons form the optic nerve connecting the retina to the brain (Sanes and Masland, 2015).

“Colour” vision requires the comparison of signals coming from at least two input channels with chromatically distinct sensitivities. In vertebrates the first stages of this comparison take place

in photoreceptors, bipolar cells and retinal ganglion cells (Baden, 2021; Baden and Osorio, 2019). RGCs with distinct chromatic sensitivities have been identified among others in primate (Dacey and Packer, 2003), zebrafish (Zhou et al., 2020) and turtles (Rocha et al., 2008), and can be expected in avian retinas. However, published electrophysiological studies reveal little about how chromatic information is encoded in avian RGCs, despite chromatic processing likely being a key feature. (Chen, 2003; Diedrich and Schaeffel, 2009; Stett et al., 2000).

This study for the first time shows how RGCs process and encode stimulus information including: stimulus polarity: Is the stimulus ON or OFF; contrast: how strong is the stimulus relative to the previous stimulus; chromatic information: which “colour” does the stimulus have; and temporal frequency: at which rate does the stimulus appear.

The recordings show that chromatic information is present at the level of RGCs, and reveal complex coding strategies, including chromatic opponent responses. This highlights a key function of chromatic information processing in avian visual systems.

RESULTS

ON OFF RESPONSES

Single RGCs responded to “white” light increments (ON steps), decrements (OFF steps) or to both (ON and OFF steps) with an increase in their spike rate (**Figure 10a&b, Figure 12a and Figure 14**). I analysed the population responses of all recorded cells to 2-s ON steps and OFF steps at different levels of contrast and calculated an average peristimulus time histogram (PSTH) (*Chapter 2: Methods*) for all cells combined to extract response amplitudes and response kinetics (**Figure 10b**).

At a population level, cells responded to ON and OFF steps between 100% and 30% Weber contrast, and solely to OFF steps at 20% contrast. The spike rate increased with contrast more steeply for OFF steps than ON steps (**Figure 10f**). Interestingly, ON and OFF response kinetics differed. After an initial peak, ON responses decayed to sustained response for the rest of the stimulus. OFF responses had faster initial decay and returned to baseline after about 1-s **Figure 11**.

Next, I compared the amplitudes of ON and OFF step responses (**Figure 14a**) calculating an ON/OFF index for each cell (**Figure 14c**). Based on this, cells were classified as ON, ON-OFF or OFF cells (**Figure 10g**). This analysis confirmed that most cells are ON-OFF cells. The proportion of ON to ON/OFF to OFF cells was marginal contrast dependent (**Figure 10 g**).

The population spiking rate of ON step responses at 100% contrast was 18 spikes per second (spks/sec), for OFF it was 16 spks/sec. The spiking rate decreased linearly with decreasing contrast and reached around 7 spks/sec for ON steps and 9 spks/sec for OFF steps at 10% contrast (**Figure 14b**). However, high standard deviations (not shown) indicated high variety in responses of individual cells.

CHROMATIC RESPONSES

To understand the sensitivities of RGCs to chromatic stimuli the retina was stimulated with light at six different wavelengths (630 nm, 560 nm, 505 nm, 480 nm, 420 nm, and 360 nm. For details of LED intensities and resulting cone excitations see (*Chapter 2: Methods*) and photoreceptor input analysis in (*Chapter 5: Functional RGC types*). Single cells differed strongly in their spectral sensitivities: some responded at long wavelengths, some only at short wavelengths and others over the parts of or the whole spectrum (**Figure 10c and Figure 13a**).

On average cells responded to ON and OFF steps at wavelengths ranging from 630 nm to 480 nm with an increase in their spike rate (**Figure 10d**). OFF steps at 420 nm didn't trigger responses at a population level. At 360 nm neither ON nor OFF steps triggered responses (*Discussion*). Chromatic ON responses were more sustained than OFF responses, and the spike rate stayed increased for the whole ON step at 630 nm, 560 nm, 505 nm, and 420 nm but not at 480 nm. At 630 nm and 505 nm, the ON response amplitude exceeded that of the OFF response, but the reverse applied at 480 nm (**Figure 10d&f**).

Individual analysis of all cells in the population confirmed cell responses to ON, OFF or ON and OFF steps in a wavelength dependent manner (**Figure 10f**). At long wavelengths, most cells responded to ON and OFF steps, while at short wavelengths cells tended to be either ON or OFF sensitive. At 505 nm and 420 nm most cells responded to the ON steps (44% and 76% respectively). In contrast, at 560 nm and 630nm only 10 % and 14% respectively responded exclusively to ON steps. At 480 nm similar numbers of cells responded to ON (32%), ON and OFF (37%) and OFF (30%), **Figure 10f**.

The amplitude of ON and OFF responses was strongly wavelength dependent. At the population level, 630 nm ON steps drove the strongest increase in the spike rate (16 spks/sec) (**Figure 14**) and ON steps at 480 nm triggered the weakest response at about 5 spks/sec. **Figure 14b** illustrates spectral tuning curves, with chicken opsin sensitivities for comparison. Unlike the ON responses, OFF response amplitudes followed a clear trend: Response amplitudes decreased with distance from the peak sensitivity of the LWS opsin, (but see *Chapter 5: Functional RGC types, part 2*). The maximal response amplitude was at 560 nm (10 spks/sec) and the weakest at

420 nm (2 spks/sec). The amplitude of responses to light stimulation at 360 nm was low for ON and OFF step responses (2 spks/sec). Due to technical limitation the 360 nm LED was about ten times weaker than all other LEDs (*Chapter 2: Methods*). Since no clear responses were found at 360 nm, 360 nm responses were not further analysed and will not be mentioned after this section.

CHROMATIC OPPONENT RESPONSES

Stimulating the retina with a single wavelength revealed simple spectral sensitivities. To further test cells' chromatic opponent responses, the retina was stimulated with a chromatic full field colour noise stimulus (FFFNoise). In this stimulus, four different LEDs (630 nm, 505nm, 480nm, and 420 nm, in the following also called "red", "green", "cyan", and "blue" respectively) are switched on or off in a pseudorandom sequence at 20 Hz. Since different combinations of LEDs are switched ON and/or OFF at random at the same time this stimulus can reveal spectral opponencies, which can be identified by reverse correlation of responses with the stimulus. This method returned first order (linear) response kernels (**Figure 15b**) which summarize the average stimulus history at a given time before the spike in combination with the information about the cell's integration depending on wavelength, (**Figure 15b**). Response kernels are a compact visualization of key chromatic response characteristics of a cell.

Response kernels have different time courses depending on how light stimuli are integrated. Common are monophasic ON or OFF types which represent cell responses to light increments or decrements respectively. Biphasic ON-OFF and OFF- ON types represent cell responses to light increments and decrements from luminance levels below or above background luminance respectively.

DIFFERENT CELLS SHOW DIFFERENT CHROMATIC OPPONENCIES

GENERAL RESPONSE CHARACTERISTICS OF RGC TO FFFNOISE.

Many RGCs responded well to full field (FFFNoise) (**Figure 15a**). STAs of single cells revealed diverse spectral sensitivities, spectral opponencies and integration times (**Figure 15c**). Nine types of responses were identified by analysing the response polarity at each wavelength, and by comparing polarities across wavelength (**Figure 15 d**), with 90% of cells falling into five of these groups (**Figure 15 b, d**). The first two groups (complex chromatic opponent cells and achromatic OFF cells) included about 60% of all cells. A few general trends could be observed: Most blue and cyan kernels were monophasic OFF, but few red kernels were monophasic OFF (**Figure 15 e**). Green kernels were common as monophasic OFF, biphasic ON-OFF and monophasic ON.

Considering the integration time, two clear trends could be observed. First, ON responses were normally slower than OFF responses. For example, as shown in **Figure 16 b**, red ON kernels were about 30 ms slower than red OFF kernels. Second, integration time was strongly wavelength dependent, on average the integration time increased with decreasing wavelength. On average, red OFF kernels had the shortest integration time (median = 85 ms). The longest integration times were observed for 420nm OFF kernel (median = 250 ms).

CELLS WITH COMPLEX SPECTRAL OPPONENCY

The 30% of cells with complex spectral opponency, fell into two subgroups (**Figure 15 d(1)** upper trace). Those in the first group had blue, cyan, and green biphasic ON OFF kernels and a red OFF ON kernel which mirrors the blue kernel with opposed polarization. The integration time was wavelength dependent, being longer at 480 nm and 505 nm than at 630nm and 420 nm.

The second type of complex opponent cells were very different from the first (**Figure 15 d(1)** lower trace). Notable was a blue monophasic OFF kernel with a long integration time of up to 500 ms and monophasic ON kernels at 630 nm and 505 nm with weaker amplitude but similar slow integration time. The cyan kernel was monophasic OFF but faster (integration time <100ms) than the blue kernel.

ACHROMATIC OFF CELLS

The second largest group of cells (29 %) had relatively fast (about 100 ms) achromatic off responses (**Figure 15 d(2)** upper), with two subtypes. The first subtype had a red biphasic ON-OFF kernel with high amplitude and green and cyan biphasic ON-OFF kernels with lower amplitudes. Interestingly, in this type, the latency difference between wavelengths was small.

The second subtype of this group had the same spectral sensitivities as the first (**Figure 15 d(2)** lower) and biphasic ON-OFF kernels. The amplitude of the kernels decreased with decreasing wavelength, but the integration time was longer than in subtype 1. The ON part of the kernel was much slower (about 300 ms) than the OFF part (150ms). In addition, kernel amplitudes were low compared to kernels in the first subtype.

RED-GREEN OPPONENT CELLS

This group of cells (10% of all recorded) had a monophasic red ON kernel and opposed green and cyan monophasic OFF kernels (**Figure 15 d(3)**). Amplitudes of the red ON kernel was like green and cyan OFF. The integration time of these cells is about 200 ms.

ACHROMATIC ON CELLS

The next largest group of cells (9 %) had achromatic monophasic ON responses (**Figure 15 d(4)** upper) with weak amplitudes similar to those of complex opponent cells subtype two. However, in contrast to the complex opponent cells, these cells had a flat blue kernel.

SHORT VS LONG OPPONENT CELLS

The fifth largest group of cells (5%) had a blue monophasic OFF kernel and opposed monophasic ON green and red ON kernel (**Figure 15 d(5)**). The integration time in these cells was wavelength dependent. The integration time of the blue kernel was about 400ms, green and red kernels were faster (200ms for blue and 180 ms for red). The blue kernel had the largest amplitude followed by the green and red kernel.

FOUR FURTHER SPECTRAL OPPONENT CELL-TYPES

10 % of cells had other chromatic opponencies as follows: i) red vs blue; ii) red vs cyan; iii) cyan m vs blue and iv) green vs cyan.

In summary, it was found that the main axis of spectral opponency in RGC is between 505nm and 480 nm. Some cells combined red and green light inputs and oppose them to light at shorter wavelength, while other cells combined green and green-blue light inputs and oppose them to red light inputs.

CHIRP RESPONSES

As seen in the previous section, RGC differed in their response kinetics. Achromatic frequency responses were tested with a chirp stimulus, which modulated the stimulus frequency from ≈ 0 Hz to 30 Hz over 30 seconds. An exponential increase was chosen to better distinguish low frequency responses. In addition to frequency-dependence, chirp responses can follow OFF phases, ON phases or both.

At a population level up to about 5 Hz, the population PSTH spike rate increased to OFF and decreased to ON phases (**Figure 17 a & b**). At a chirp frequency of about 5 Hz the sinusoidal fluctuation in average PSTH decreased, but the spike rate remained elevated compared to the unstimulated condition. The bin size (0.05s) limited detection of sinusoidal fluctuation in the PSTH. Another limitation in the analysis was the alignment between the sinusoidal fluctuation of the response with the PSTH bins. While the frequency of the PSTH histogram remained constant throughout the stimulus, the frequency of the sinusoidal population response changed over time. Because of this, interference patterns between PSTH and responses emerged. Consequently, PSTHs were hard to read at higher chirp frequencies and were not ideal to understand cell responses.

To circumvent these limitations the integration time of each cell was tested. This was done by calculating the average delay of a cell's response to either an ON step or OFF step (data not shown). The chirp was then divided into ten different parts (3 seconds in duration, over different frequency ranges) and for each part the phase lock between the chirp stimulus and the cell's response was calculated under consideration of the cell's integration time. If the spike train of a cell is aligned with the stimulus, most spikes will fall within a defined window relative to the chirp sequence. In other words, the better aligned the spikes are (under consideration of the response delay) with the peaks or minima of the chirp (depending on whether the cell is sensitive to ON or OFF stimulation), the better the cell follows this stimulus. The strength of the alignment of spikes with the stimulus was mathematically represented as vectors. Finally, the resulting vector strength was calculated (the more vectors point into the same direction, the stronger the resulting vector strength). Consequently, the resulting vector strength indicates how well a cell follows the chirp stimulus.

On a population level the average vector strength between chirp frequencies of ≈ 0 and 10 Hz is above 0.5 (**Figure 17d**). This indicates that most cells followed these frequencies. The vector strength decreased almost linearly with increasing chirp frequency bins. At the highest frequencies (25-30 Hz) the average vector strength was about 0.38.

To test which vector strength could be expected from a random spiking cell just by chance, 1000 randomly spiking cells were created, and the average vector strength was calculated for these cells (**Figure 17c**, red scatter plot). The mean vector strength of random spiking cells was about 0.25. Based on this a 95% confidence interval was calculated to indicate at which point the vector strength could be the result of a random alignment between randomly triggered spikes and the stimulus. Interestingly the mean vector strength of the RGC population stayed above this confidence interval at all frequency bins (blue line in **Figure 17 d**) confirming that the RGC population can follow the frequency chirp up to frequencies of 30Hz. However, a large proportion of the cells had a vector strength of around 0.2 at a stimulus frequency of 30 Hz while for a smaller group of cells the vector strength remained high at 0.8 and above. This indicates that two different groups of cells were present within the population. One group remained phase locked throughout the entire stimulus and another group lost phase lock at higher frequencies. Another indication for diversity within the population response was a high standard deviation of vector strengths. Analysis of single cell chirp responses confirmed differences in phase lock (**Figure 18**), this will be further analysed in (*Chapter 6: Response Shapes*).

In summary, while the population response of RGC followed the chirp from ≈ 0 to 30 Hz, single cells differed in their frequency responses, with some being more sensitive to low frequencies and some more sensitive to high frequencies.

DISCUSSION

KEY FINDINGS

The results presented in this chapter reveal some key response characteristics of avian RGCs for the first time. Strikingly, most RGCs were classified as ON-OFF cells with differing response kinetics (sustained vs transient) to stimulus onset and offset. ON responses showed complex chromatic sensitivities. OFF responses broadly scaled with the LWS opsin spectral sensitivity (but see *Chapter 5: Functional RGC types, part 2*). The majority of RGCs showed complex, time dependent chromatic opponency. Because of this, it is interesting that most RGCs showed low frequency tuning, with cut offs around 3 Hz. However, some cells followed high frequencies and on population level RGCs responses up to 30 Hz were measured.

ON AND OFF RESPONSES

Interestingly, most RGC were excited both by "white" ON and OFF steps (**Figure 11 g**) but on population level the OFF response was more transient than the ON response (**Figure 11 b & d**). Hence, my data suggests that ON and OFF could be encoded by response kinetics (transient vs sustained) and secondarily by specialist ON or OFF RGCs. In addition to this, RGCs likely encode stimulus contrast as response amplitude in ON and OFF responses.

How does this compare to other vertebrates?

Traditionally RGCs are classified as ON or OFF cells depending on whether the centre of their receptive fields is sensitive to light increase (ON) or decrease (OFF) (Van Wyk et al., 2009; Werblin and Dowling, 1969). Separation between ON and OFF pathways is a core principle of visual processing (Hartline, 1938; Kuffler, 1953) and is established in bipolar cells (Werblin and Dowling, 1969). Both, ON and OFF cells can show transient or sustained responses. For example, primate midget cells, and mouse alpha cells (sustained) (Kolb and Marshak, 2003; Krieger et al., 2017) or transient alpha cells found in mouse, cat and primates (Crook et al., 2008; Krieger et al., 2017; Peichel and Wässel, 1981) . Because of this, it is surprising that I found a majority of ON-OFF sensitive cells.

The ON to ON-OFF to OFF RGC type ratio differs between vertebrate species, perhaps as a function of number of spectral receptor types (i.e. input channels). Species with few photoreceptors tend to show more ON or OFF RGC types (mouse, primate). In contrast, in species with a higher number of photoreceptors, more cells are sensitive to both ON and OFF

steps (salamander, fish). Further investigations are necessary to establish this hypothesis. A broad comparison between vertebrates with few input channels and those with many input channels would be ideal.

Salamanders have six receptor types, which is comparable to chicken and has a majority of ON-OFF cells (Pang et al., 2002). Cross talk between the ON and OFF pathway does exist in a subset of ganglion cells (Pang et al., 2007). Interestingly, in zebrafish, which have five input channels, the proportion of ON and OFF cells differs depending on the position in the retina (Zhou et al., 2020), which indicates that certain visual information is preferably encoded in either the ON or OFF pathways.

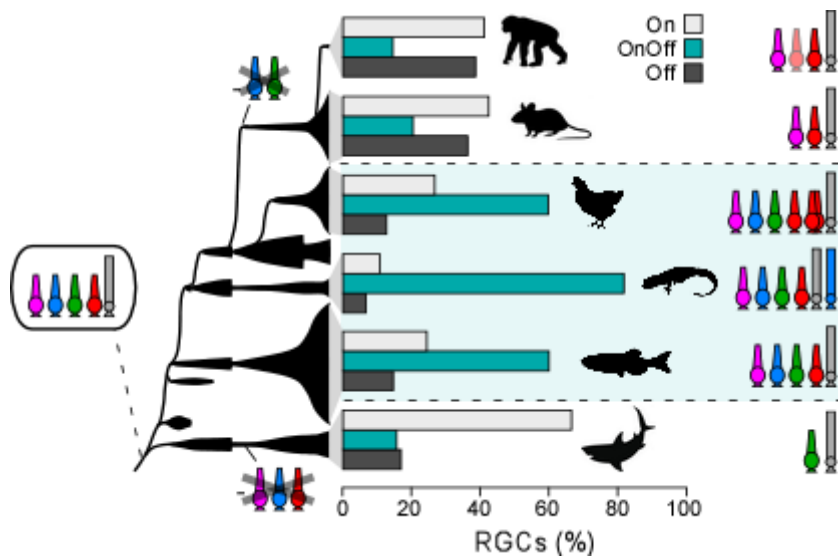


Figure 10: ON OFF dominance by species. Different species have different coding strategies. Species with fewer input channels (shark, mouse primate) have fewer ganglion cells that encode both ON and OFF steps than species with relatively more input channels (chicken, salamander).

CHROMATIC RESPONSES

I tested chicken RGC chromatic sensitivities in two ways. First as full field stimuli at different fixed wavelengths. Second, as full field binary chromatic noise stimulus (see pros and cons for both methods below). Regardless of the stimulus used, the majority of RGCs show complex wavelength dependent sensitivities and/or opponencies.

OFF responses were likely primarily driven by cone types that contain LWS opsin (LWS cone or double cone inputs or a combination of both), given that OFF spectral tuning curve scales with distance to the peak sensitivity of the LWS opsin. Chromatic noise stimulation revealed 30% of all cells had achromatic OFF kernels whose amplitude scaled with the LWS cone sensitivity. These kernels are faster than those of cells showing chromatic opponent kernels. I will show in (*Chapter 5: Functional RGC types*), that these cells form two functionally distinct cell types and

in (*Chapter 6: Response Shapes*), that these cell types have faster responses than any other identified cell types.

ON responses must receive more complex inputs from different cones, given the complexity of the ON tuning curve over the spectrum. ON tuning curves differed fundamentally from OFF tuning curves in two ways: 420 nm responses were much stronger in ON than OFF and the differences between 480 nm responses and 420 nm or 505 nm responses were large. SWS2 and the MWS cones are sensitive to 480 nm light. The absence of strong responses suggests that inhibitory and excitatory signals cancel each other out at this point on the population level.

Population responses to 420 nm are interesting. 420 nm stimuli triggered strong ON responses but no OFF responses when present as full field flash from black. In contrast, 420 nm stimulation during FFFNoise lead to OFF kernels. The reason for this difference is puzzling. It may lay in the fact that the full field colour noise adapts the retina to an intermediate luminance level from which light at a specific wavelength is either decreased or increased. Possibly light at around 420 nm is subtracted as “background” and thus 420 nm responses highly depend on the adaptation state of the receptor/circuit. In any case, full field noise stimulation is fundamentally different to full field flashes at distinct wavelengths. Specifically designed stimuli, testing 420 nm responses in different adaptive states could help understanding the observed differences.

RESPONSE KINETICS

As shown above, ON and OFF responses differed in their time courses. More interestingly, response kinetics were wavelength dependent. Response kernels revealed integration times at 420 nm at up to 400 ms in some cells. This is surprisingly slow. For example macaque RGCs show max response kernel amplitudes at about 0.05 seconds before spike and integration times no longer than 200 ms (Chichilnisky, 2001). Response kernels with very long integration times are puzzling, and their function unclear. It is possible, that long time delays between stimulation and spike are a recording artefact (see Limitations of the methods). More likely, wavelength dependent response latencies contain spectral information, and are used to code for chromatic stimulus content. This theory will be addressed in detail in (*Chapter 6: Response Shapes*)

CHIRP RESPONSES

The chirp stimulus tested frequency tuning. Behavioural experiments and electroretinography find that chickens have flicker fusion frequencies of up to 90 Hz, depending on the luminance (Lisney et al., 2012, 2011). Population response to the chirp stimulus used here peaked at about 5Hz but followed the stimulus up to 30 Hz. Full field noise stimulation revealed specific achromatic cells that rely on long wavelength inputs and show faster response kernels. The

analysis of chirp responses of all cells in the population showed that one fraction of the cells follows the chirp only below 3 Hz, while another group follows the chirp up to 30 Hz. (*Chapter 5: Functional RGC types*) will describe functional RGC types with fundamentally different frequency sensitivities.

LIMITATIONS OF THE METHODS

FULL FIELD STIMULATION

Since this study is first to study avian RGCs in depth, the visual stimuli were kept simple. The main concern was to gather enough data to establish a first general understanding of chicken RGC electrophysiology. Full field stimulation has the advantage that RGC receptive field properties (size, polarity orientation) are not of concern. However, this also represents a major limitation. RGCs commonly have receptive fields consisting of a centre and a surround, of which one inhibits responses and one promotes responses (Hubel and Wiesel, 1959). Depending on how strong the inhibitory part of the receptive field is, full field stimuli may not reliably trigger responses. Spatially non-uniform stimulation would be required to test receptive field sizes. Spatial chromatic noise stimulation (Chichilnisky, 2001; Field et al., 2010) was tried during the study and did return responses in one experiment. However, since chicken receptive field sizes are small, spatial noise stimulation needs to use small pixel sizes which in turn require a prolonged presentation of the stimulus and require extensive analysis. With the improved recording protocol this experiment should be possible in the future.

LINEAR KERNELS

Linear kernels as presented in this study assume a linear correlation between different chromatic inputs and response. However, neurons often show nonlinear responses. Thus, linear kernels may not be able to explain the full extent of correlations between stimuli and responses. For example, nonlinear chromatic opponencies might explain the observed slow response kernels at 420 nm. To gain further insights into chromatic sensitivities and opponency ideally nonlinear kernels should be calculated alongside linear kernels. However, nonlinear analysis is mathematically more advanced, and results are harder to interpret, which is why it was not a priority in this study.

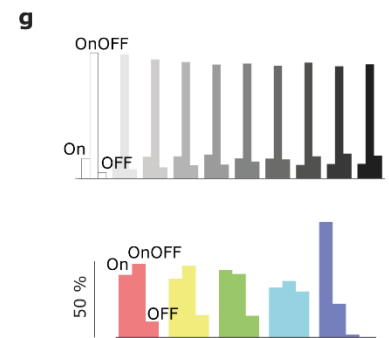
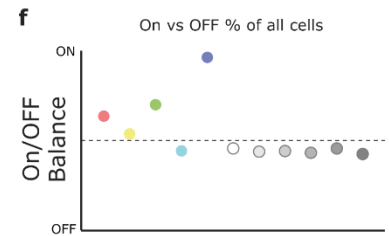
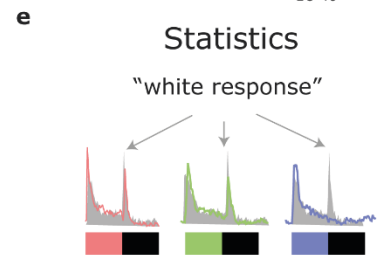
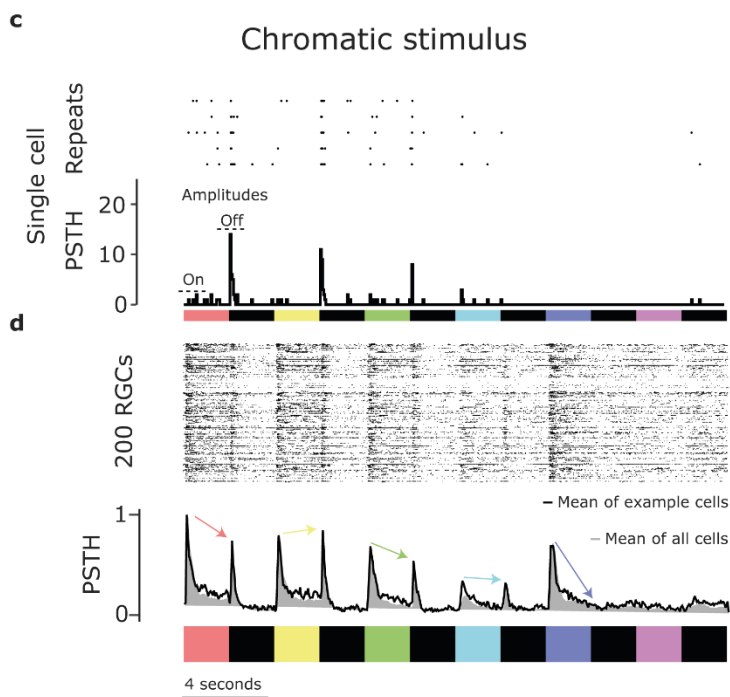
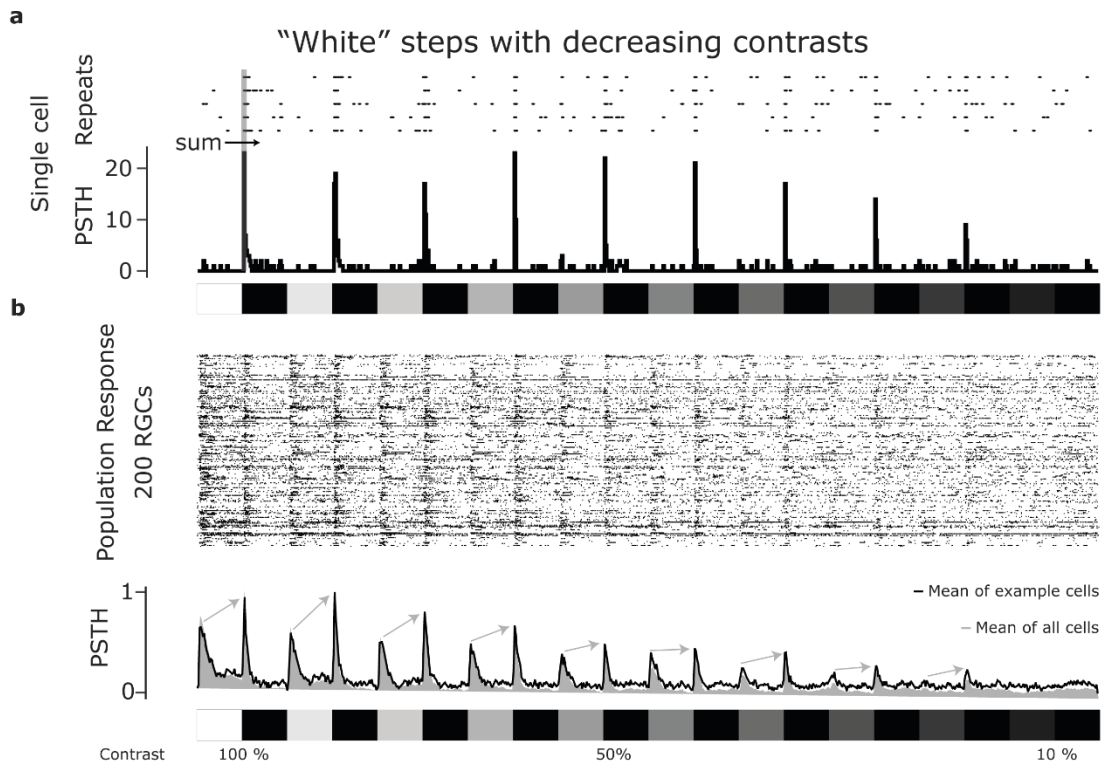


Figure 11: RGC responses to white and chromatic ON and OFF steps.

a. A single cell response to five repeats of the “white” contrast steps stimulus is shown. The spike trains of all repeats are plotted time aligned as rows of dots (indicating the time of the spike) to highlight times of consistent responses over all five repeats. Below the resulting peristimulus histogram (PSTH) for this cell is plotted as dark line further highlighting synchronous spiking patterns over all repeats. The resulting spike frequency is calculated as $nr. \text{ spikes per bin} * \frac{1}{\text{bin size} = 0.05}$. This cell responded to OFF steps at contrast from 100% Weber contrast to 10% contrast.

b. Same as **a.** but for 200 randomly picked example cells. Single cell spike trains of all 5 stimulus repeats are plotted overlaid as one combined spike train per cell. Below the normalized PSTH for the example cells is plotted as dark trace and the normalized PSTH for all cells in the population is plotted as grey area below. The population responded to ON and OFF steps at between 100% Weber contrast and 20% Weber contrast.

c. Same as **a.** but for stimulation at six different wavelengths as follows (red = 630 nm, yellow = 560 nm, green = 505 nm, cyan = 480 nm, blue = 420 nm, magenta = 360 nm). This cell responded to red, yellow, and green OFF steps.

d. Same as **b.** but for the chromatic stimulus illustrated in **c.** The population responded to ON and OFF steps at wavelengths between 630 nm and 480 nm light and to ON steps at 420 nm light.

e. Overlaid population responses to red, green, and blue light (traces in the respective colours) and the 100% Weber contrast ON step from **b.** The population response to 100% weber contrast resembles closest the population response to the red chromatic stimulus.

f. ON OFF balance calculated as $\frac{ON \text{ step amplitude}}{OFF \text{ step amplitude}}$. The amplitude was calculated based on the population response as indicated by the arrows in **b** and **d.** All “white” step responses are OFF dominated while the ON OFF balance varies depending on the wavelength for the chromatic stimulus.

g. Histogram of ON ONOFF OFF cells in the entire population. Plotted are histograms for different contrasts of the “white” step stimulus and different wavelengths of the chromatic stimulus. The proportion of ON vs ONOFF vs OFF cells was wavelength dependent.

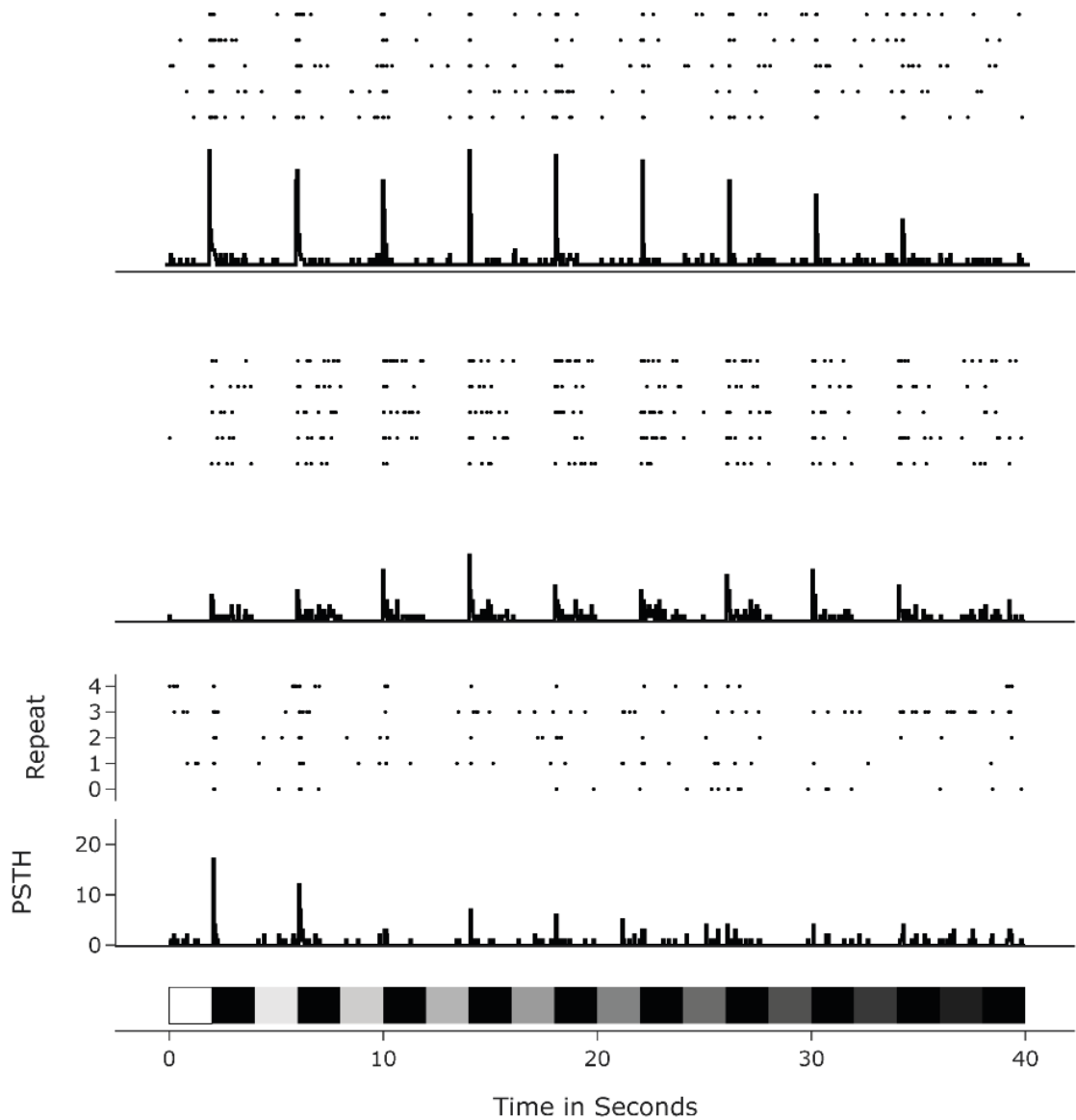


Figure 12: Examples of single cell responses to the “white” step stimulus. Three different example cells are shown. Plots as described for **Figure 11a**. The first cell responded to the OFF steps over a range of different contrasts. Responses were transient. The second cell interestingly had a sustained OFF response. The third cell only responded to OFF steps at 100% and 90 % contrast.

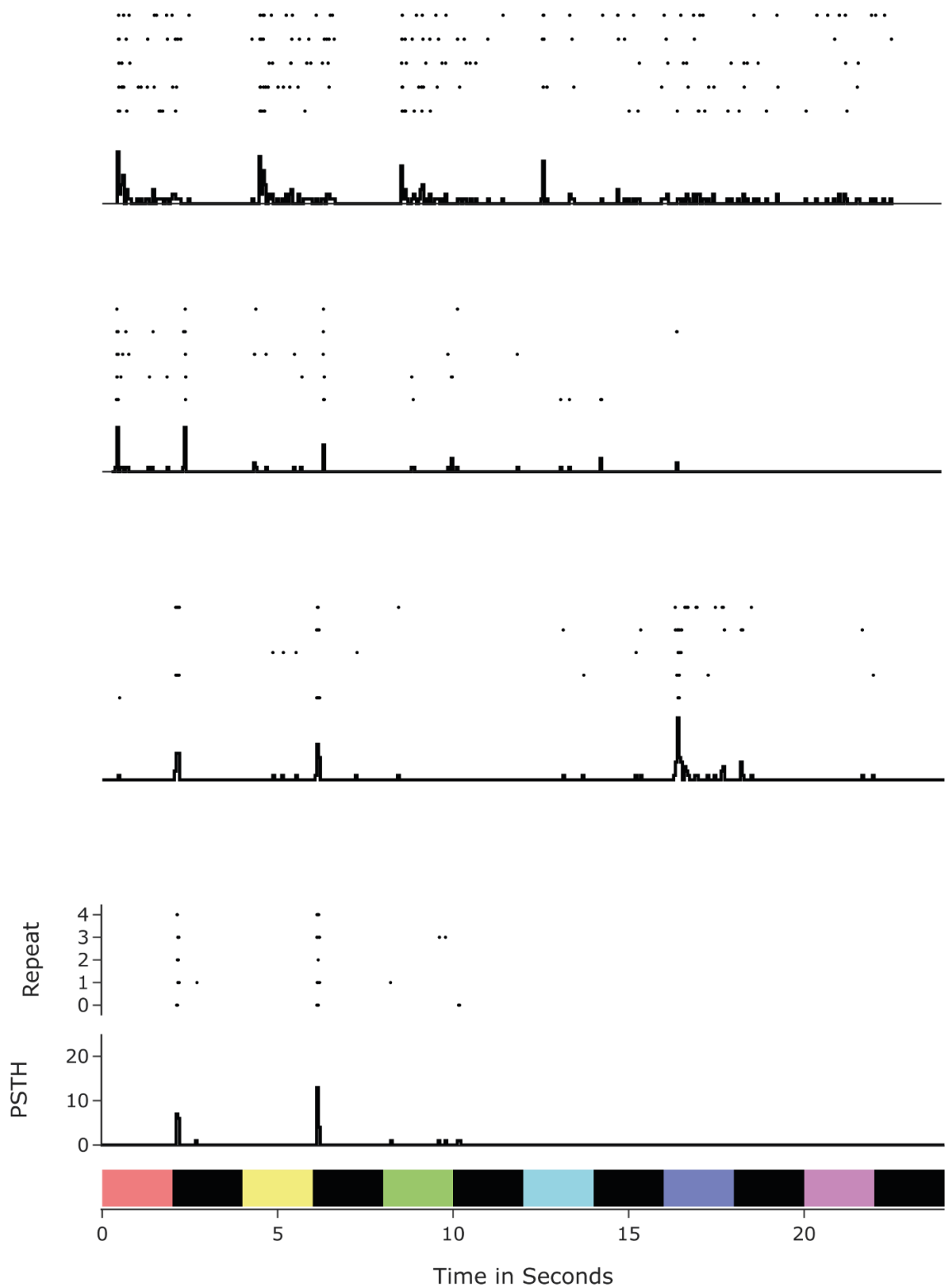


Figure 13: Examples of single cell responses to chromatic stimuli. The first cell responded sustained to ON steps at 630 nm – 480 nm. The second responded to ON and OFF steps at 630 nm and 560 nm. The third showed reliable responses only at 420 nm. The fourth cell responded to OFF steps at 630 nm and 560 nm.

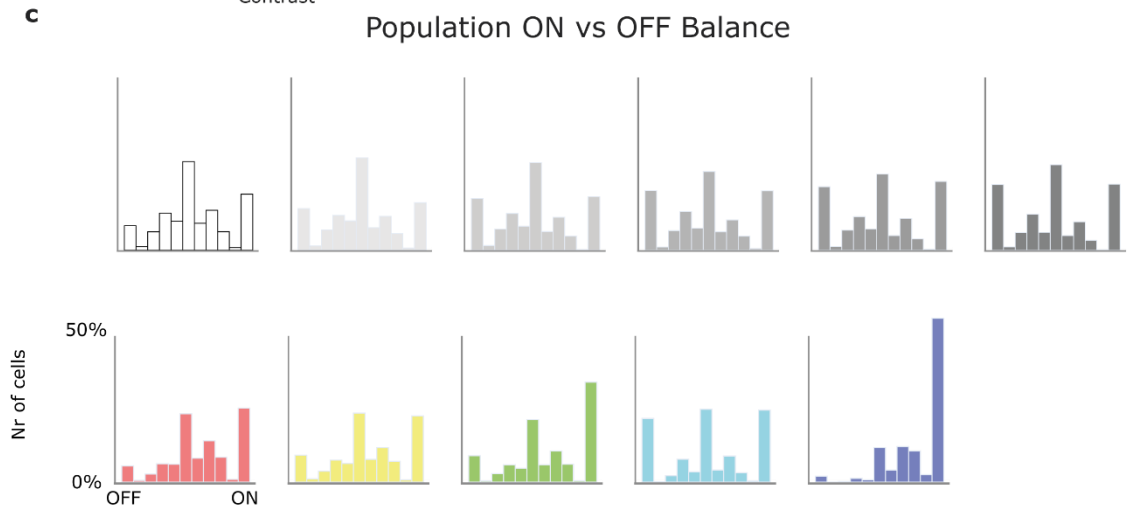
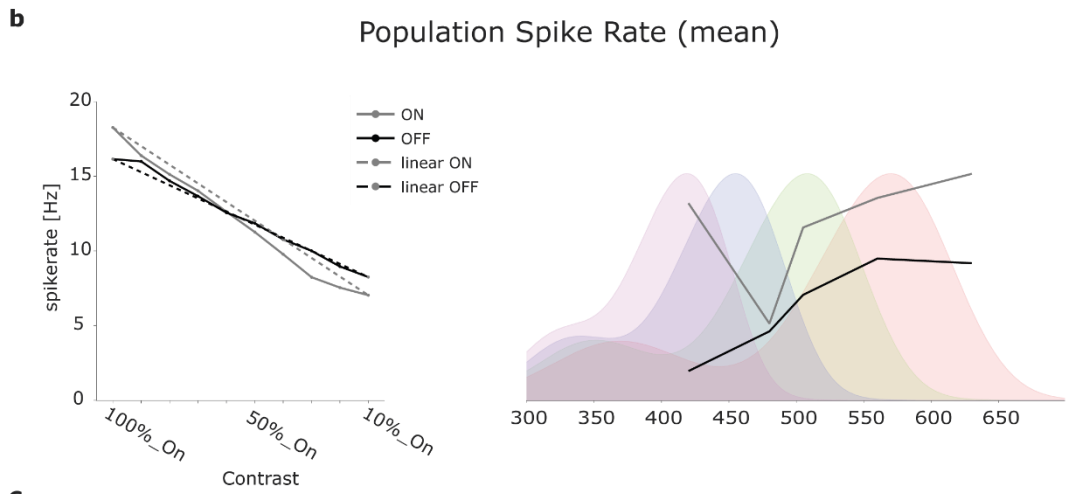
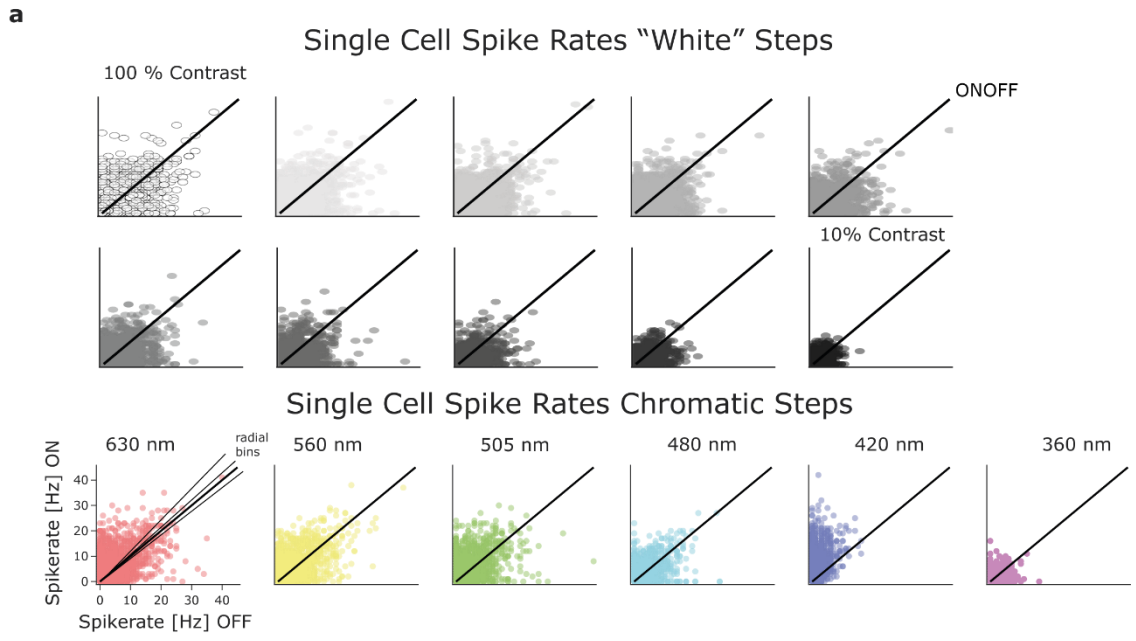


Figure 14: Comparisons of ON and OFF response amplitudes.

a. Scatterplot comparing the maximal spike rate in response to ON steps (y-axis) and OFF steps (x-axis) for the different contrasts “white” step stimulus and the chromatic stimulus for each cell in the population. The mean spike rates for each stimulus condition are plotted in **b**. Clear differences in spike rate to ON and OFF steps could be seen for some chromatic steps (505 nm and 420 nm) but not for the “white” steps.

b. Mean response amplitude plotted as functions of contrast and wavelength. The maximal spike rate showed a linear correlation with contrast. For chromatic stimuli, the spike rate of OFF responses decreased with distance from the wavelength of the maximum absorption of the LWS opsin. The spike rate of the ON responses had a more complex pattern.

c. Histogram of the scatter plots shown in **a**. The points in the scatterplot were assigned to eleven “radial” bins, to indicate how many cells show responses only to ON or OFF steps and which cells show responses that lay in between. After further condensation of the data **Figure 11 g** was obtained.

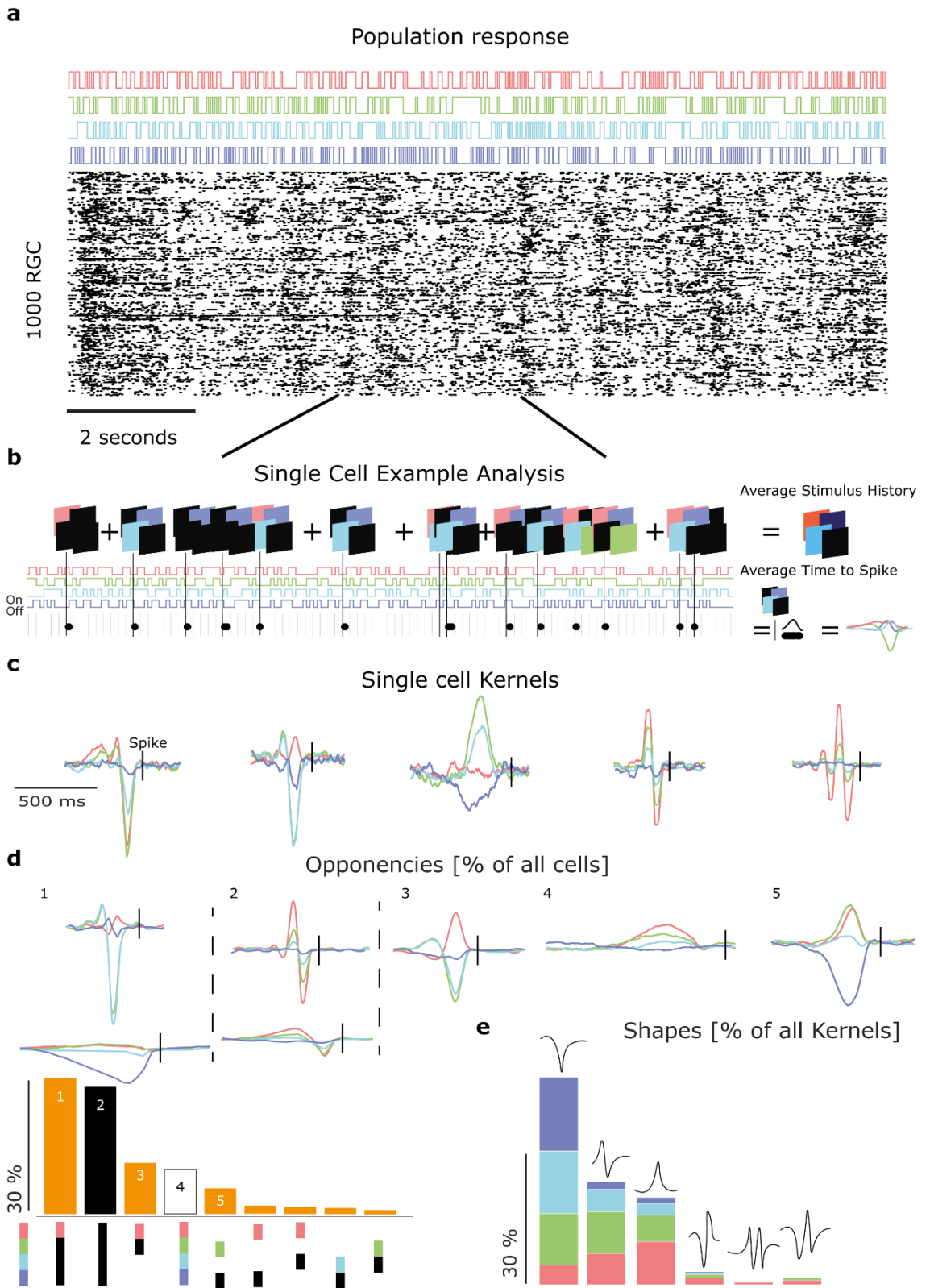


Figure 15: Full Field Colour Noise

- a.** Spike trains of 1000 example cells showing the cell responses to a small subset of the stimuli. The binary noise sequence for the four LEDs (red = 630 nm, green = 505 nm, cyan = 480 nm, blue = 420 nm.) is plotted above the spike trains. Certain noise sequences (LED combinations) caused increased spike rates in many cells in the population.
- b.** Illustrative analysis of a spike train that shows how spike triggered averages (STA) are computed. The stimulus history that preceded each spike is summed over time (a window of 1 second before a spike was considered stimulus history) and the STA is calculated as the average stimulus that preceded a spike. In addition, a time “kernel” is calculated, which indicates the distribution of time differences between the summed stimuli and the triggered spike.
- c.** The response kernels of five cells are plotted. The first is a monophasic achromatic OFF cell sensitive to light from all four LEDs. The second is a biphasic achromatic OFF cell, which is most sensitive to 630 nm. The third is a biphasic opponent cell, which is inhibited by 420 nm, 480 nm, and 505 nm, but excited by at 630 nm. The fourth is a multiphasic OFF cell most sensitive to light at 630 nm. The last cell is a monophasic opponent cell, which is inhibited by 420 nm and excited by 480 nm and 505 nm.
- d.** Different types of cells could be identified based on their response kernels. Five types of kernels contained about 90% of all cells: 1 = complex opponency cells, 2=achromatic OFF cells, 3 red ON (630 nm) vs green OFF (505 nm) cells, 4=achromatic ON cells, 5=green ON (505 nm) vs blue OFF (420 nm) opponent cells. The averaged traces of all cells within a group are shown next to a histogram indicating the proportion of cells that fall within a certain group.
- e.** Histogram of the proportion of different kernel types found in the population, classified by colour. Most common were monophasic OFF responses, followed by biphasic ON OFF and monophasic ON responses. Less common were OFF ON responses and more complex waveforms like triphasic or multiphasic kernel.

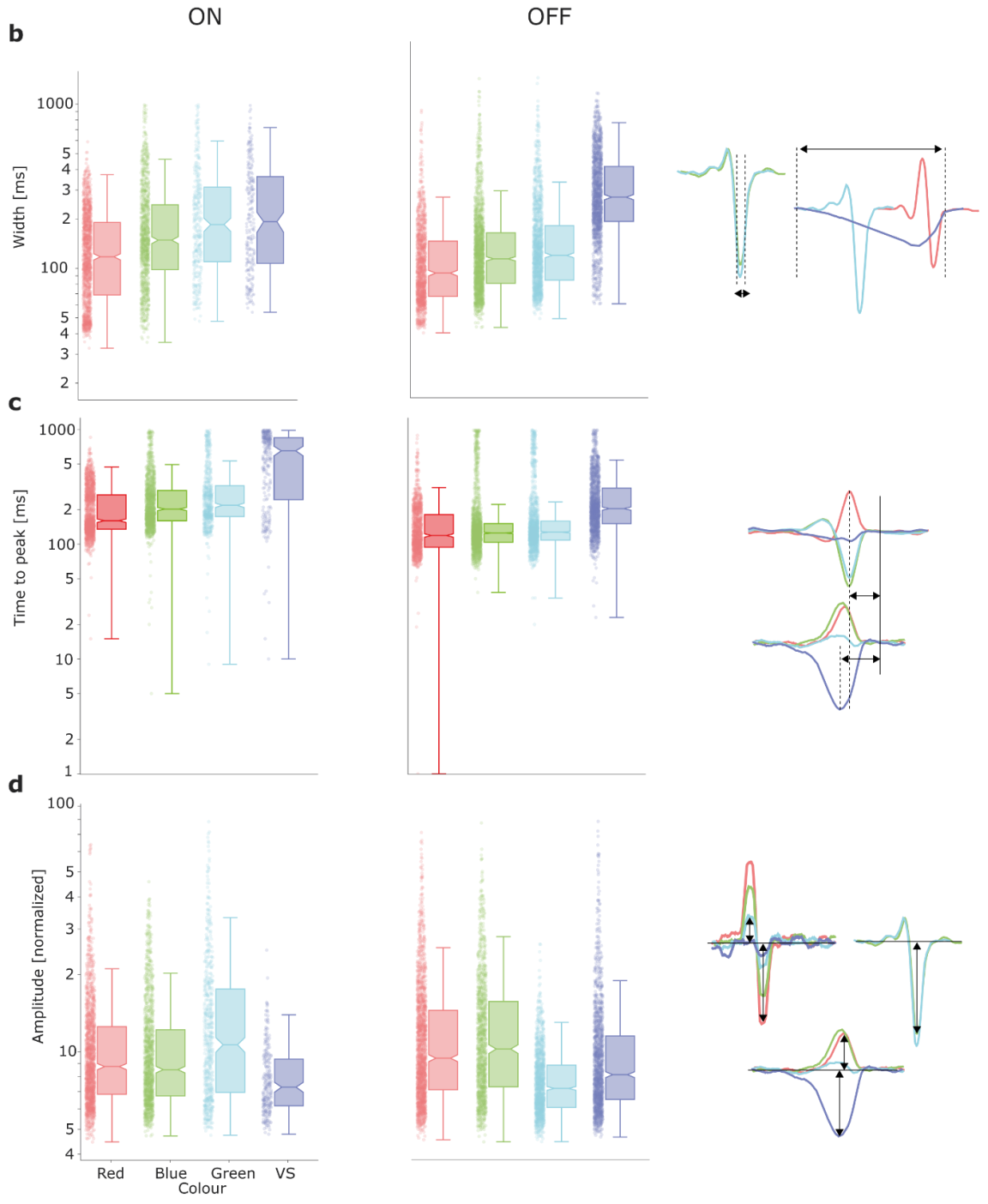
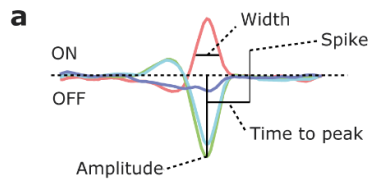


Figure 16 Full Field Colour Noise: general kernel properties.

a. Illustration of how kernel polarity, width, amplitude, and time to peak were calculated. Kernels that deflect down from the mean are OFF, kernels that deflect up from the mean are ON. The width was calculated as the full width at half maximum. The amplitude was calculated at the height of the peak above the mean. The time to peak was calculated as time from the peak of a kernel to the time of the spike.

b. Width of the kernels of all cells in the population, sorted by colour and ON and OFF. The width is an estimation of the speed of the integration time. ON responses had a higher width than OFF responses. For ON responses red (630nm) kernels were fastest and blue (420 nm) kernels were slowest. The integration time decreased with wavelength. The same as true for OFF responses, but the trend was less pronounced. However, OFF kernels at 420 nm were the slowest kernels, on average, they were twice as slow as kernels from any other colours.

c. Time to peak. The time to peak is another estimation of the integration time of a cell. It is the time after a given stimulus at which a spike is most likely triggered.

d. Amplitudes of the kernels in the population. This is an estimation of how strong a cell is driven by a stimulus. However, the relationship can be complex due to opponency. Different colours can inhibit each other and thus reduce the amplitude.

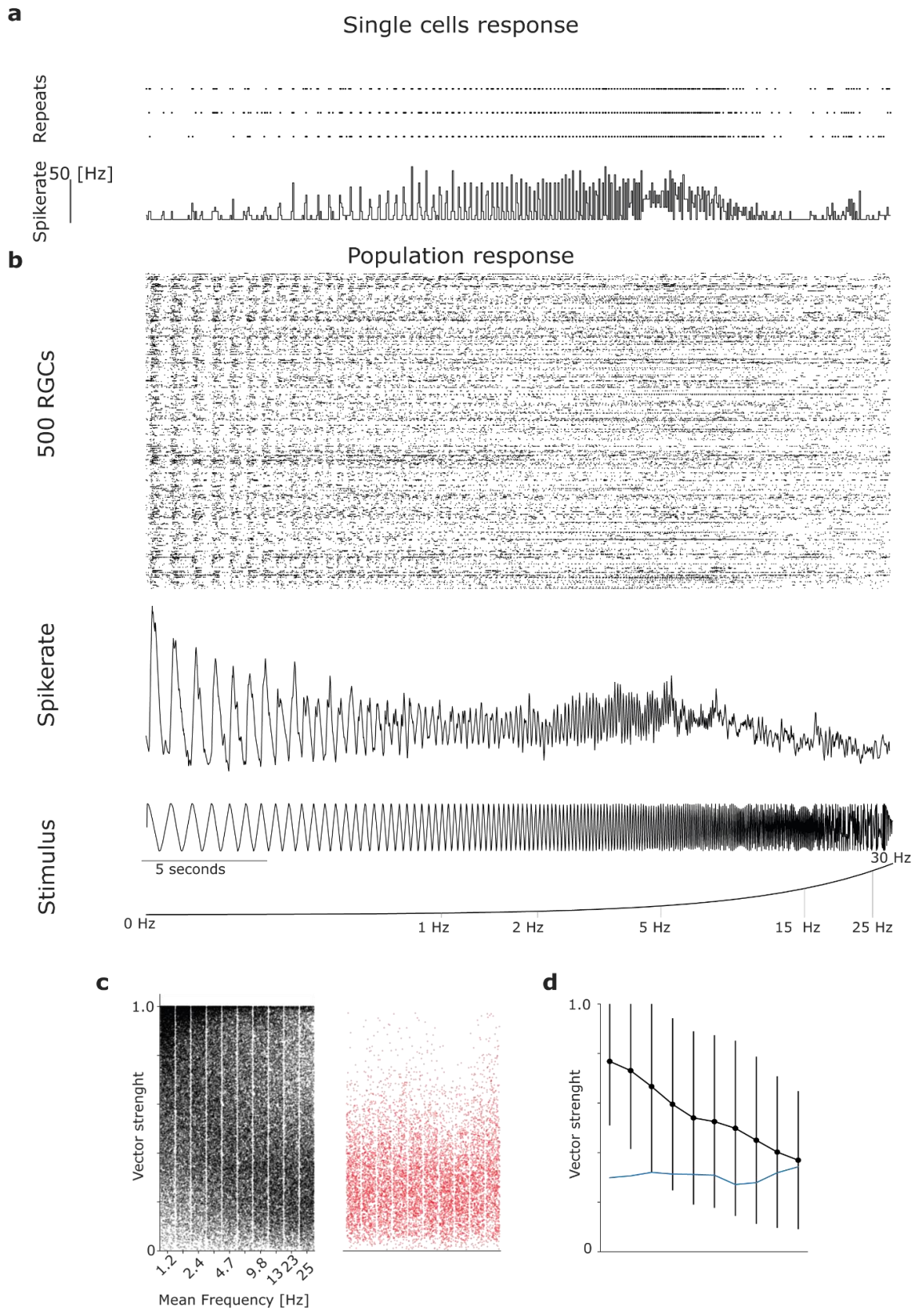


Figure 17 Chirp Responses Overview

a. Single cell response to the frequency chirp stimulus. The figure structure is like the one described for **Figure 11a**. Stimulus trace same as in **b**. This cell did not respond to the lowest frequencies but followed the stimulus up until 10 Hz.

b. Chirp response of 500 example RGCs. Structure of the figure is similar to **Figure 11b**. The Population responded well to low frequencies up to 5 Hz. Above 5 Hz the population response is harder to read, but spike rate stayed increased up until 25 Hz on population level. Two stimulus traces are presented. The first shows the chirp stimulus as a function of light intensity over time. The second shows the chirp stimulus as a function of frequency over time. Note, that the frequency increased exponentially. The duration of the whole stimulus was 30 seconds.

c. (Left) Phase lock analysis of the chirp responses for each cell in the population. The quality of the phase lock is represented as vector strength. 1 indicates that the spikes are 100% locked with the stimulus, 0 indicates no response. **(Right)** Phase lock of artificially created spike trains with random spiking patterns. Random spike trains have the chance to follow the chirp stimulus by chance thus creating vector strengths higher than 0. To test which vector strength would be expected for a non-responsive randomly spiking cell, 1000 randomly spiking cells were created. The mean vector strength of these artificial cells remained at around 0.2 on average. Thus, at a vector strength of 0.2 a badly phase locked cell is indistinguishable from a randomly spiking cell.

d. Vector strength of the population response plotted for ten different parts of the chirp stimulus. On population level, the vector strength was highest at the lowest frequencies and decreased exponential with increased chirp frequency (consider that the decrease looks linear, but the x axis is in log scale). Error bars indicate the standard deviation. The error was high at all parts of the stimulus, indicating a big variance of the vector strengths between cells.

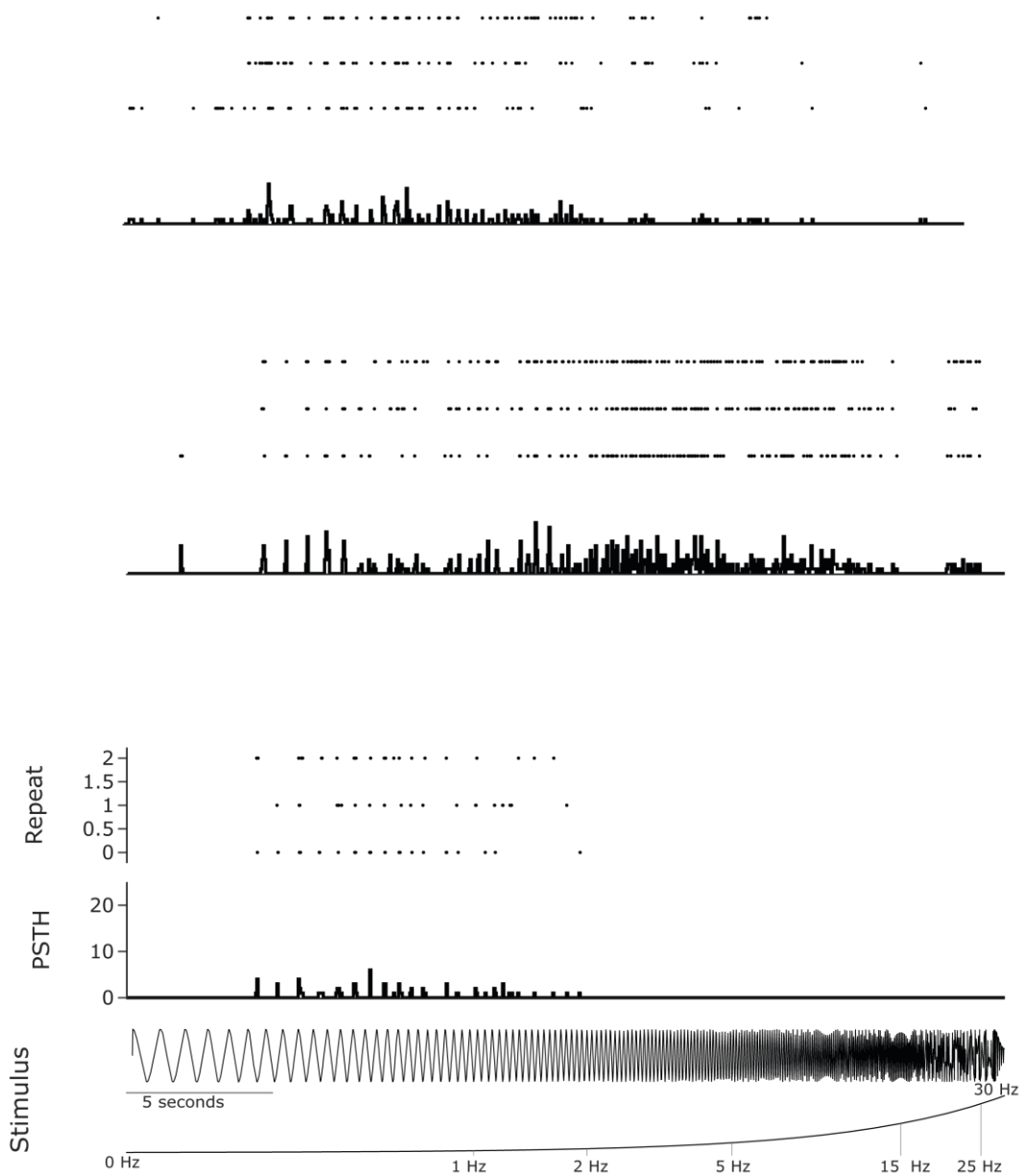


Figure 18 Chirp responses of single cells.

a. Figure structure like **Figure 12**. Shown are three cells that followed different parts of the chirp stimulus. Cell 1 followed low and medium frequencies but not high frequencies. Cell 2 followed low and high frequencies. Cell 3 followed only low frequencies. Stimulus trace similar as described in **Figure 17b**

CHAPTER 5: FUNCTIONAL RGC TYPES

SHORT SUMMARY

Identification of functionally distinct types of RGCs is key for the understanding how information is processed within the chicken retina. A Gaussian mixed modelling clustering approach returned 27 “functional types” of chicken RGCs. Clusters differed strongly in chromatic sensitivities and response kinetics. Most functional types showed complex time dependent integration of spectral information and colour opponent responses. Most functional types responded both to the onset and offset of stimuli, alongside a minority of more classical OFF clusters. Functional types with chromatic opponent responses show sensitivity to slow temporal contrast modulation while achromatic OFF types are sensitive to high temporal contrast modulation.

Photoreceptor input modelling revealed at least two major axes of chromatic opponency amongst RGC clusters: MWS versus LWS and SWS2 versus MWS. In contrast, responses in the minority of achromatic OFF clusters were consistent with non-opponent and dominant drive from long wavelength sensitive cones and/or double cones, potentially alongside more minor contributions from MWS cones. These results suggest that a large proportion of different functional RGC types in the chicken retina encode spectral information and might be used to convey spectral information to the brain, while a minority of achromatic circuits appears to track rapid temporal changes in the stimulus.

INTRODUCTION

In the previous chapter RGC population responses and single cells responses were described. General trends in RGC responses were summarized, but it was also shown that single RGCs might differ substantially from the population response. Therefore, identifying specific, functionally distinct types of RGCs is important to understanding how visual information is organized at the output level of the chicken retina. The way of classifying RGC types is subject of an ongoing debate. Traditionally, RGCs have been classified based on basic response characteristics, like ON vs OFF preferences (Hartline, 1938), based on morphology (Naito and Chen, 2004b), or based on molecular signatures (Farkas et al., 2004; Kölsch et al., 2021; Laboissonniere et al., 2019; Rheaume et al., 2018). Ideally, all three are combined (Goetz et al., 2021). Since each type of RGC encodes information about a specific feature of the visual scene, more recently RGCs were also classified based on their responses to specific sets of stimuli or based on responses in combination with genetic profiles using unsupervised clustering approaches (Baden et al., 2016; Farrow and Masland, 2011; Goetz et al., 2021; Hilgen et al., 2022, 2017a; Jouty et al., 2018). One advantage of a clustering approach is that it does not rely on pre-selecting arbitrary response

properties for categorization by hand. Rather, clustering identifies distinct high-density clouds of cell-types in a multi-dimensional space.

How many RGC types do different vertebrates have? 42 RGCs were found in the mouse retina based on a combination of molecular, anatomical and functional data (Baden et al., 2016; Goetz et al., 2021) while in the order of 30 were molecularly described in zebrafish. In primates, at least 17 different types have been described (Grünert and Martin, 2020).

Using transcriptomic profiling (Yamagata et al., 2021) identified 41 genetically distinct types of chicken RGCs which is comparable to the number of types found in the mouse, and notably about twice that of primates. Approximately in agreement, we know from morphological classifications of chicken RGCs that they display a sizable variety of dendritic tree sizes and stratification patterns in part depending on the position of the cell in the retina ((Naito and Chen, 2004b; Seifert et al., 2020), see general introduction). Based on this, a high number of different chicken RGC types can be expected, but the number of functionally different chicken RGC types and their function remains unknown: answering this question is one aim of this chapter.

Which RGC types exist in other vertebrates? In primates, five major types numerically dominate. By far the most numerous are On and Off midget RGCs. They show sustained responses to continuous illumination and stochastic chromatic opponency between red cone and green cone inputs based on random outer retinal wiring (Crook et al., 2011; Field et al., 2010; Grünert and Martin, 2020). In the primate fovea, they establish a 1:1:1 pathway between (red or green) cones, BCs and RGCs, providing high spatial resolution. Second most common are On and Off parasol RGCs which exhibit transient responses to sustained contrast changes, and which readily follow temporal flicker up to several 10s of Hz (Grünert and Martin, 2020).

Third most common are small bistratified cells. This type shows opponency between blue cone ON signals and yellow OFF signals (red and green cone signals combined) (Dacey and Lee, 1994) and famously projects to the koniocellular layer of the LGN where it provides the probably dominant spectral channel underpinning primate blue-yellow colour vision

The mouse retina has more types of RGCs than the primate retina. They can be broadly categorized into types that are OFF, slow ON, fast ON or ON OFF sensitive and further into more specific subtypes. Some types encode for very specific information of the visual scene. Perhaps most notably, mice possess seven types of direction selective RGCs, alongside probably three types of orientation selective RGCs (Sun et al., 2006; Weng et al., 2005). No cells with such response profiles are known to exist in primate.

In summary, different RGC types process different types of visual information like contrast, colour, and motion. Their responses commonly differ in polarity (ON vs OFF), kinetics (sustained vs transient) and colour opponency (for example red vs green), as well as a profusion of properties linked to the encoding of space. While many RGC types encode broad features of visual stimuli, like contrast information, others may encode for very specific stimuli like specific forms of motion.

How is chromatic information encoded in chicken RGCs?

Two hypotheses seem plausible. First, all different input channels (i.e. cones) could get their own primate like midget pathway, i.e. a “private line”. This would predict the existence of several RGC types that display spectral responses consistent with individual cone types, which may be opsin shaped, or indeed already opponent based on outer retinal processing as in fish. In any case, this would predict that RGCs differ notably in the overall spectral tuning. Notably, already from known BC connectivity with cones showing that no cone has a private line (Günther et al., 2021), this model seems unlikely. Second, it is possible that signals from different input channels will be much more integrated with each other and thus most chicken RGC types resemble the primate small bistratified type. This would then be further promoted by the complexity of the stratification of chicken RGCs. (Naito and Chen, 2004b) showed that many chicken RGCs show large dendritic trees that project to multiple layers of the inner plexiform layer potentially receiving input from ON and OFF pathways. Consistent with this second model, and as described in (*Chapter 4: General RGC responses*), most RGC in the chicken retina are sensitive to both ON and OFF stimulation.

Here I used an unsupervised clustering approach to identify types of chicken RGCs based on their responses to four different stimuli. My findings show that chicken RGC types differ strongly in their response kinetics and the chromatic information they encode, showing at least four types of chromatic opponency responses. However, despite a profusion of nuanced differences that lead to these opponencies, their overall spectral shapes are remarkably homogeneous. In addition, specific achromatic RGC types for fast temporal contrast coding exist.

RESULTS

PART 1: FUNCTIONAL RGC TYPES

Cell responses were clustered using a Gaussian mixed model clustering algorithm (methods). The clustering was performed based on responses to chromatic full field flashes, “white” flashes, and frequency chirp or response kernels (full field chromatic binary noise). The initial clustering was intentionally set up to find more clusters than predicted based on Bayesian information

criterion (BIC). This was done to avoid “under – clustering” which could result in overlooking small but important clusters.

The clustering was set to find 100 different clusters. In a second step, clusters were thereafter recombined by hand based on similar average response properties. Through this, the initial 100 clusters were condensed to 35 clusters, of which eight comprised fewer than five cells and were discarded from further analysis, yielding a total of 27 remaining clusters. One additional cluster was removed from the analysis because it contained no meaningful responses to any of the stimuli. Thus 26 clusters were considered for further analysis (in the following referred to as functional RGC types).

Figure 23 shows the mean responses of all 100 initial clusters and the average responses of the resulting 35 clusters after recombination.

RGC clusters differed strongly by the number of cells they contained. The largest cluster contained 557 cells and the smallest seven cells. The first four types contained almost 50% of cells in the population and the first ten RGC clusters accounted for about 80% of the population (**Figure 20 b**). Not all 26 clusters were present in all recordings, but cells contributing to the ten largest clusters were found in all recordings (**Figure 20 a & c**).

FUNCTIONAL RGC TYPES SHOW LITTLE VARIATION IN RESPONSE POLARITIES AND KINETICS BUT STRONG VARIATIONS IN CHROMATIC SENSITIVITIES

Most individual chicken RGCs showed both ON and OFF responses (*Chapter 4: General RGC responses*). Consequently, most cluster also showed ON-OFF responses. Since functional RGC types are traditionally sorted into OFF, ON-OFF and ON types, all 26 functional RGC types were sorted from OFF dominant via ON OFF to ON dominant and are presented in (**Figure 22**) in this order (based on comparison between ON and OFF mean chromatic response amplitudes). Of these, only two functional RGC types (C1 and C2) showed stronger OFF than ON responses and resembled classical OFF Functional RGC types. Seven functional RGC types were ON types. The remainder displayed ON-OFF responses.

Moreover, only three functional RGC types were sensitive to frequency modulation above 3 Hz. The most notable differences between functional RGC types were their spectral tuning curves of ON responses and the polarities of their response kernels. Understanding similarities and differences between all 26 clusters can be challenging, therefore the ten functional RGC types containing the most cells as well as four additional hand-picked functional RGC types with interesting properties will be described in detail in the following.

THE FIRST TEN FUNCTIONAL RGC TYPES DIFFER STRONGLY IN THEIR ON STEP RESPONSES OVER DIFFERENT WAVELENGTHS

Responses to chromatic ON steps differed more between functional types than OFF responses (**Figure 20 a**). These differences were most apparent at wavelengths below 630 nm. All but two of the first ten functional types had strong ON responses at 630 nm. In contrast, only two of these functional types had equally strong ON responses at 505 nm, another two had medium responses, and the remaining had weak responses. In all first ten clusters, ON responses at 480 nm were weaker than ON responses both at 505 nm and 420 nm, following the trend described in (*Chapter 4: General RGC responses*). Responses at 420 nm varied strongly between types. Some had maximum responses at this wavelength, others had almost no response. In summary, the ON step tuning curves of some functional RGC types were considerably different to the mean

tuning curve of the average population response of all cells as presented in (*Chapter 4: General RGC responses*). The main differences between population response and responses of some functional types were seen at the shorter of the tested wavelengths: 560 nm, 505 nm, and 420 nm.

In contrast to “colour” step responses, “white” step responses followed very similar trends in all first ten types: The response amplitude decreased with decreasing stimulus contrast. A small nonlinearity existed in some functional RGC types and eight of the first ten functional RGC types had strongest OFF responses at 90% contrast rather than 100%.

The ON vs OFF response dominance differed between functional types and was dependent on the wavelength. None of the first ten types had strong OFF responses at 420 nm, while at other wavelengths, functional types differed in their ON and OFF dominance (**Figure 20 c**). “White” step ON and OFF dominance differed between functional types as well (**Figure 20 d**).

SEVEN OUT OF THE FIRST TEN FUNCTIONAL TYPES SHOW CHROMATIC OPPONENCIES

Seven out of the first ten functional types had chromatic opponent responses when presented with full field chromatic noise stimulus (**Figure 21**). (*Chapter 4: General RGC responses*) described different subtypes of the five most common STA kernel types in the population identified by comparing kernel amplitude and polarity for each wavelength. Seven out of the first ten functional had five of the different subtypes described in (*Chapter 4: General RGC responses*) (complex opponency: cluster 13, 24, 5; achromatic OFF: cluster 1; red vs green: cluster 7; green vs blue: cluster 4). Notably, the most common functional type (cluster 7) had strong chromatic opponency: red ON vs green OFF while most other types had opponencies between blue OFF cyan ON stimulation (**Figure 21**).

ONLY TWO ON FUNCTIONAL RGC TYPES WITHIN THE FIRST TEN FUNCTIONAL RGC TYPES

Functional RGC type 20 and 16 were the only functional RGC types that had low sensitivities to OFF stimulation (**Figure 20**). Functional RGC type 20 was most sensitive to ON steps at 630 nm while functional RGC type 16 was most sensitive to ON steps at 420 nm. functional RGC type 16 did not show responses to “white” ON or OFF steps at different contrasts.

ONLY ONE ACHROMATIC FUNCTIONAL RGC TYPE EXISTS WITHIN THE FIRST TEN FUNCTIONAL RGC TYPES

Functional RGC type 1 was the only of the first ten functional RGC types that had stronger OFF responses than ON responses to chromatic stimuli and “white” step stimulation (**Figure 20**). A strong OFF response was also present in red, green, and cyan response kernels. The red kernel had the biggest amplitude, and the amplitude of the other kernels decreased with decreasing wavelength.

GREEN ON FUNCTIONAL RGC TYPES

Functional RGC type 21 had sustained ON responses to chromatic and achromatic full field stimulation (**Figure 20**). Interestingly, light stimulation at 505 nm triggered the strongest ON responses, followed by stimulation at 560 nm and 630 nm. In contrast, light responses at 480 nm were weak. Functional RGC types with strong responses to stimulation at 505 nm were often more sustained than Functional RGC types that did not show strong responses at 505 nm (also see functional RGC types 19, 21, 22, and 25).

BLUE ON FUNCTIONAL RGC TYPES

Functional RGC type 26 was the only functional RGC type that did not respond to light stimulation at 630 nm and only responded to ON steps at 420 nm (**Figure 20**). “White” ON or OFF steps did not trigger any responses.

FUNCTIONAL RGC TYPE WITH OSCILLATING RESPONSES

Functional RGC type 8 had strong ON responses over all wavelengths and strong OFF responses to stimulation above 420 nm (**Figure 20**). It also responded to “white” ON and OFF steps. This functional RGC type had interesting response kinetics. After the peak of the initial response, the spike rate decreased to zero at about 200 ms after the stimulus onset. After this initial decrease, the spike rate increased again and reached another peak about 200 ms to 300 ms after the initial peak. This was consistent across all wavelengths and was also present in responses to “white” light. However, in case of “white” light stimulation, the peak of the second response was delayed by about 500 ms relative to the peak of the initial response.

LONG AND MEDIUM WAVELENGTH SENSITIVE OFF FUNCTIONAL RGC TYPE

Functional RGC type C2 shared many features with functional RGC type C1 (**Figure 20**). It had stronger OFF responses to light stimulation above 420 nm and to “white” step stimulation. The response kernels of this cluster were complex. Red, green, and cyan response kernels were biphasic ON OFF while the blue kernel was monophasic OFF. In addition, red kernels were faster than green and cyan kernels. Both types had fast red kernels, when compared to other functional RGC types.

CHROMATIC FUNCTIONAL RGC TYPES ARE SENSITIVE TO LOW FREQUENCIES

The frequency tunings of first ten functional RGC types had interesting differences (**Figure 20** and **Figure 21**). The average vector strength (as described in Chapter 4: General RGC responses and the methods section) was calculated for each functional RGC type. Seven out of the ten functional RGC types had strongest phase lock with the chirp stimulus at low frequencies below 3 Hz and the vector strength decreased with increasing chirp frequency. All these seven functional RGC types had chromatic opponent kernels (**Figure 21**).

On contrary, classical OFF Functional RGC types (functional RGC type 1 and 2) had high vector strengths over all frequencies of the chirp responses and peak vector strengths at 7 Hz and 5 Hz respectively.

In accordance with the observation that most functional RGC types were sensitive to low temporal frequencies, most functional RGC types did not show increased spiking rates at higher chirp frequencies. Only the two achromatic OFF functional RGC types had a high spiking rate throughout the chirp stimulus and reached peak spiking rates at a chirp frequency of 12.5 Hz (see *Chapter 6: Response Shapes*).

ADDITIONAL GENERAL OBSERVATIONS

While on population level 480 triggered weaker responses than at 420 nm and/or 505 nm, seven functional RGC types (3, 8, 10, 11, 15, 19 and 25) had ON responses with similar amplitude at 480 nm at 420 nm and/or 505 nm. Most of these functional RGC types responded to ON steps at all tested wavelengths (**Figure 22**).

Some functional RGC types had ON responses at 505 nm at similar amplitude than ON responses at 560 nm. 14 functional RGC types had this trend (2, 3, 4, 8, 9, 10, 11, 12, 13, 15, 19, 21, 22 and 25), (**Figure 22**).

Few functional RGC types had no or only weak responses to full field stimulation at 560 nm (7, 18, 26), (**Figure 22**).

Most functional RGC types had ON and OFF responses when stimulated with “white” light. However, seven functional RGC types (1, 2, 7, 16, 18, 23 and 26) had no or only weak responses to ON steps. Functional RGC type 7 is of particular interest since it did not show strong ON responses at 630 nm and 420 nm but weak ON responses to “white” light, (**Figure 22**).

Eight functional RGC types (6, 9, 10, 16, 18, 23 and 26), (**Figure 22**), had weak or no OFF responses when stimulated with “white” light at different contrasts. These eight clusters could be sorted into three groups based on their responses to chromatic full field stimulation. The first group contained clusters that show strong ON responses at 420 nm but weak responses at all other wavelengths. The second group contained functional RGC types that had strongly sustained ON responses that did not fully return to baseline at the onset of the OFF step. The third group contained functional RGC types that only respond to light stimulation at 630 nm and 560 nm.

Eight functional RGC types (6, 9, 10, 12, 19, 21, 25, and 26), (**Figure 22**), did not show any responses to the frequency chirp stimulus. Interestingly, of those clusters, only functional RGC

type 6 had a meaningful STA kernel. Generally, functional RGC types without chirp responses had either very sustained ON responses to full field stimulation or were not sensitive to light stimulation at 630 nm.

Another group of seven functional RGC types (7, 11, 16, 17, 18, 20 and 23) (**Figure 22**), did respond to chirp stimulation but did not follow chirp frequencies above 1 Hz.

In summary, most functional RGC types responded to ON and OFF and only few functional RGC types responded only to ON or OFF stimulation. ON responses varied strongly between functional RGC types depending on the wavelengths of stimulation, while OFF responses were more uniform across functional RGC types. Many functional RGC types only responded to very low frequencies (<3 Hz) while only a few clusters had strong responses over the whole frequency range of the chirp.

PART 2: PHOTORECEPTOR INPUTS

LINEAR MODEL

In the first part of this chapter, 26 functionally diverse functional RGC types were described. A large proportion of these functional RGC types show differences in their response tuning curves to chromatic stimulation and chromatic opponent kernels when stimulated with chromatic full field noise. Summarized: One of the main functional differences of different RGC lies in their differential chromatic sensitivities. Which input channels contribute to chromatic opponent responses in these functional RGC types? To answer this question, I modelled RGC responses by linear combination of input channels based on the known opsin expression of each cone-type.

RESULTS

The number of photoisomerization was calculated for single cone opsin and each LED under consideration of LED powers (**Figure 24 a**). Assuming a linear correlation between the number of photoisomerization and response amplitudes of RGCs, example tuning curves were modelled for cases in which RGCs get single inputs from either LWS, MWS, SWS2 or SWS1 cones, (**Figure 24 b**). In a next step, inputs from multiple cones were linearly combined (addition or subtraction) to simulate functional RGC types that sum inputs from multiple cone types or combine excitatory and inhibitory inputs (**Figure 24 b**) (example: LWS cone + MWS cone). A search algorithm was set up to identify linear cone input combinations that result in tuning curves that match experimentally derived tuning curves. The goodness of the model was calculated as the absolute difference between the normalized modelled tuning curve and the normalized tuning curve derived from real data. **Figure 24 c** shows tuning curves of the first ten functional RGC types and handpicked four functional RGC types together with the modelled tuning curves.

In general, the linear combination of photoreceptor inputs let to surprisingly good models of experimentally collected tuning curves. The mean goodness of fit was 0.8 (range 1 (best fit) -0 (worst fit), std =0.2). By modelling tuning curves for each functional RGC type, photoreceptor contributions to each functional RGC type were identified (**Figure 24 c**).

The majority of functional RGC types shared similar photoreceptor inputs for ON responses. Out of the first ten functional RGC types, the modelled SWS2 cone provided inhibitory inputs in eight cases. In six out of these eight cases, modelled SWS1 photoreceptors and MWS photoreceptors provided excitatory inputs. This would suggest that the majority of functional RGC types have two chromatic opponency axes: SWS1 inputs vs SWS 2 inputs and SWS2 inputs vs MWS and/or LWS inputs, (**Figure 25**). Notable exceptions from this trend exist. The most abundant functional RGC type did not get inhibitory inputs from modelled SWS 2 cones but from modelled MWS cones resulting in opponent inputs between SWS 1 and 2 vs MWS and LWS vs MWS. Functional RGC type 26 was a classical long wavelengths vs short wavelength opponent functional RGC type, receiving excitatory inputs from SWS 1 and SWS 2 and inhibitory signals from MWS and LWS. Functional RGC type 21 was MWS vs SWS1 and SWS 2 opponent. The tuning curves of some functional RGC types could be explained by single photoreceptor input. For example, the spectral response shape of functional RGC type 20 is consistent with a near exclusive drive from LWS inputs.

For OFF responses, two different general trends were observed. SWS 2 was the main provider of inhibitory inputs as is the case for ON responses. However, in many functional RGC types, SWS1 did not provide strong inputs, resulting in chromatic opponency over a single axis: LWS+MWS – SWS2 inputs. A second input weighting was common, which does not rely on inhibitory inputs: Combination of LWS and MWS inputs (functional RGC type C1 & C2).

DISCUSSION

FUNCTIONAL RGC TYPES

26 functional RGC types encoding distinct features of visual information were segregated by performing a Gaussian mixed model clustering and concurrent recombination of clusters by hand. Based on morphological studies (Yamagata et al., 2021) and under consideration that cells were only tested using full field stimulation (see *Chapter 4: General RGC responses discussion*), identification of 26 different Functional RGC types likely underestimates the full diversity. It is likely that additional functional types will emerge upon expansion of the tested stimulus battery.

In primates, five different types account for a large majority of all RGCs (Grünert and Martin, 2020). Most numerous are On and Off midget RGCs which have small receptive fields and sustained responses, and some show colour opponent centre surround responses based on random outer retinal wiring (Dacey, 1993). They provide the brain with information about contrast in the visual scene at high spatial resolution and are thought to centrally underpin our ability to differentiate “greens” from “reds”. Functionally similar types (beta cells) are found in the cat retina (Enroth-Cugell and Robson, 1966; Peichel and Wässel, 1981) but since cats lack the LWS duplication that leads to primate trichromacy, they are generally not thought to be spectrally informative in this case. (Zhang et al., 2012) Moreover, cat RGCs are poorly understood, and drawing direct parallels seems premature. No clear counterpart of midget RGCs has been found in mice, although several particularly small RGCs are functionally reminiscent, but nowhere near as abundant as they are in primate. Based on this, it seems that as far as we know, a true midget like pathway remains unique to primates. (Zhang et al., 2012) Do chicks have a midget-like RGC circuit?

A direct comparison is challenging. The most common functional RGC type (C7) found in this study had chromatic opponent responses between short and long wavelength stimulation, which is not a common feature for a midget RGC. Unfortunately, it was not possible to measure the receptive field size of these cells. Since small receptive field size is a key feature of midget cells, comparison is difficult. Further complicating comparison is the fact that functional RGC types did not differ strongly in terms of how sustained or transient their responses are. In primates, midget cells show strongly sustained responses in contrast to parasol cells which show transient responses. Chicken RGCs types cannot be distinguished in a similar way. The most chicken like functional RGC type in primates is the small bistratified RGC. It shows ON OFF responses to white light stimulation (Cowan et al., 2020; Reinhard and Münch, 2021) and more complex chromatic opponency between red+green cone and blue cone inputs. Since the chicken’s retina has more input channels than any mammalian retinas it might not be surprising, that most chicken functional RGC types resemble primate small bistratified types.

Complex integration time differences between ON and OFF and chromatic responses, one of the main distinctions of chicken functional RGC types, has not been noted as distinguishing feature of primate, cat or mouse functional RGC types. In the turtle, which has the same number of input channels as chicken, 12 different types of chromatic opponent ganglion cell types have been suggested based on random single-unit sampling (Rocha et al., 2008). Multiple chromatic functional RGC types have also been identified in the zebrafish retina (Zhou et al., 2020). While this chapter presented less than 12 different functional RGC types with chromatic opponent

responses, most types did present chromatic opponency and only few types show achromatic responses. In addition, many RGCs had complex chromatic opponent responses.

Chromatic processing likely becomes more and more complex with increasing number of input channels. Morphological findings support this hypothesis. Commonly, ON OFF and ON-OFF functional RGC types are morphologically separated by their projection pattern in the IPL. For example, primate midget cells are monostratified and project to either the ON or OFF layer within the IPL. In contrast, small bistratified cells project to both ON and OFF layers. Many chicken RGCs show very complex stratification patterns (Naito and Chen, 2004b, 2004a; Seifert et al., 2020) and project to multiple different layers within the IPL. The findings presented in this chapter, in combination with morphological findings confirm that a large proportion of chicken RGC receives complex ON and OFF inputs. However, monostratified cells do exist and so do pure ON and OFF cells. The density of RGC in the chicken eye is not uniform and cell density increases in the area centralis and a dorsal area of high acuity (Morris, 1982). RGC at the periphery have larger dendritic trees and thus likely larger receptive fields. Recordings in this study were performed exclusively in the dorsal part of the retina and it is possible that the ratio between ON and OFF and ON OFF cells changes in the area centralis where monostratified RGC exist. Retinal specialization is a common feature among vertebrates (for example the fovea in humans (Yan et al., 2020) or the “strike zone” in zebrafish (Zimmermann et al., 2018)). It remains to be shown, how different areas of the chicken retina differ in their electrophysiology.

CHROMATIC FUNCTIONAL RGC TYPES

In (*Chapter 4: General RGC responses*) spectral tuning curves for ON and OFF responses of the whole population were presented. It was shown that the ON responses resulted in more complex tuning curve over wavelength than OFF. It was also noted that strong variations between different cells exist. By identifying functional RGC types based on response properties, it was possible to show that notable differences in chromatic tuning curves exist between different functional RGC types. Summarized, ON tuning curves of functional RGC types fall into one of four different groups:

1. Functional RGC types that respond exclusively to short wavelength stimulation
2. Functional RGC types that respond exclusively to long wavelength stimulation
3. Functional RGC types that respond indifferent of the wavelength of stimulation
4. Functional RGC types that show complex wavelength dependent responses

By far the most functional RGC types belong to group 4. One theme in this group is particularly common: Tuning curves reveal stronger responses at 630 nm and 420 nm and weaker,

differential responses in between these two wavelengths. One common theme is that responses at 480 nm tend to be weak. The reason for this was revealed by modelling the likely photoreceptor contributions for each functional RGC type. In the most common functional RGC type (C7), modelled MWS cone inputs provide inhibitory, while SWS2 cones and LWS cones provided excitatory inputs. This explains a weak response at 480 nm and 505 nm. In contrast, many other functional RGC types receive inhibitory inputs from SWS2 cones and excitatory inputs from SWS1 and MWS. This also leads to weak responses at 480 nm.

Functional RGC type C26 belongs to group 1 and shows only responses to stimulation at 420 nm. Interestingly, photoreceptor input modelling revealed that this functional RGC type likely receives excitatory inputs from SWS 1 and SWS2 cones but inhibitory inputs from MWS and LWS cones. In other words, this functional RGC type is a classical long vs short wavelength opponent type. Despite the fact, that this type receives excitatory inputs from SWS 2 cones, responses at 480 nm are weak. Taken together, this reveals one major finding: 480 nm responses are weak on population level, because many functional RGC types receive opponent inputs from MWS cone and SWS 2. The nature of that opponency may differ (MWS and SWS2 may provide inhibitory or excitatory inputs respectively and vice versa). No functional RGC type seems to combine inputs from MWS cones and SWS 2 cones. Pure ON cells exist which receive inputs from all cones, including MWS and SWS 2 but those show no chromatic opponent responses.

Few functional RGC types belong to group 2. Exclusive long wavelength responses either rely solely on LWS cone inputs (for example functional RGC type C 20) or require complex input interactions. This is because tuning curve models predict that 630 nm responses should be stronger than 560 nm responses if only LWS cone inputs are provided. Most functional RGC types with exclusive long wavelength responses show stronger 560 nm responses than 630 nm responses, which would require additional MWS inputs. However, because 480 nm responses in these functional RGC types are often weak, this would also require inhibitory inputs from SWS 2 cones because otherwise the model would predict strong responses at 480 nm provided via MWS cone inputs (For example functional RGC type C17). A special case is functional RGC type C 21 as the model predicts that it receives excitatory MWS cone inputs but no LWS inputs.

The third group is rarer and is not represented within the first ten functional RGC types. However, a few smaller functional RGC types exist that show ON responses independent of wavelength. Photoreceptor input modelling suggests that these types receive equal inputs from all cones (functional RGC type C8).

Surprisingly, the model predicted that many OFF responses are constituted by more complex input interactions than expected based on tuning curves alone (see *Chapter 4: General RGC responses*). This is for the same reason as explained for group 2. Sole LWS cone inputs predict stronger 630 nm responses than 560 nm responses, but most functional RGC types show stronger 560 nm responses than 530 nm responses. It is possible, that LWS cone inputs are not linear, and provide maximal responses at 560 nm rather than 630 nm since 560 nm is close to the peak sensitivity of the LWS opsin. Assuming nonlinear LWS inputs, OFF response tuning curves could likely be explained by LWS inputs alone, but this remains to be tested.

Functional RGC type C2 is “special” in far as its OFF response can be explained simply by a summation of excitatory LWS and MWS inputs.

STA Kernels received from full field chromatic noise stimulation often show chromatic responses that contradict chromatic full field flash responses and thus modelled photoreceptor inputs. The reason for this remains unclear but is likely due to the different nature of the stimulus, as described in the discussion of (*Chapter 4: General RGC responses*). Undoubtedly, a more sophisticated input model is needed to explanation of functional RGC type responses over different stimuli.

Taken together, the data presented in this chapter suggests that four major types of chromatic opponency exist (within the ten biggest functional RGC types and four addition picked types):

Table 4 Most common types of chromatic opponencies and their modelled inputs as displayed by functional RGC types.

	SWS 1 cone	SWS 2 cone	MWS cone	LWS cone
Opponency 1	+	+	-	+
Opponency 2	+	-	+	+
Opponency 3	+	+	-	-
Opponency 4	-	-	+	+

In addition, some smaller functional RGC types show additional types of chromatic opponency.

LIMITATIONS

It is likely that some of the identified functional RGC types will contain more subtypes, which encode information about more specific visual stimuli like movement, visual patterns or more specific stimuli that drive distinct chicken behaviours. Future studies could focus on identifying receptive field sizes and motion or direction selective functional RGC types.

Some of the kernel types that were identified in (*Chapter 4: General RGC responses*) don't show up in any functional RGC type presented in this chapter. This is likely because despite over-clustering, cells with rare kernel shapes got mixed up into bigger clusters. Therefore, both results presented here and in *Chapter 4: General RGC responses* must be considered for a complete picture of existing kernel types.

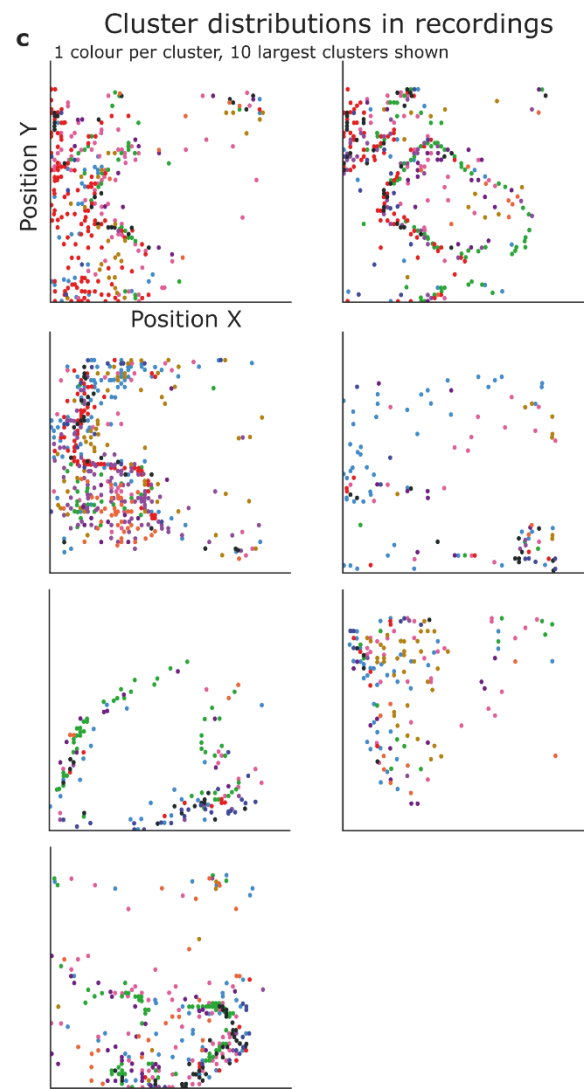
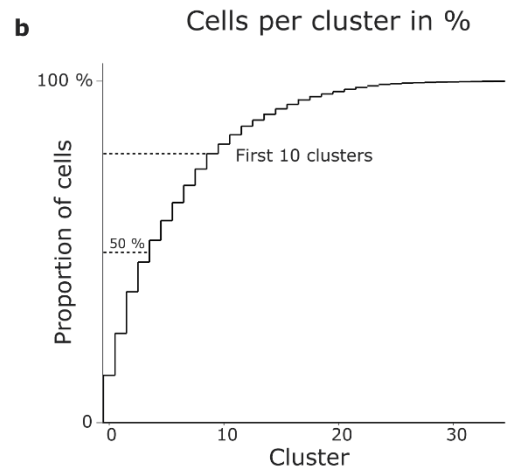
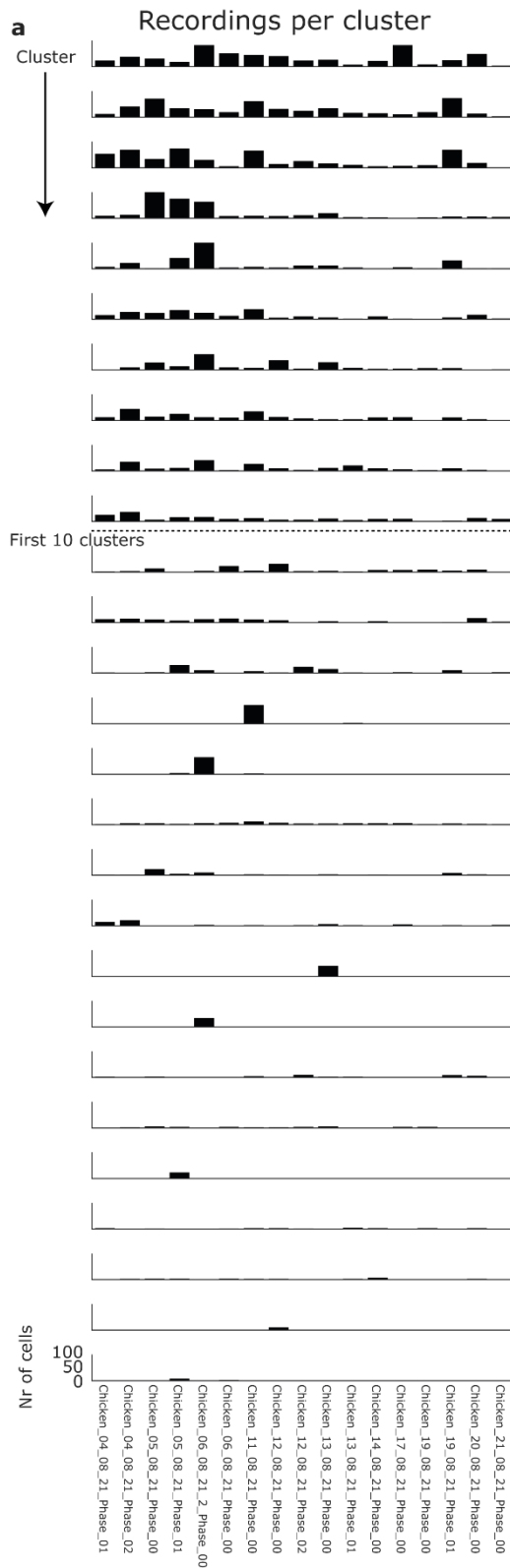


Figure 19 Basic clustering statistics. a. Overview over the proportion of recordings and the number of cells per recording that contribute to a cluster. All recordings contribute cells to the first 12 clusters. For clusters >12 sometimes only a few recordings contribute.

b. Number of cells per cluster, plotted as an accumulative histogram. The first four clusters contain almost 50% of all cells in the dataset. The first ten clusters contain 80% of all cells.

c. Location and spread of clusters across the multielectrode array. Shown are eight example recordings. Some clusters are in a denser less equally distributed fashion, while others seem to be organized in some sort of mosaic. In some recordings, a specific area of the chip contains most of the responsive cells.

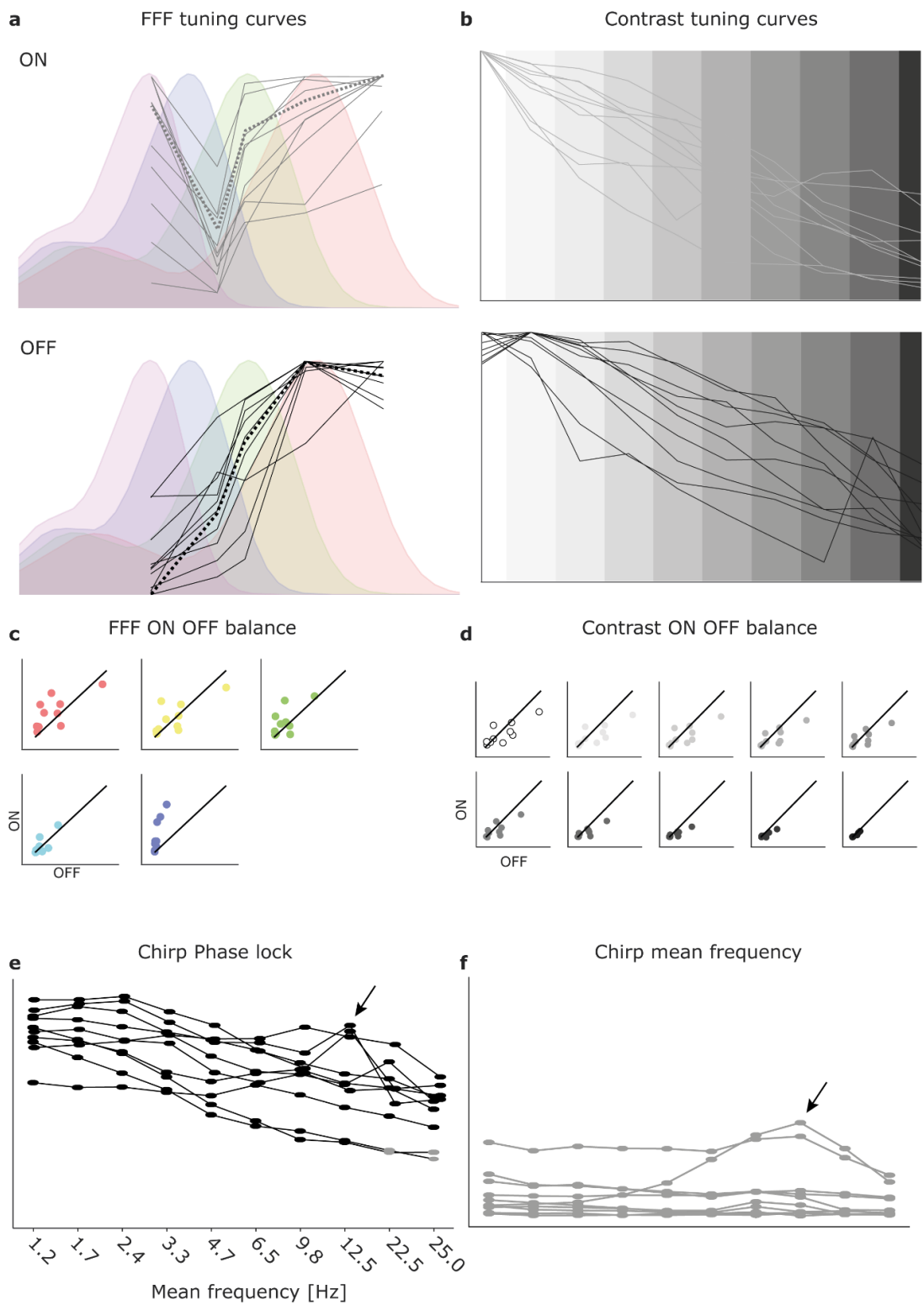


Figure 20: General response properties of the ten biggest clusters.

a. Tuning curves of ON (top) and OFF (bottom) responses plotted relative to chicken opsins (black and grey solid lines) and population response averages as comparison (dashed lines). The traces for ON and OFF responses are each normalized to maximal responses. Interestingly, ON tuning curves differ much more between clusters and from the average than OFF tuning curves. OFF tuning curves of all ten clusters were similar to the average population response and followed the same trend described in (*Chapter 4: General RGC responses*) (the amplitude of the response decreased with increased distance of the stimulation wavelength from the wavelength of the LWS peak sensitivity). There were two main axes of variations in ON responses. The first axis was at 505nm (the peak of the MWS opsin). Some clusters had strong ON responses at 505 nm while other had weak responses at that wavelength. The second axis was found at 420 nm. Some clusters responded strongly to ON stimuli at 420 nm (and 630 nm) while other barely responded at all.

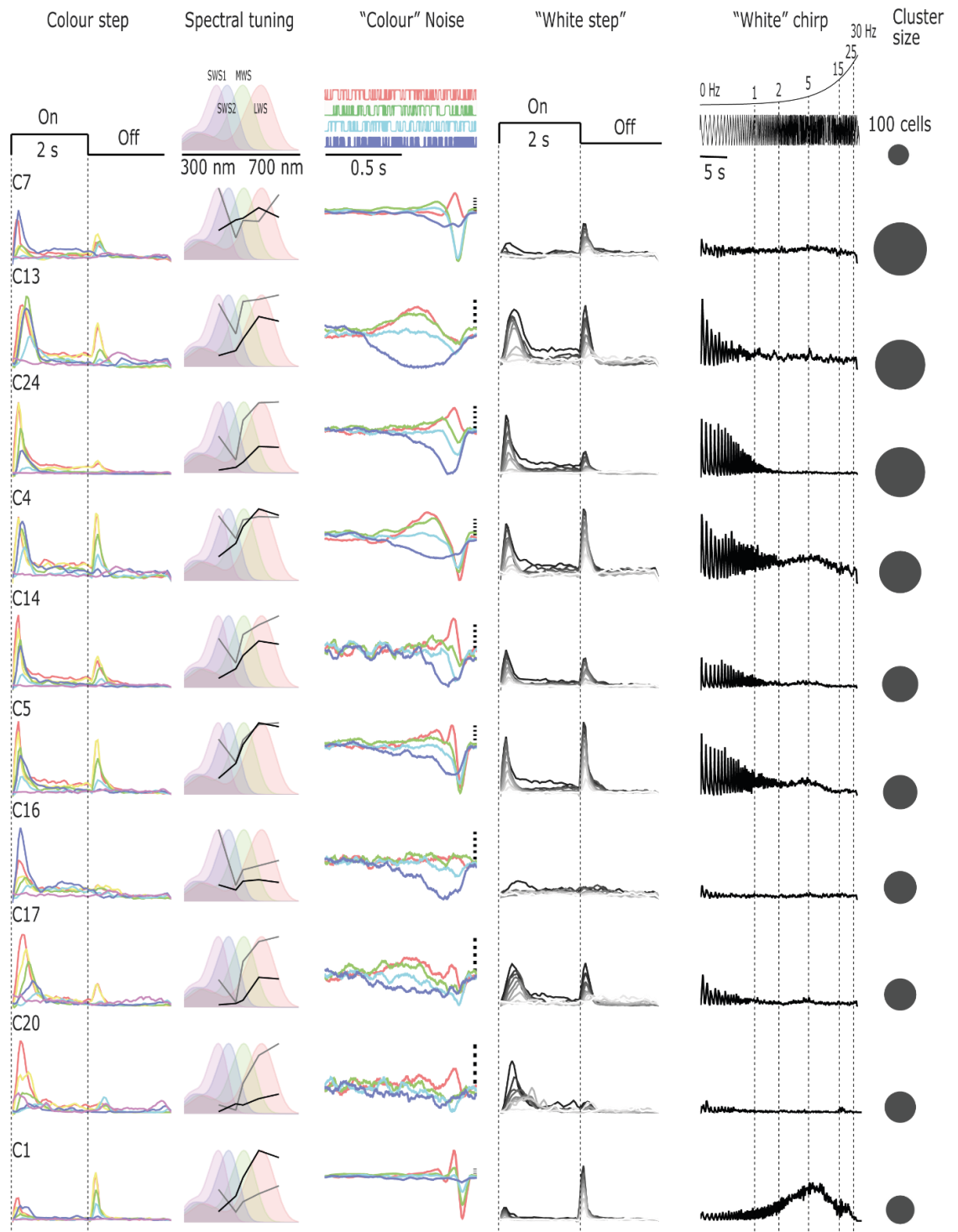
b. Tuning curves of ON and OFF “white” steps at different levels of contrast. ON and OFF responses were each normalized to the maximal response. The amplitudes of all clusters were correlated positively with the contrast of the stimulus. However, for OFF stimuli, the peak sensitivity of most clusters was reached at 90% contrast and not 100 % contrast.

c. Amplitude of ON responses (y axis) plotted as function of the amplitude of OFF responses (x axis) for the ten biggest clusters. Responses at 630 nm and 420 nm were more ON dominant while at 560 nm, 505 nm, and 480 nm ON and OFF responses had similar amplitudes.

d. Amplitude of ON responses (y axis) plotted as function of the amplitude of OFF responses (x axis) for the ten biggest clusters for achromatic stimuli at different contrasts. Interestingly, the amplitude differences between ON and OFF responses were not affected by the contrast and stayed balanced over all tested contrasts.

e. Vector strength (*see Chapter 4: General RGC responses* and *Chapter 2: Methods*) for chirp responses of the ten biggest clusters plotted over bins of increasing frequencies. Most clusters had their strongest vector strengths at low frequencies below 2.4 Hz. For clusters, the vector strength decreased linearly over the frequency bins. One cluster had constant high vector strengths for most of the frequencies (up to 22.5 Hz) and two clusters had peak vector strength at 12.5 Hz (arrow).

f. Spike frequency of chirp responses of the ten biggest clusters. In most clusters, the spike frequency did not change much over the duration of the frequency chirp and remained low at about 2-4 Hz. One cluster had high spike frequencies over most of the chirp stimulus and highest spike frequencies at 22.5 Hz. Another cluster had peak spike frequencies at 22.5 Hz as well (arrow) but in this case, the spike frequency increased with increasing chirp frequency up to 22.5 before the spike frequency decreased again.



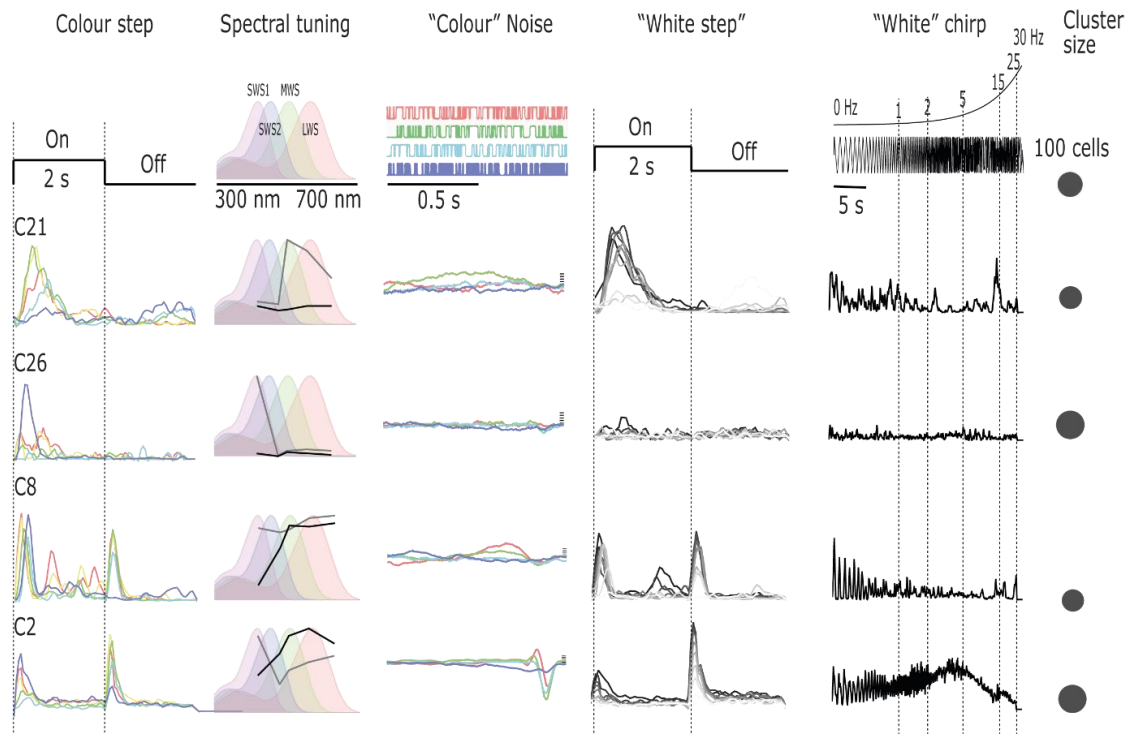


Figure 21 Overview over responses of the ten functional RGC types with the most cells (sorted by cell number, rows) and four additional handpicked functional RGC types.

First column. Overlaid ON and OFF responses (PSTH, bin size = 0.05) to Full field flash stimuli at five different wavelengths (630 nm = red, 560 nm = yellow, 505 nm = green, 480 nm = dark blue, 420 nm = cyan blue). Functional RGC types differed in their sensitivity to certain wavelengths and their ON vs OFF peak amplitude balance.

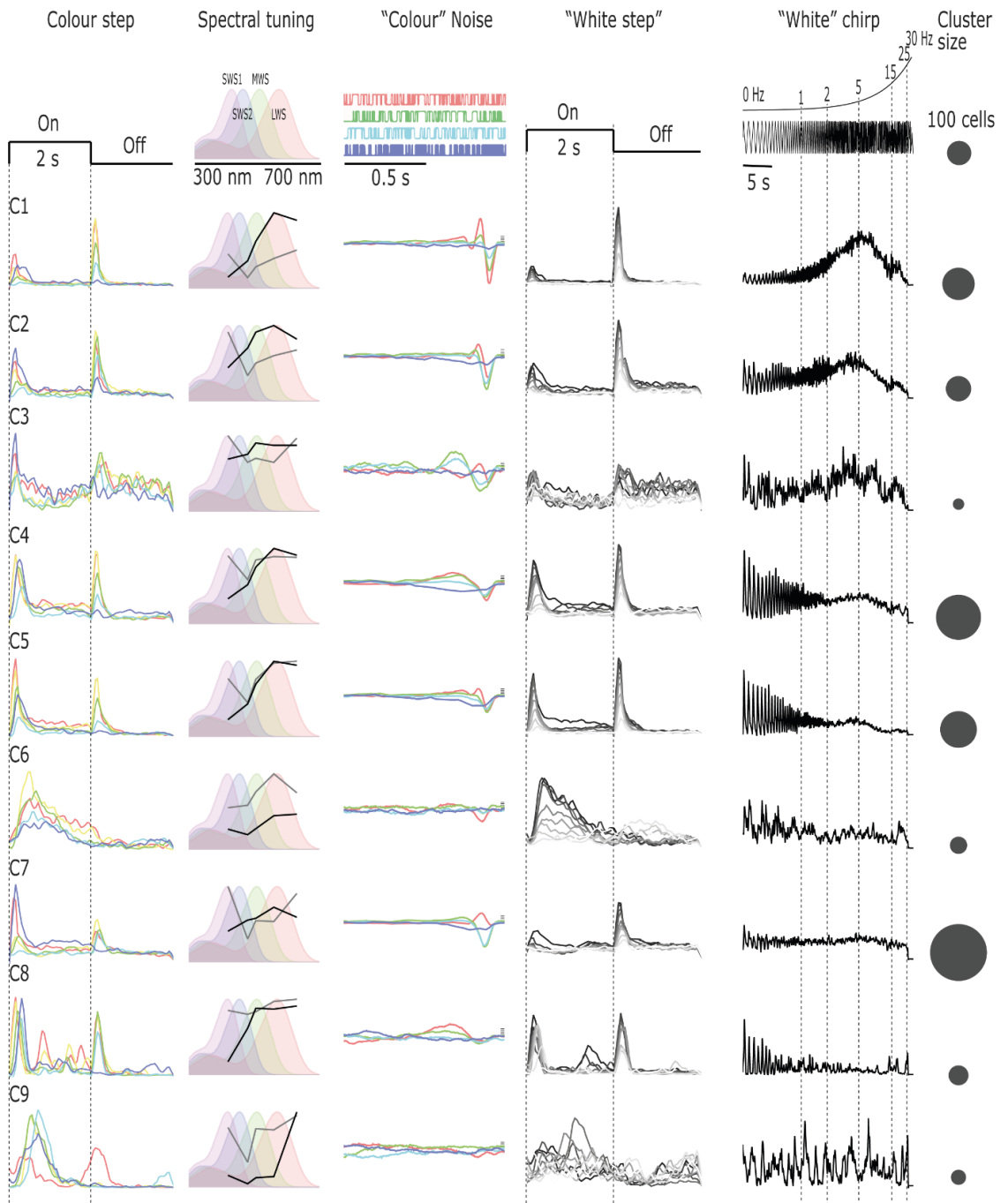
Second column. Normalized response amplitudes of ON (grey line) and OFF (black line) step responses at five different wavelengths (as shown in column 1). The amplitudes are plotted on top of the chicken opsin spectral sensitivity curves. Functional RGC types 1, 2, 4, 7, and 10 had complex tuning curves for ON step responses. Functional RGC type 1 had a complex tuning curve for OFF step responses. The remaining functional RGC types had simpler OFF step tuning curves, which in general followed the LWS opsin's sensitivity curve.

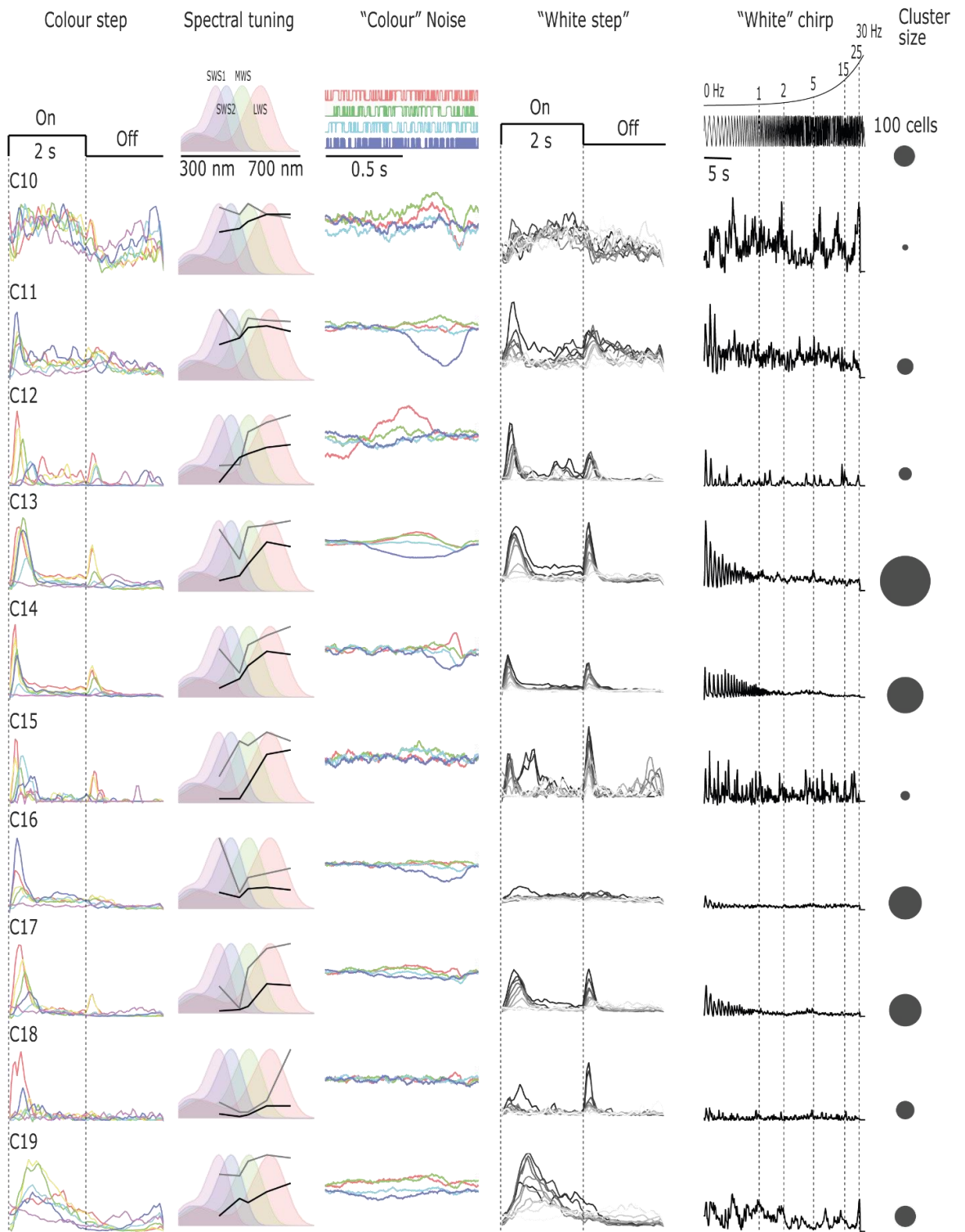
Third column. Full field noise kernels (same colours as in first column). The first ten functional RGC types had a great variety of different colour opponency time coding and kernel shapes. Some clusters had very weak kernels.

Fourth column. "White step" responses (PSTH, bin size = 0.05) at different levels of contrast plotted overlaid. For better readability, the colour scheme was inverted (100% contrast = black, 10% contrast = bright grey). "White" step responses differed between clusters. Some were more sensitive to ON, other were more sensitive to OFF, most were sensitive to ON and OFF.

Fifth column Chirp responses (PSTH, bin size = 0.01) of functional RGC types. Most functional RGC types (2, 3, 4, 5, 6 and 8) responded well to low frequencies. While functional RGC type 10 responded well at high frequencies. Functional RGC type 4 and 6 also responded at intermediate high frequencies. Some functional RGC types 1, 7, and 9 had very weak chirp responses in general.

Sixth column Number of cells per functional RGC type. The first functional RGC type contained 557 cells, the 10th cluster contains 180 cells.





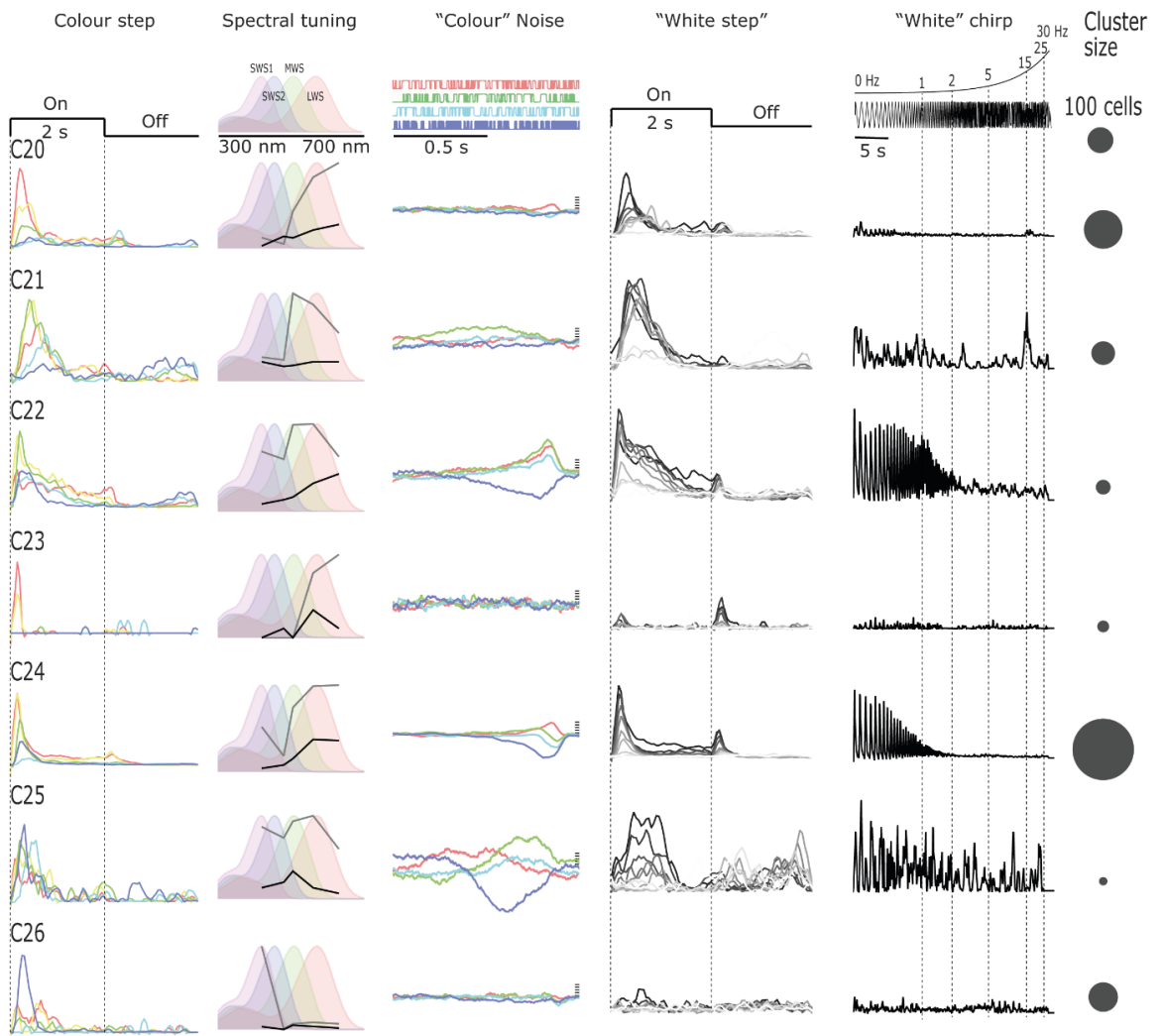


Figure 22 Overview over response properties of all clusters (rows).

Functional RGC types sorted by OFF to ON sensitivity based on mean responses to chromatic full field flashes. Columns as in **Figure 21**. Most functional RGC types were ON OFF sensitive. Two functional RGC types were most sensitive to OFF. The first, most OFF dominated cluster had an OFF tuning curve that was correlated to the sensitivity of the LWS opsin. In contrast, the second most OFF dominated cluster had strong OFF responses at peak sensitivities of the LWS opsin and the MWS opsin.

Interestingly, OFF dominant functional RGC types responded better to the chirp stimulus than ON dominated functional RGC types. Many ON dominant functional RGC types did not respond to the chirp stimulus and those that did cut off below 3 Hz. In contrast, OFF and OFF ON dominated clusters had strong chirp responses throughout the chirp stimulus and often peaked at around 5Hz.

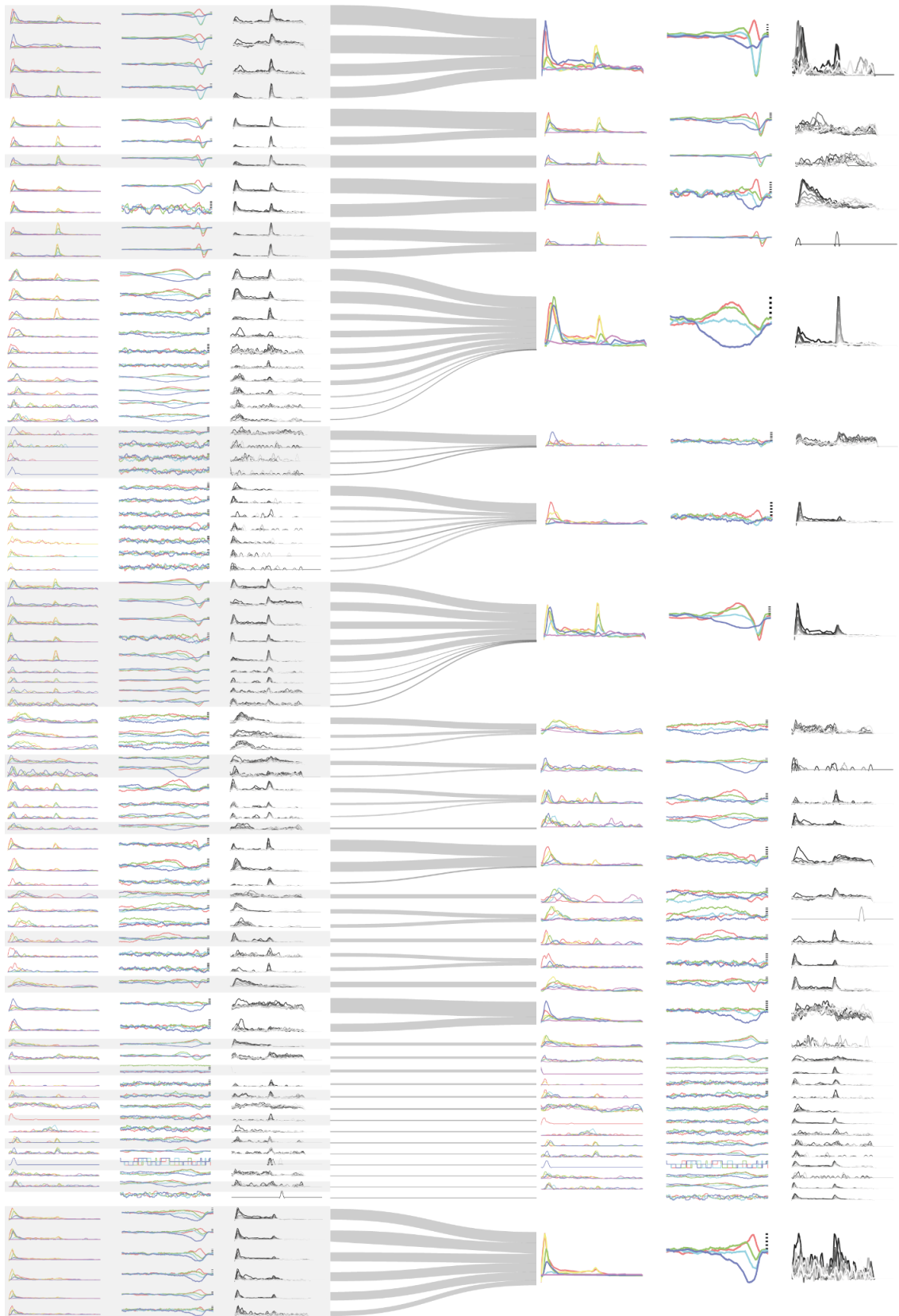


Figure 23: Condensation of 100 clusters into 27.

Flow diagram displaying how the 100 clusters, that were returned by the initial clustering were combined into 27 clusters. The strenght of the connections of the flow chart indicates the number of cells that the initial 100 clusters contained. Clusters displayed in order in which they were returned by the clustering algorithm.

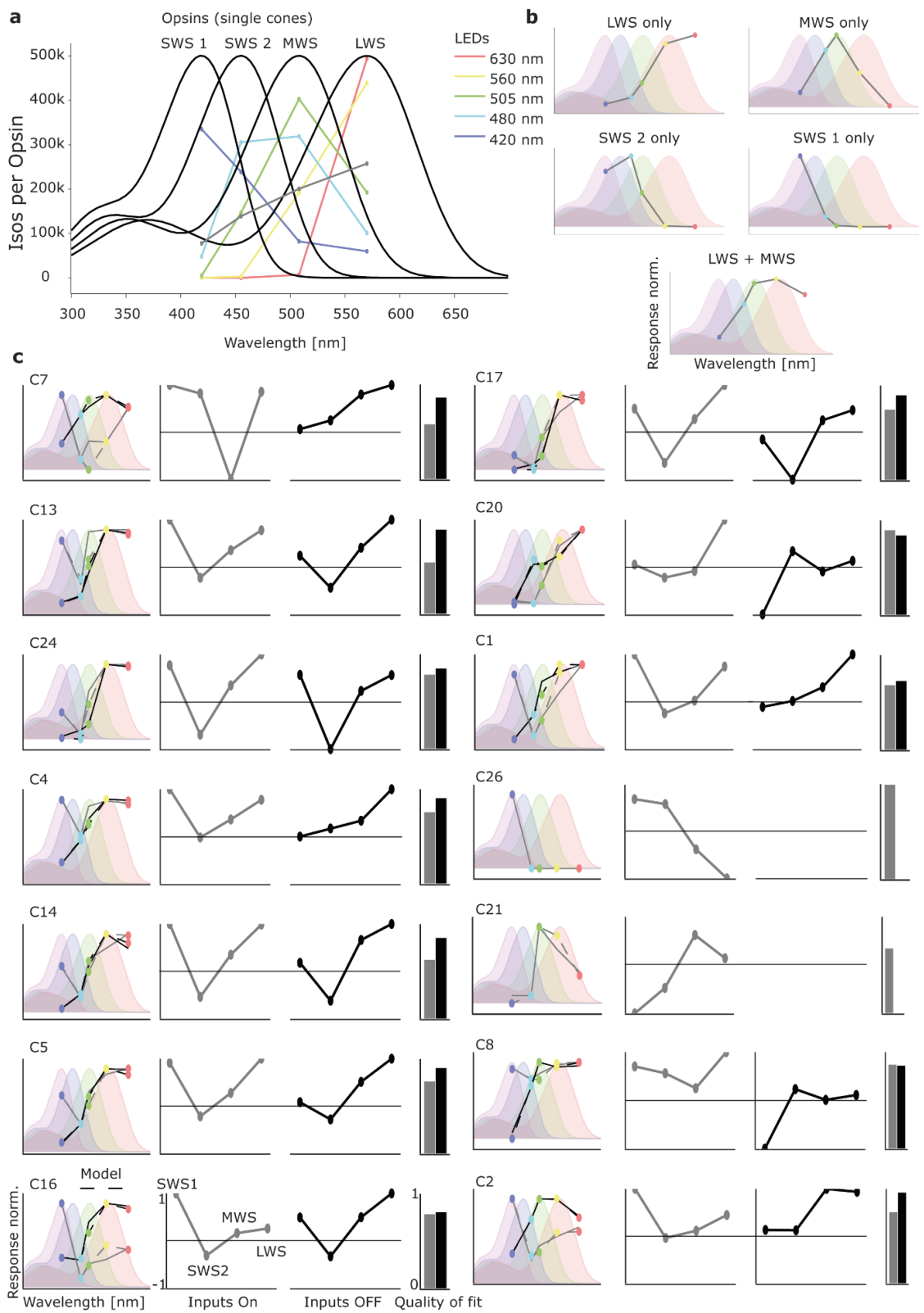


Figure 24 Modelling of photoreceptor inputs of functional RGC types.

a. Photoisomerizations per opsin. Note: LEDs are indicated by colour, not by their position on the x axis. For each opsin the number of photoisomerizations was calculated for stimulation by a given LED. For example: 630 nm LED (red trace) triggered about 500,000 isomerizations in the LWS opsin and close to zero isomerizations in the MWS opsin.

b. Example modelled tuning curves for pure LWS, MWS, SWS2 and SWS1 stimulation. Single LWS inputs were obtained by rotating the y axis from **a** into x for a given opsin and normalization to max. For example: The LWS opsin received 500,000 isomerizations at 630 nm, about 400,000 isomerizations at 560 nm etc.

c. Tuning curves and modelled photoreceptor inputs for different functional RGC types (rows). First column: ON and OFF tuning curves derived from mean functional RGC type responses (solid lines) and modelled ON and OFF tuning curves with the best fit (dashed lines). Second column: modelled photoreceptor inputs for the ON model. Third column: modelled photoreceptor inputs for the OFF model. Fourth column: Goodness of the fit of ON and OFF models. Fifth to eighth columns: Same as columns one to four.

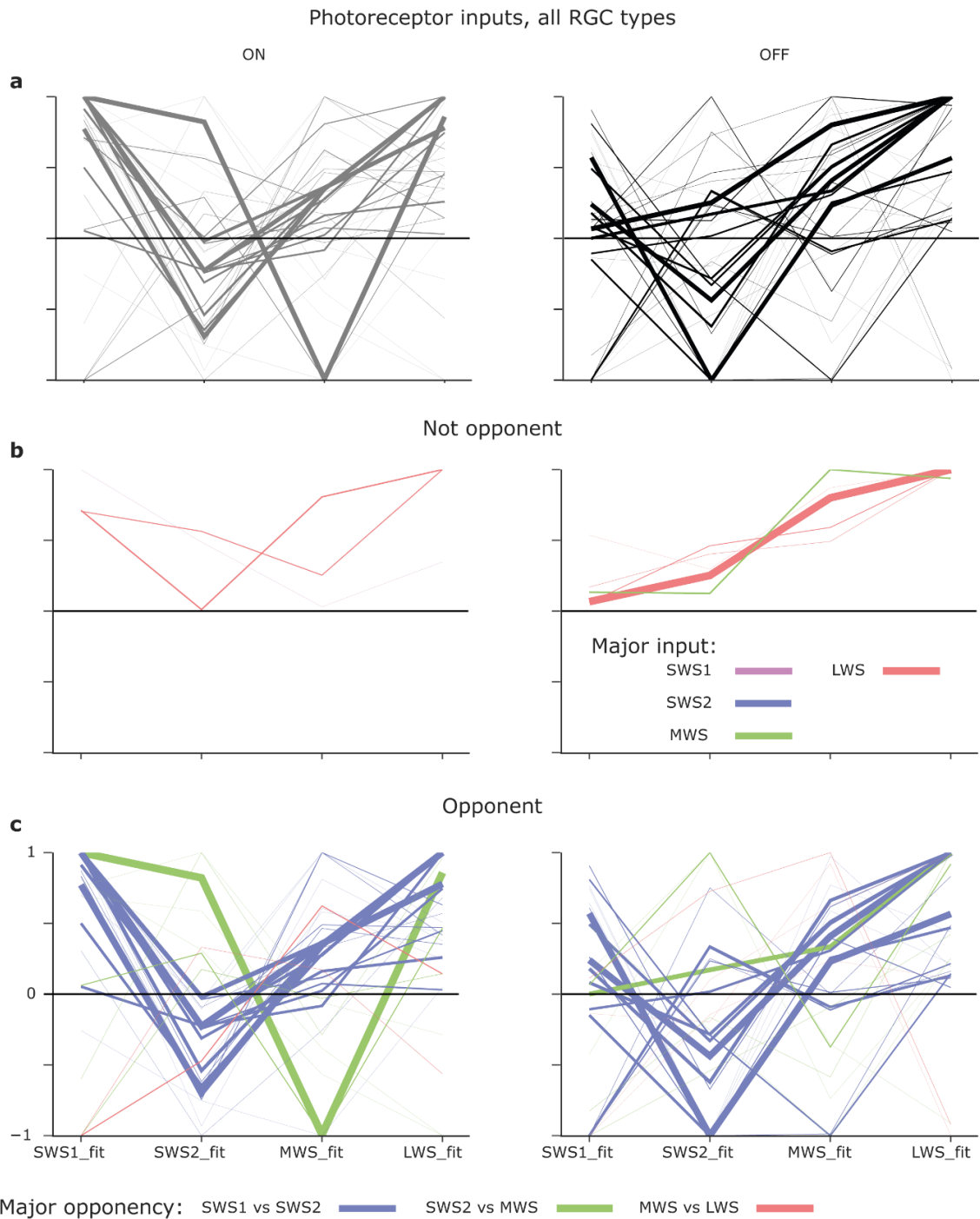


Figure 25 Major chromatic opponency axes in chicken RGCs

a. Modelled cone inputs of all functional RGC types. The line weight = number of cells that a given functional RGC type contained. Functional RGC types received diverse cone inputs, but most followed one of three trends as highlighted in **b** and **c**.

b. Summarized modelled cone inputs for functional RGC types that received excitatory inputs for ON and OFF responses (left, right respectively). Colours indicate the photoreceptor that contributed the strongest input. Many of these functional RGC types received strongest input from the LWS cone.

c. Summarized modelled cone inputs for functional RGC types that received inhibitory inputs from at least one cone type. Line weights indicate number of cells belonging to that type. Colours indicate the major opponency axis (biggest difference between inputs of two cones). Functional RGC types had one of two major chromatic opponencies: SWS1 cone inputs vs SWS2 cone inputs (blue) and MWS cone inputs vs SWS2 inputs (green).

CHAPTER 6: RESPONSE SHAPES

SUMMARY

Chicken functional RGC types show interesting complex wavelength dependent integration time differences. Further analysis revealed that response shapes (combination of response amplitude and time course) are wavelength and contrast dependent. Chromatic responses have different response shapes than “white” step responses. Principal component analysis highlights how these differences could principally be used by RGCs to independently encode chromatic and contrast information, although the exact code remains unknown. Beyond spectral coding, a minority of functional RGC types are specialised for fast, achromatic contrast coding, showing highly synchronized responses.

The findings presented here suggest the existence of distinct slow chromatic and fast achromatic pathways in the chicken retina. Modelling suggests that the latter is consistent with predominant LWS and double cone drive, while the former required inputs from diverse combinations of single cones.

INTRODUCTION

Time is an important dimension in neuronal coding. For example, the specific integration times of excitatory and inhibitory postsynaptic potentials fundamentally underpin a profusion of neuronal functions (Bliss and Lømo, 1973; Brombas et al., 2017; Coombs et al., 1955). Many neuronal circuits have been described in which time delay and input summation are the key functions by which information is encoded. In vision, time delays combined with signal summation establishes motion vision (Barlow and Levick, 1965; Borst, 2000; König et al., 1996). Neuronal coincidence detectors that compare inputs coming from the left and right ear are common in auditory circuits in different species (Campbell and King, 2004). Another time dependent coding mechanism found in auditory circuits is the comparison of relative time delays to first spike between different neurons in the population (Chase and Young, 2007).

In view of this background, chromatic dependent time differences as described in (*Chapter 4: General RGC responses*) and (*Chapter 5: Functional RGC types*) are an interesting finding. Could avian retinas encode chromatic information in their temporal dimension of neuronal responses? And how could such a time dependent coding be decoded? A latency dependent neuronal code that allows to distinguish different chromatic stimuli faces multiple challenges: Latency must encode chromatic content and “saturation” of the stimulus, that is, the spectral width of the stimulus, how “white” is the stimulus. In addition, and perhaps even more fundamentally, such

a code must allow reliably differentiating between amplitude changes and changes of the chromatic constitution of the stimulus.

A further question is how differences in latencies between different retinal output channels are integrated. Time delays that originate in movement in the visual scene must be disentangled from the time delays caused by the neuronal coding.

As shown in (*Chapter 4: General RGC responses*), changes of stimulus intensity of “white” steps are encoded as changes in response amplitudes. However, wavelength is also encoded in amplitude changes. Because of this, the proposed code cannot simply rely on amplitude but would require a combination of both, amplitude and timing (in the following called response shape), to encode chromatic content and stimulus amplitude.

In this chapter, response kinetics (time to first spikes, synchronization between population responses, time course of population responses) are analysed for the information that could be encoded in them. I will show how chromatic responses differ from “white” responses and how individual functional RGC types show fundamentally different response shapes. Further, the possible functional significance of different response kinetics will be discussed.

RESULTS

The response kinetics of the population response of RGCs were analysed based on three different aspects: General response shape, time to first spike, and synchronization of times to first spikes (in the following called first spike synchronization). Kernel density estimations of times to first spike were calculated to estimate the probability density function of first spikes of all cells in the population. Tighter distributions mean higher first spike synchronization. The peak of the distribution is the time at which first spikes occur in closest temporal proximity (hereafter called “population first spike”).

RESPONSE SHAPE

At a population level the response shape was dependent on wavelength, differed between responses to chromatic and “white” stimulation and between “white” step responses depending on contrast, (**Figure 26** and **Figure 28**). For ON responses, response latency generally decreased with wavelengths as follows (630 nm < 560 nm < 420nm, < 505 nm < 480 nm). 420 nm responses were an exception to trend. Interestingly 480 nm responses were not only slowest, but also most sustained, 630 nm responses were not only fastest but also least sustained. In contrast, “white” step responses were more sustained than chromatic responses at 630 nm and 560 nm despite comparable latencies.

Population first spike differs similarly depending on wavelength and contrast, (**Figure 26** and **Figure 28**). Population first spike was fastest at 630 nm (0.11 s) and slowest at 480 nm (0.3 s). “White” step responses had population first spike times in the range between 0.12 s and 0.2 s depending on contrast. Similarly, the first spike synchronization decreased with wavelength and with contrast. In summary, population first spike time was faster at all ‘white’ contrast levels than at full contrast at 480 nm.

OFF responses did not have the same differences, (**Figure 28**). OFF responses were generally faster than ON responses on population average and differences in population first spike times were less wavelength and contrast dependent. In addition, first spike synchronization was higher and less wavelength or contrast dependent.

Response shape is the combination of response amplitude and response latency. Both variables are not independent from each other, which makes interpretation of differences in response shape difficult. For a summarized comparison, first and second principal components (PCs) were extracted from all response shapes and PC weights were compared between wavelength and contrast levels, (**Figure 27**). This was done to test two hypotheses: First, if it is possible to distinguish “white” step responses from chromatic responses based on response shapes. Second, if it is possible to separate chromatic responses dependent on wavelength. Both hypotheses were tentatively confirmed by PC analysis in case of ON steps but not OFF steps, (**Figure 27 b & c**). Most of the variance of “White” step ON responses can be explained by the first PC (The weights for the second PC are close to 0 at all contrast levels). However, to explain chromatic response shapes both first and second PC are needed. This analysis was performed using different time windows – it was found that using response shapes as coding strategy works sufficiently within the first 200 ms after the onset of the stimulus (data for other time windows not shown).

INDIVIDUAL FUNCTIONAL RGC TYPES

At a population level, response shape differences could therefore principally be used as a coding strategy for chromatic stimulus information. But how uniform are response shape differences across different functional RGC types as delineated by clustering in (*Chapter 5: Functional RGC types*)? To answer this, I performed the same analysis as described above for the population response on the level of functional RGC type populations.

I selected six different example functional RGC types to evaluate differences in response kinetics in detail. Functional RGC types with different chromatic sensitivities and frequency tunings were chosen to evaluate how response kinetics differ in functional RGC types which encode for

different visual information (chosen types are, C1, C2, C5, C7, C8, and C16 as introduced in *(Chapter 4: General RGC responses)*).

In some cases, response shapes differed strongly between different functional RGC types (**Figure 29 a**). In *(Chapter 5: Functional RGC types)* it was shown that response amplitudes differed between individual functional RGC types depending on chromatic sensitivity and/or contrast. It was shown that response kernels have wavelength dependent integration times. In addition, response shapes of functional RGC types differed surprisingly strongly. PC analysis revealed that many functional RGC types could use the differences in ON but also OFF response shapes to encode chromatic stimulus information, (**Figure 29**). In many functional RGC types responses at 630 nm and 560 nm were near “white” step responses of high contrast in PC space while responses below 560 nm occupied a more distinct place. However, some functional RGC types differed strongly from this trend, for example C1, and C7 and to some extent C16. Here, responses at 630 nm differed strongly from responses at 420 nm while all other wavelengths and “white” steps occupied a different place in PC space, (**Figure 29**).

Differences in population time to first spikes were more pronounced for ON responses than OFF responses. Commonly, population time to first spike was fastest at long wavelength (630 nm and 560 nm), and functional RGC types C2 and C1 had the fastest population times to first spike of all functional RGC types. Responses at 480 nm were slow across all functional RGC types but population time to first spike differed strongly at 420 nm, (**Figure 30**).

Furthermore, first spikes were more synchronized in OFF responses than in ON responses and synchronization increased with long wavelength, (**Figure 30**). In ON responses first spike synchronization differed strongly between different functional RGC types. OFF responses had more similar spike synchronizations. The strongest synchronization of all functional RGC types was found in functional RGC type C1. Spikes were highly synchronized across all wavelengths and 560 nm responses were the fastest across all functional RGC types ON and OFF responses. The population time to first spike is about 0.1 s.

In summary, response kinetics differed between chromatic and achromatic stimulation and depending on level of contrast and wavelength of stimulation.

CHROMATIC VS ACHROMATIC VISION

Interestingly, the small minority of “truly” achromatic OFF functional RGC types (C1, C2) exhibited substantially faster population time to first spikes, which were moreover less wavelength or contrast dependent and a higher synchronization in the time to first spike than chromatic functional RGC types (for example C16, C5) or achromatic ON functional RGC types

(C8). Time difference between different functional RGC types is most apparent when comparing chirp responses, (**Figure 31**). Chromatic functional RGC type did follow the chirp stimulus at low frequencies (below 3 Hz). At higher frequencies the spike frequency and vector strength decreased. In contrast, achromatic OFF functional RGC types increased their spike rate with increasing chirp frequencies and the vector remained high throughout the chirp stimulus. Functional RGC type C 16, which responded fastest to 420 nm stimulation showed low phase locking of its response to the chirp stimulus, only responding at very low frequencies below 1 Hz, (**Figure 31**).

DISCUSSION

GENERAL

How is chromatic stimulus content encoded by chicken RGCs? As shown in (*Chapter 4: General RGC responses*) and (*Chapter 5: Functional RGC types*), a profusion of functional RGC types displaying chromatically opponent responses do exist in the chicken retina. In principle, this allows separation of “colours” along specific opponency axes in the light spectrum. However, opponency does not appear to be the only possible source of spectral information in the RGC’s activity patterns. First, stimulus integration time is also strongly wavelength dependent (*Chapter 4: General RGC responses* and *Chapter 5: Functional RGC types*), and second, as shown this chapter, the kinetic response shapes add further possible information to this code. However, response shape is a ‘bulky’ term, a combination of response amplitude and response latencies and thus finding appropriate parameters for analysis and comparison is challenging. The results in this chapter by no means prove that chromatic information is encoded in response shapes. However, they show that such a code could be possible. Strikingly, it was possible to separate responses to different wavelength and “white” step responses in PC space. PC analysis is a dimensionally reduction of the response shape that aims at finding common shapes that explain the most variance in the data. This operation is mathematically not trivial, but it seems plausible that a neuronal circuit can identify response shape differences, for example by analysing both the time to first spike and the distribution of subsequent spikes over time.

Time to first spike differed remarkably between different wavelengths and between ON and OFF responses. Independent from the question if chromatic information is encoded in integration time delays, these findings suggest that ON responses have fundamentally different physiology than OFF responses. The reason for this on circuit level remains unclear, but some general consequences for stimulus encoding in RGC can be derived from this finding:

First, the OFF pathway seems more suitable for the encoding of fast temporal contrast changes. In support, two achromatic OFF functional RGC types were identified in (*Chapter 5: Functional RGC types*). Both types had fast OFF responses, and functional RGC type C1 had the fastest OFF responses of all functional RGC types. Both types had strong responses to frequency chirp stimulation even at high frequencies. No fast ON functional RGC type with similarly strong frequency chirp responses was identified. The second interesting general trend my data reveals is that responses were fastest at long wavelength (630 nm & 560 nm) slower at intermediate wavelength (505 nm and 480 nm) and again faster at 420 nm (but see *Chapter 4: General RGC responses, slow blue response kernel discussion*). This finding is supported by behavioural studies measuring flicker fusion frequencies in the pigeon (Delius et al., 2017) and to some extent in chicken (Rubene et al., 2010). Both studies show that flicker fusion frequency are fastest at the long and short wavelength edges of the visible spectrum and slower in between. In addition (Rubene et al., 2010) argues that UV light plays a key role in increasing flicker fusion frequency. My data contradicts these findings to some extent, showing that long wavelength stimuli drive the fastest responses which is in accordance with findings by (Delius et al., 2017). The results by (Rubene et al., 2010) have to be considered with some caution as the number of tested animals was very low and the LEDs used for the test were arguably suboptimal. The data presented in this study has identified specific functional RGC types that rely on long wavelength inputs for the encoding of fast temporal contrast information.

"DOUBLE CONE-RGCs"?

At this point, I want to discuss one of the perhaps most interesting questions regarding avian vision: What is the function of the double cone? Double cones consist of two electrically coupled members that both contain the LWS opsin (like the LWS single cone) but a different oil droplet than the LWS cone (P-Type) (Bowmaker and Knowles, 1977; Goldsmith et al., 1984; Hart, 2001; Morris and Shorey, 1967; Toomey et al., 2015). The different oil droplet in double cones likely shifts the peak absorption of the LWS opsin to shorter wavelengths compared to the LWS cone although P-Type oil droplet absorption has not been sufficiently modelled yet; compare (Hart and Vorobyev, 2005) and (Wilby et al., 2015; Wilby and Roberts, 2017). A prominent hypothesis suggests that double cones are primarily used for achromatic vision (Potier et al., 2018; Sun and Frost, 1997; v. Campenhausen and Kirschfeld, 1998). However, this hypothesis fails to explain some observations: For example, double cones are absent from the raptor fovea (Potier et al., 2018) and both members of the double cone form various connections to bipolar cells that also receive inputs from single cones (Günther et al., 2021).

Based on my data, I would like to suggest a different role for the double cone in avian vision: The double cone as primary input to a fast temporal contrast processing pathway. This hypothesis is built on the fact that chicken show fast flicker fusion frequency up to 90 Hz, depending on luminance levels (Lisney et al., 2012, 2011) but most functional RGC types identified in this study had comparatively slow temporal contrast resolution. However, notable exceptions to this general slowness are two clusters, C1 and C2. Both were strongly OFF-biased, in accordance with the observation that the ON pathways in chicken was generally slower than the OFF pathway. Moreover, importantly, both functional types followed chirp frequencies up to the maximum tested (30 Hz), and their spectral responses were best explained by dominant input from an LWS opsin-expressing cone (*Chapter 5: Functional RGC types, part 2*). C1 is particularly LWS dominated, while C2 requires additional, inputs from MWS cones. Even though both are OFF biased, they are still technically OnOff cells, and here C2 had fastest ON responses of any functional RGC type while type C1 had the fastest OFF responses of any functional RGC type. In addition, times to first spike were highly synchronized in both types in contrast to other functional RGC types. All these response properties make these two functional types ideal for the processing of fast temporal contrast – perhaps superficially reminiscent of alpha cells in a mice, or parasol cells in primate

A DOUBLE CONE PATHWAY?

Avian retinas face some unique signal processing challenges during flight. Behaviour guidance must be fast; thus, signal processing must be fast. Commonly, vertebrates use LWS single-cones for achromatic vision like motion vision (for example in zebrafish, see (Krauss and Neumeier, 2003) in combination with (Baden, 2021).) Chicken also have LWS single-cones which could serve as major input to the achromatic pathway, however, these contain oil droplets that effectively cut off the short wavelength sensitivity of the LWS opsin (Wilby et al., 2015; Wilby and Roberts, 2017). If achromatic vision in chicken would solely rely on LWS cone inputs, this pathway would not receive visual signals at wavelengths below about 560 nm which would presumably come at the cost of signal/noise ratio and, consequently, maximum resolvable temporal frequency. Thus, it is not surprising that functional RGC type C2 combines inputs from LWS-opsin expressing cones and MWS. This spectrally extends the window of wavelengths that can provide input to such a pathway. However, combination of multiple cone inputs has a downside: The signals from two different types of cones must be combined by synaptic transmission and excitatory postsynaptic potential integration. This may lead to time delays, time differences between input channels and overall, less synchronized and accurate neuronal representation of fast visual stimuli independent of chromatic content. Moreover, it is likely that avian cones receive diverse forms

of feedback signals from horizontal cells in the outer retina, which might – as in fish – spectrally and temporally segregate their responses from another. My data shows, that in functional RGC type C2 integration times differed between 630 nm and 505 nm (see response kernel in (*Chapter 5: Functional RGC types*) and population time to first spike in this chapter).

Based on in this I propose the following hypothesis: The chicken retina uses two different “fast” temporal contrast coding pathways. One of which relies on combined LWS and MWS cone inputs as described above. The other mainly relies on double cone inputs and is represented in my data as functional RGC type C1. Relying on the double cone for temporal contrast processing has many advantages over a hypothetical LWS + MWS single-cone channel.

First, double cones have P-type oil droplets which result in higher LWS cone sensitivities at lower wavelength in double cones compared to LWS cones. In addition, the accessory member of the double cone does not have an oil droplet (although different types of double cones with different types of oil droplets might exist (López-López et al., 2008; Seifert et al., 2020)). As a result, the double cone is likely sensitive to a broader range of the visual spectrum, and probably also most sensitive overall. An achromatic pathway solely based on double cone inputs does not need to integrate signals between different types of cones and more synchronized responses over different wavelengths can be expected. Response amplitude would scale with the LWS opsin. My data supports this hypothesis. Functional RGC type C1 had very synchronized OFF responses between 630 nm and 480 nm.

Consequently, functional RGC type C1 can process fast temporal contrast changes at least up to 30 Hz. Functional RGC type C2 did follow the chirp stimulus to high frequencies and cuts off before C1. Another prediction of the proposed hypothesis is that functional RGC types which show complex chromatic opponency that relies on the summation or subtraction of inputs of many different cones fail to encode fast temporal contrast. The data presented in this chapter supports this. For example, functional RGC type C7, which had complex opponent responses, had strong wavelength dependency in population time to first spike in ON and OFF and did not follow frequency modulation above 3 Hz.

Further investigations must be conducted to test the proposed hypothesis. Ideally, response time courses of all input channels would be known. Chirp responses should be tested over different isolated wavelength. Behavioural studies could be set up by saturating the double cone and LWS cone with red light while flicker fusion frequency is tested at lower wavelength.

In summary, this chapter shows how manifold response shapes differ depending on stimulus conditions and functional RGC types. The extent to which integration time differs between

different wavelength is astonishing and needs to be further investigated. In combination with the abundance of functional RGC types that show complex chromatic opponent responses, my results suggest a complex neuronal coding strategy of chromatic and achromatic stimulus information on the level of chicken RGC.

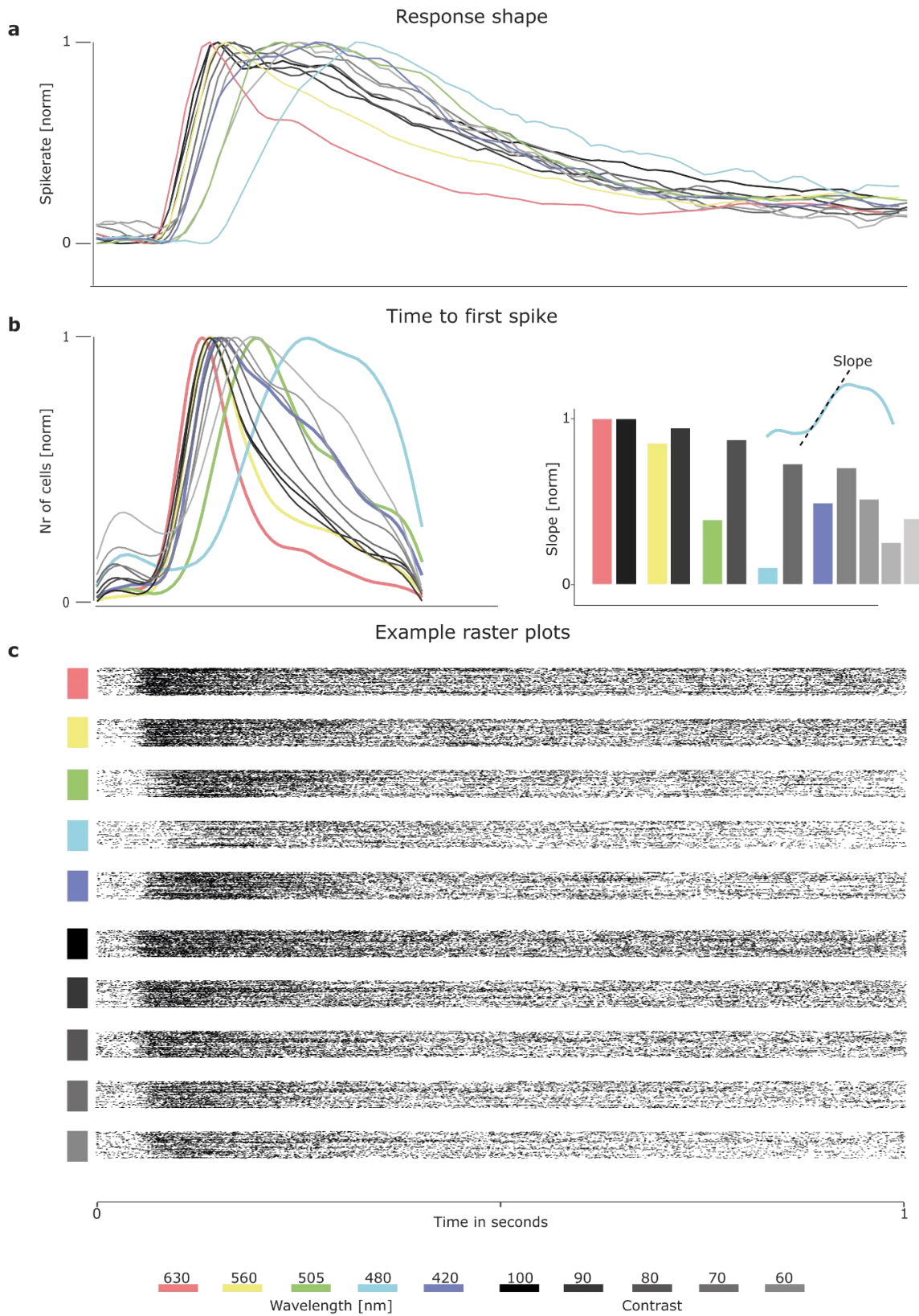


Figure 26 Response shapes and population time to first spike depend on stimulus wavelength and contrast.

a. Response shape of chromatic and “white” step responses. “White” step responses were more sustained than chromatic responses and in general shorter wavelength responses were more sustained than longer wavelength responses. Time to response onset also increased with increasing contrast and decreasing wavelength of the stimulus. 420 nm responses did not follow this trend and were faster than 505 nm responses.

b. Population time to first spike of chromatic and “white” step responses plotted on the same x time axis as **a**. Population time to first spike increased with decreasing wavelength and decreasing stimulus contrast. (420 nm being an exception to the rule). First spike synchronicity decreased with decreasing wavelength and contrast of the stimulus. The slope of onset of first spikes also decreased with decreasing wavelength and stimulus contrast.

c. Example raster plots of 200 randomly picked example cells plotted for five different wavelength and contrast levels. X axis (time) matches **a** and **b**.

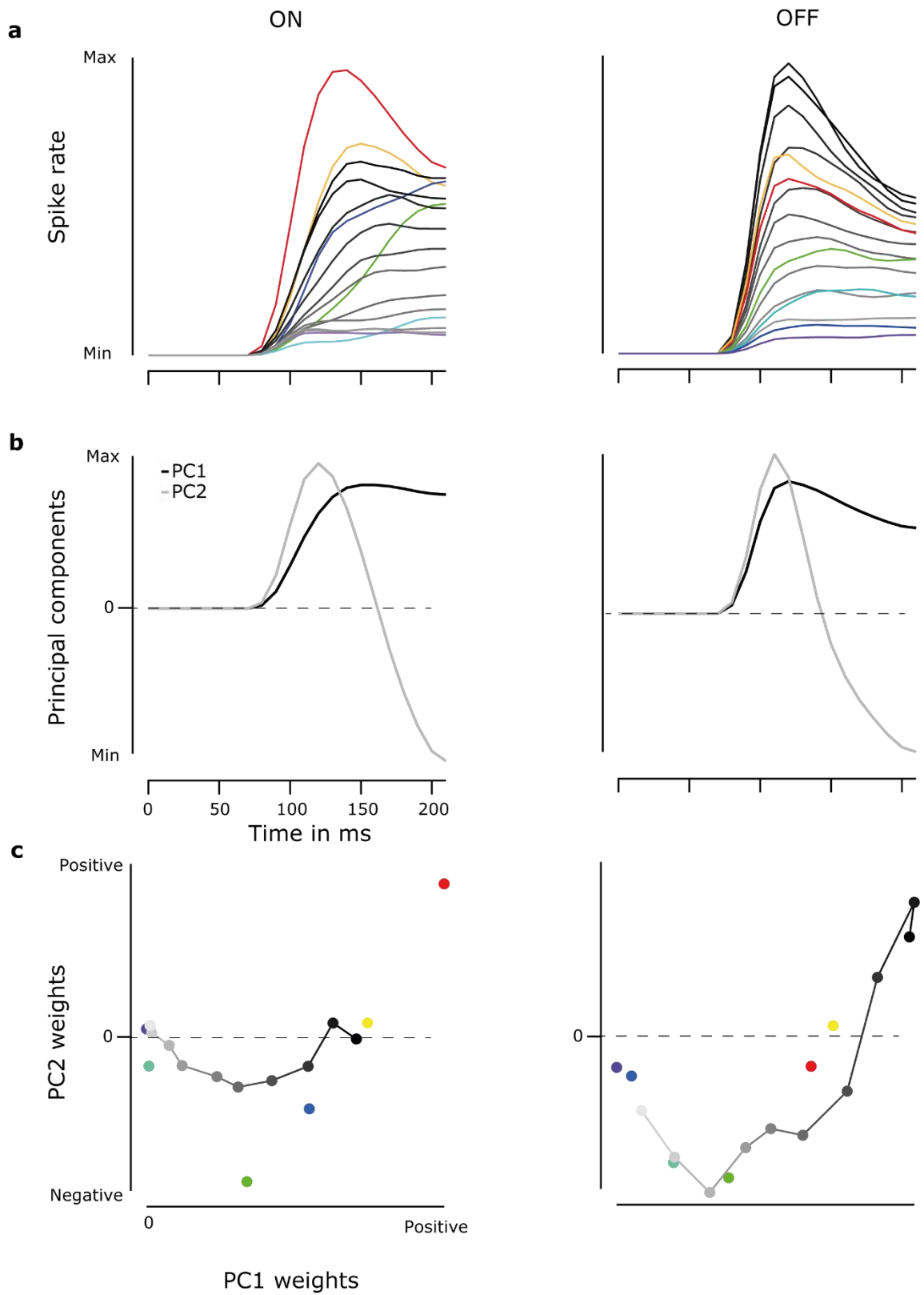


Figure 27 ON responses at different wavelength and contrast levels follow different trajectories in PCA space in contrast to OFF responses.

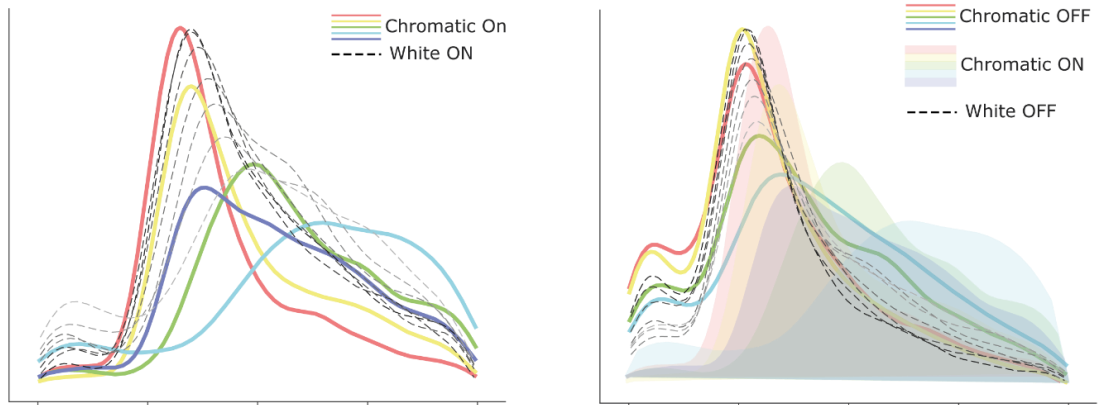
a. Response shapes of population ON and OFF responses at different wavelength and contrast levels. ON responses had more diverse shapes within the first 200 ms than OFF responses, possibly containing more information about chromatic content of the stimulus.

b. Principal components derived from responses shown in **a**. The first PC resembled the general response shape while the second PC resembled the responses time courses.

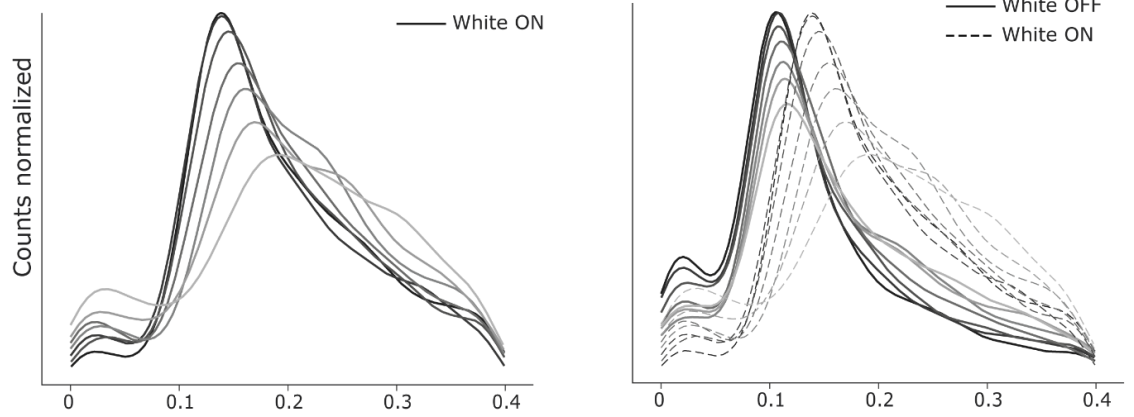
c. The PC weights of each tested stimulus condition (wavelengths and contrast). ON: “White” step responses were mostly scaled versions of PC1 (**b**). In contrast, chromatic responses were best explained under consideration of PC 1 and PC 2. OFF: Both, chromatic and “white” step responses were best explained by a combination of PC 1 and PC 2.

Time to first spike (whole population)

a



b



c

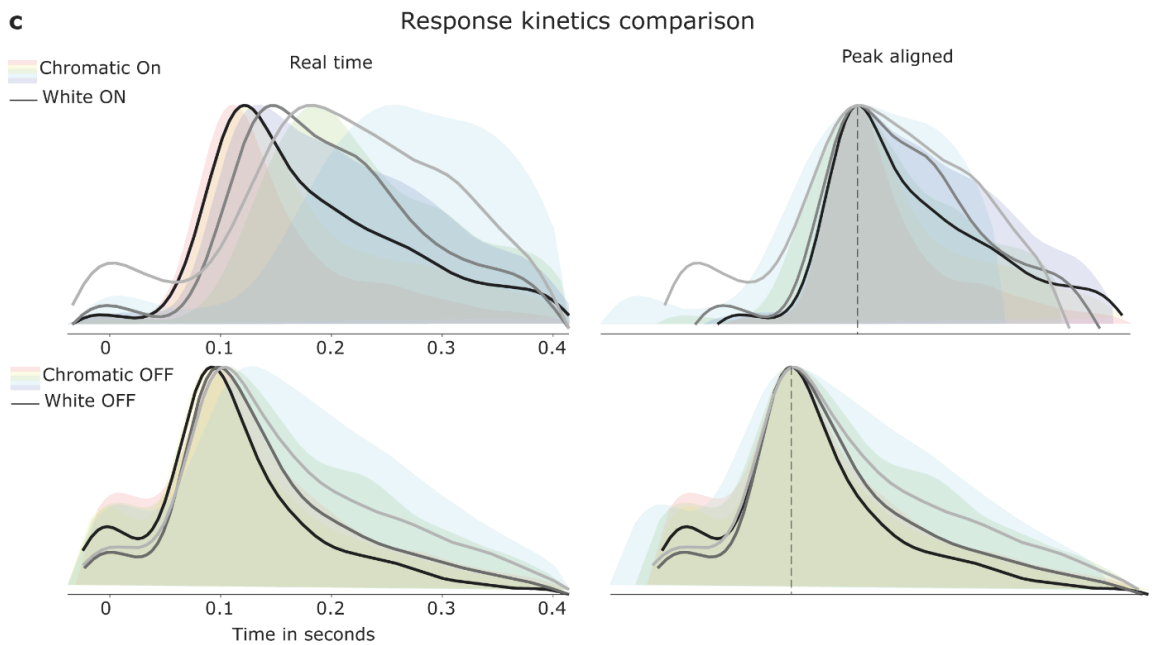


Figure 28 Comparison of population responses response shapes at different wavelengths and stimulus contrast levels and between ON and OFF.

a. Chromatic and “white” step responses had different times to first spike and different first spike synchronicity. Shown is the kernel density estimation of first spikes of all cells in the population.

b. Population time to first spike differed between “white” ON and OFF responses. OFF responses were faster and more synchronized.

c. The distribution of population first spikes differed between chromatic and “white” step responses between wavelengths and contrast levels. 630 nm triggered the most synchronized spikes, 480 nm the least synchronized spikes.

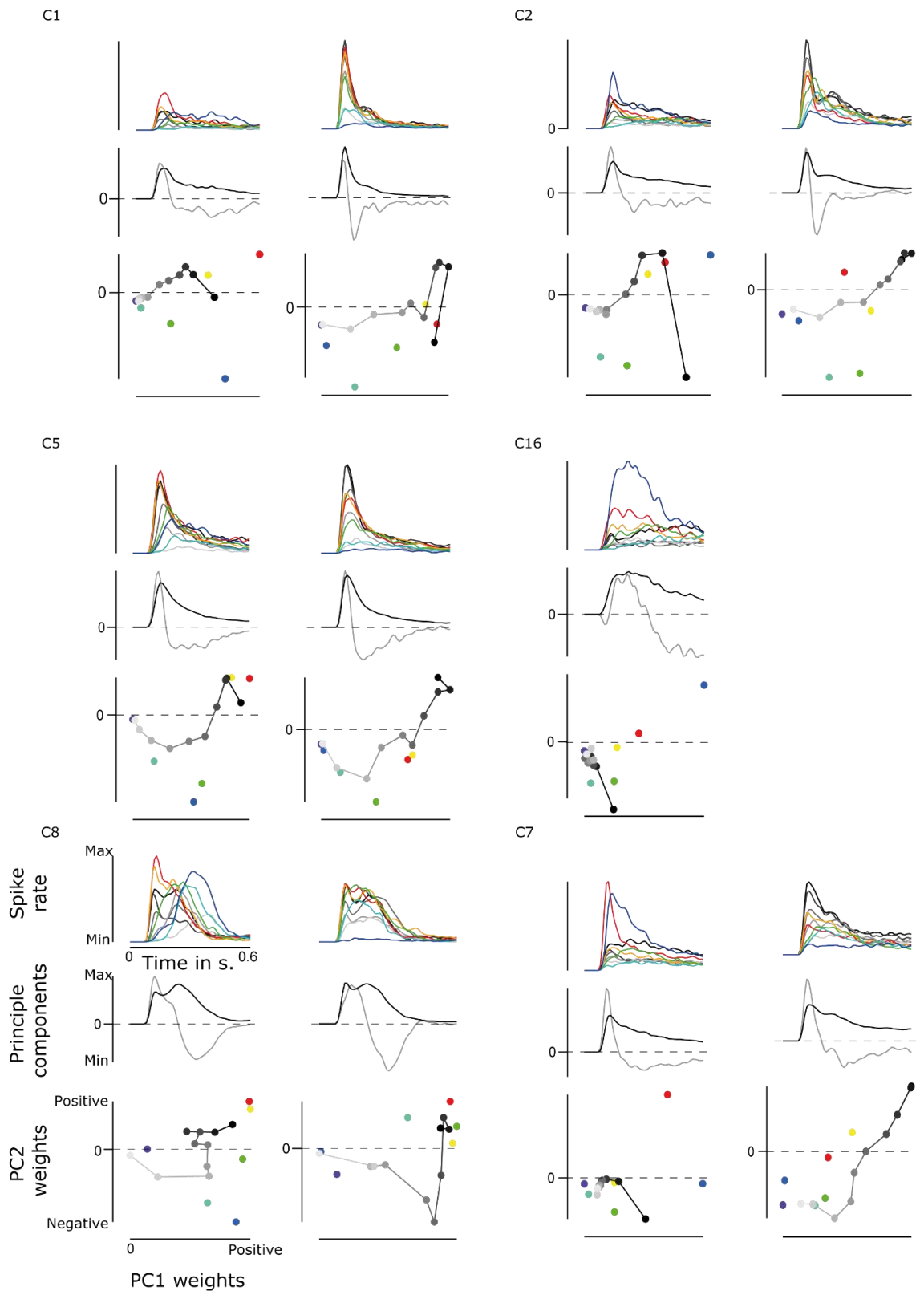


Figure 29 Response shape differences of single functional RGC types evaluated in PC space. Same as shown for the whole population in **Figure 27**. In On responses of most functional RGC types, chromatic and “white” step responses followed different trajectories in PC space, while in OFF responses chromatic on “white” step responses occupied more similar spaces. Generally, responses at 420nm, 480 nm, and 505 nm had negative PC1 weights, while responses at 560nm and 630 nm had positive PC1 weights. Exception from this rule exist (type C16 and C2). In most functional RGC type, responses at 560 nm and 630 nm occupied spaces that are close to “white” step responses (Exceptions are C1 and C7).

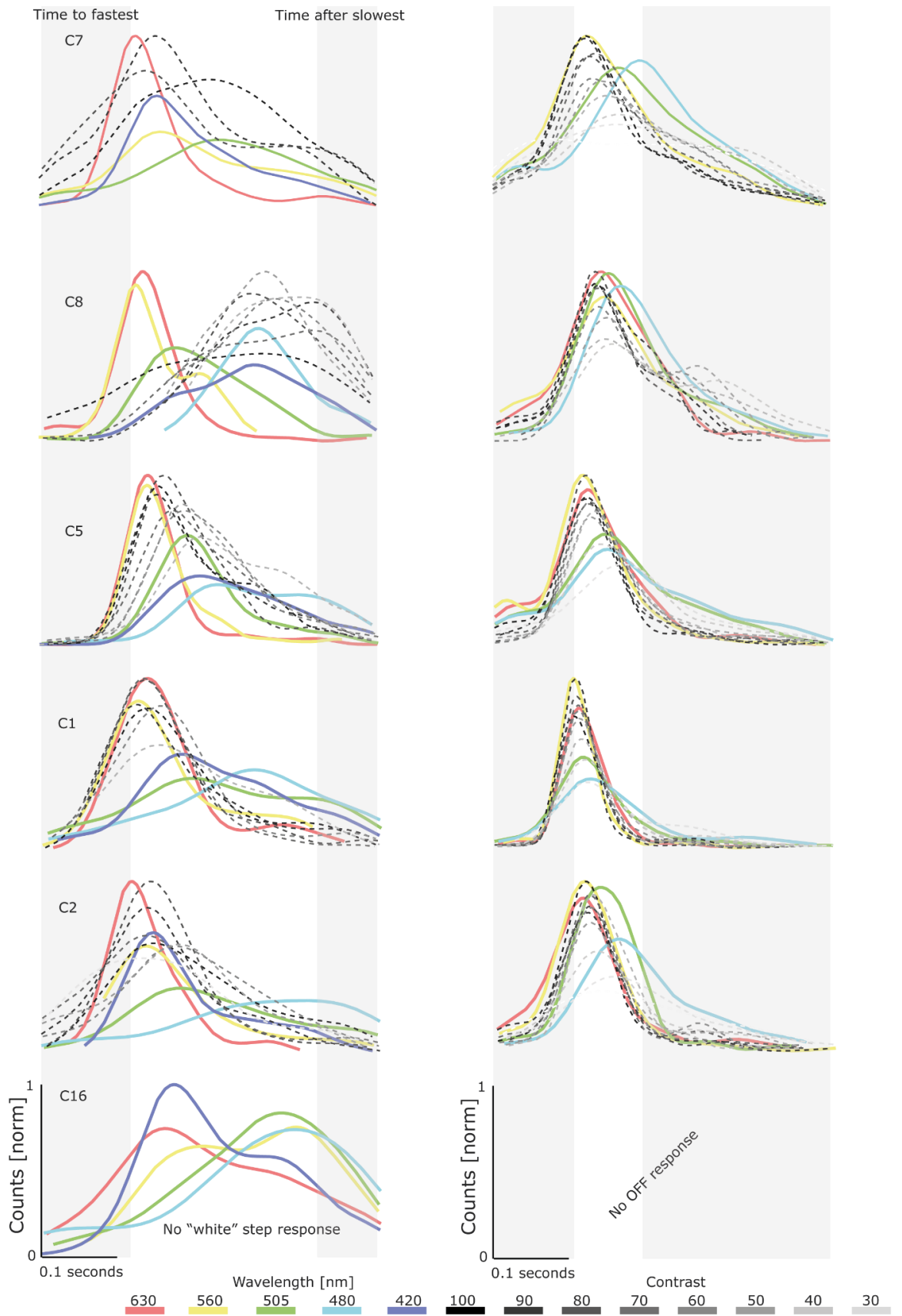


Figure 30 Time to first spike differences between different functional RGC types. Same functional RGC types as in **Figure 29** are shown. Same as shown for the whole population in **Figure 28**. Chromatic and “white” steps responses are overlaid. First grey zone indicates the population first spike time of the fastest functional RGC type. The second grey zone indicated the time between the slowest population first spike time of any functional RGC type to the end of the time window.

All functional RGC types had faster and more synchronized population first spike times in OFF responses (if OFF responses exist). Population first spike times of ON responses were slower, and less synchronized. functional RGC types C1 and C2 were the fastest functional RGC types (560 nm OFF and 630 nm ON response respectively). The population time to first spikes at individual wavelength and contrast levels differed partially strongly between functional RGC types (for example compare C2 ON and C16 ON or C1 OFF and C8 OFF)

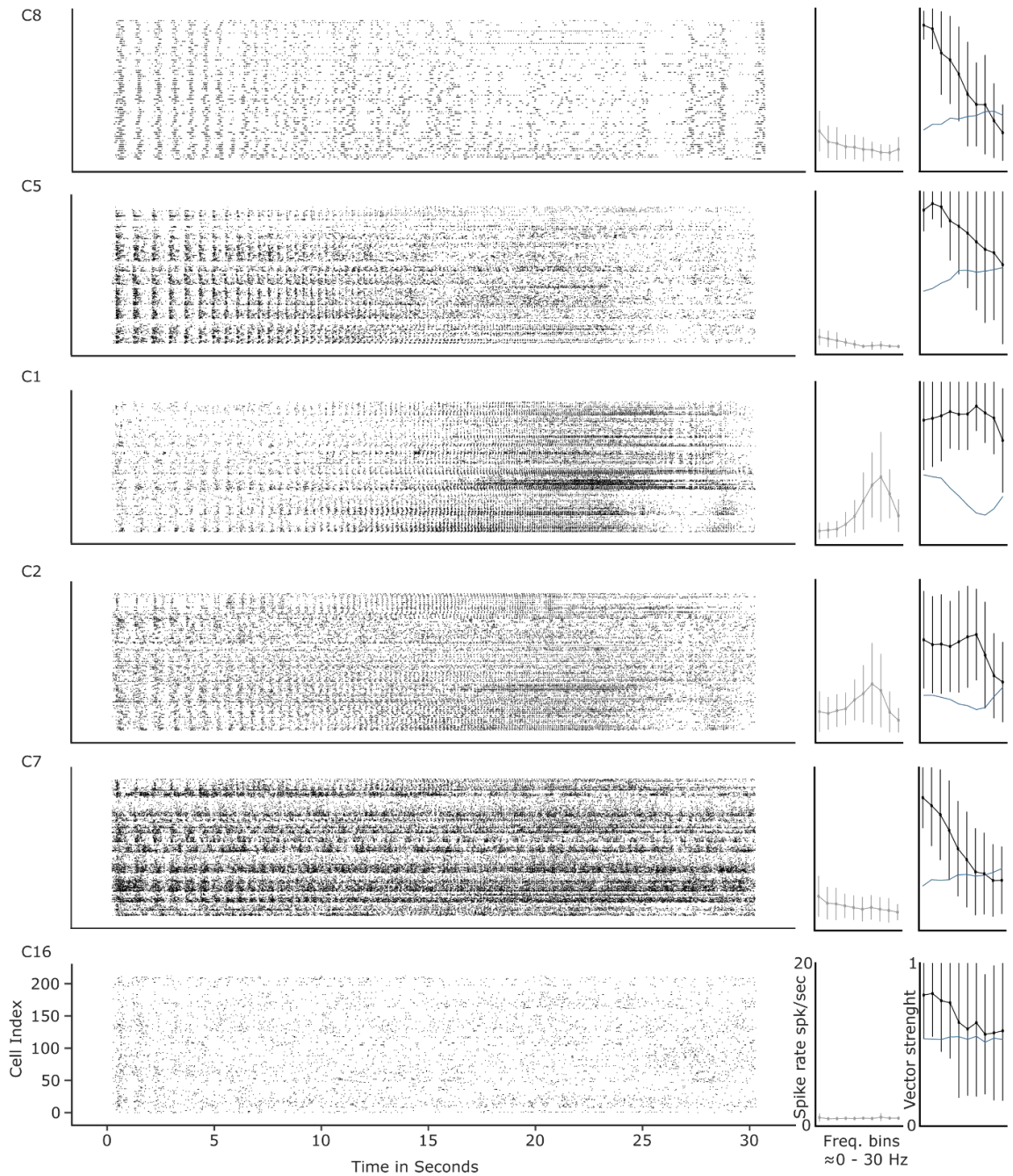


Figure 31 Comparison of chirp responses between different functional RGC types. Same clusters as in **Figure 30**. functional RGC types C1 and C2, which had more synchronized population time to first spike followed the chirp stimulus from low to high frequencies (30 Hz) as indicated by the vector strength. In addition, spike rates of these functional RGC type increased with increasing chirp frequencies up until 7 Hz. In contrast, functional RGC type that had less synchronized population time to first spike follow the chirp only at low frequencies (<3 Hz) and did not have increased spike rates at higher chirp frequencies. Functional RGC type C16, was most sensitive to light at 420 nm and responded to the chirp only at very slow frequencies. Interestingly, functional RGC type C7 had low vector strength at higher chirp frequencies but retained similar high spike rates during the chirp stimulus.

CHAPTER 7: CONCLUSION

SIGNIFICANCE OF FINDINGS

To understand similarities and differences in visual processing between different vertebrate species a good understanding of the avian retina is necessary. Prior to this study, limited insights existed and questions about chromatic processing in the avian retina were left almost completely unaddressed. The first aim of this study was to establish the chicken retina for electrophysiological MEA recordings. Maintaining avian retinas *in vivo* has been proven challenging. As shown in (*Chapter 3: Chicken retina MEA recordings*), this is likely due to spreading depressions which are triggered easily in the chicken retina. However, a sophisticated dissection protocol presented in that chapter has proven to prevent the triggering of spreading depressions successfully. It remains to be seen, if spreading depressions are a common phenomenon in avian retinas or specific to the chicken. If they are chicken specific, this might disqualify the chicken retina as a good model for electrophysiological research in comparison to other birds.

Being able to record electrical signals from chicken RGCs for multiple hours, this study addressed fundamental questions about RGC electrophysiology by recording about 6000 RGCs from multiple animals. Based on this, it was possible to get a first, fundamental understanding about avian visual processing: 27 functionally distinct functional RGC types were identified, which together showcase key conceptual similarities and differences to well-described RGC functions of other species. The vast majority of RGCs are ONOFF cells and had complex wavelength dependent ON responses. Typically, these RGCs leveraged complex combinations of ‘classical’ spectral opponency alongside spectrally dependent differences in response-timings. This diverse majority of “slow, colour-coding cells” is likely conceptually reminiscent of a greatly diversified set of small-bistratified-like cells as found in the primate retina – or possibly of several functional groups of RGCs found in fish. In contrast, a very distinct minority of Off-biased RGCs were essentially achromatic and “fast” – potentially providing a “alpha/parasol-like” pathway for achromatic contrast vision. The spectral tuning of these fast cells was approximately consistent with the expected spectral tuning of double-cones, hinting that these neuron population might be functionally linked.

Colour information could be readily read out in several ways. For example, spectrally broad “white” stimuli yielded a high population synchronicity for the Off response, while all “coloured” stimuli, independent of wavelength, instead yielded a relatively decreased population synchronicity for the On-response. Moreover, the kinetics of On-responses varied in a strikingly wavelength dependent manner: On average, and except for near-UV responses, long-

wavelength On-responses had shortest latency and most synchronised responses, systematically followed by shorter wavelengths. Using principal component analysis across flash-responses showed, that in general, greyscale and “colour” stimuli appear to be encoded in a near-orthogonal manner in PC space.

Summarized, this highlights the complexity of the neuronal code that is present at the level of RGC in the avian retina. The here presented dataset offers a first fundament based on which further studies investigation avian vision can be conducted.

LIMITATIONS

Many of the findings presented in this study can be called “preliminary” and require further validation. Because almost nothing was known about avian visual processing prior to this work, visual stimuli used were kept very general. It was not possible to establish a stimulus that would reliably allow for detection of receptive field sizes of RGCs. Full field stimulation activates both, receptive field centres and surrounds. Receptive field dynamics in RGCs can be complex and establishing a stimulus for receptive field detection should be a priority in future work.

The 27 identified function functional RGC types likely only represent a subgroup of the existing number of functional RGC types. Based on genetic markers, 41 functional RGC types were identified. It seems likely, that more complex stimuli, like moving gratings or spatial noise would allow for the detection of more functional RGC types.

Although response shapes differed depending on wavelength, identification of a latency dependent neuronal code would require specific stimuli that could test the proposed latency dependent coding. A deep understanding about how stimulus amplitude and “whiteness” of the stimulus effect latency is required. This could be done by creating stimuli that mix different wavelength and compare response latencies.

The recording protocol must be further enhanced. Since now weight could be used to assure the attachment of the retina, experiments would often yield only a few hundred responsive cells. To understand the mosaic of functional different functional RGC types, it is necessary to record from as many cells as possible.

Finally, this study was limited by the absence of any available information about visual processing in the bird retina, which made it harder to establish hypotheses to test. For example: The function of the double cone is entirely unknown. Despite many trends and hints that were revealed in my experiments, understanding of the double cone would require proof of its

necessity and sufficiency for a specific aspect of avian visual processing. Before such a proof can be attempted, many more investigations are needed.

With the advance in genetics (Crispr) it seems plausible that questions regarding the double cone function can be address on a broad front soon. The more experimental data is collected, the easier it will be to establish a deep understanding.

OUTLOOK

If we want to increase our knowledge about the avian retina, more electrophysiological studies, studying all the different aspects of avian vision are needed. Preferably, these studies would be conducted on multiple different bird species, to get an overview over “bird typical” concepts. The chicken is a good model organism, but morphologically, its retina seems to be one of the “simpler” bird retinas. It does not contain a fovea, yet many bird have not one but two foveae. A high density of RGCs can be challenging to record and analyse, even when using a MEA. Although this study was focused on the periphery of the chicken retina, spike sorting took several days because millions of spikes were recorded in a single recording. It seems unlikely, that current MEAs offer a high enough resolution for good recordings of the bird fovea. In the near future, answering simpler questions, that this work has raised should be considered. The role of the double cone in the avian retina remains to be uncovered, although this study offers a first hint at its possible function. It would be useful to functionally examine the double cone pathway under the hypothesis that it provides fast temporal contrast information to the brain. This could be done even by performing intracellular recordings, behavioural experiments and anatomical investigations (as previously started by (Günther et al., 2021).

A key feature of bird retinas is the high specialization of different areas. Investigating these areas could provide interesting findings about retinal specialization. For example, using MEAs, the here described experiments could be repeated in the whole chicken retina and functional cell types could be compared between different areas. It seems highly likely, that specialized areas contain specialized functional RGC types.

Finally, this requires a better behavioural understanding about how vision is guiding behaviour in the chicken (or other birds). The available literature often doesn’t account for specific behaviours, yet for example flight requires very different visual information than pecking food (Martin, 2017).

LITERATURE

- Amesbury, E.C., Schallhorn, S.C., 2003. Contrast Sensitivity and Limits of Vision: *International Ophthalmology Clinics* 43, 31–42. <https://doi.org/10.1097/00004397-200343020-00006>
- Araki, M., Kimura, H., 1991. GABA-like immunoreactivity in the developing chick retina: differentiation of GABAergic horizontal cell and its possible contacts with photoreceptors. *Journal of Neurocytology* 20, 345–355. <https://doi.org/10.1007/BF01355531>
- Baden, T., 2021. Circuit mechanisms for colour vision in zebrafish. *Current Biology* 31, R807–R820. <https://doi.org/10.1016/j.cub.2021.04.053>
- Baden, T., 2020. Vertebrate vision: Lessons from non-model species. *Seminars in Cell & Developmental Biology* 106, 1–4. <https://doi.org/10.1016/j.semcdb.2020.05.028>
- Baden, T., Berens, P., Franke, K., Román Rosón, M., Bethge, M., Euler, T., 2016. The functional diversity of retinal ganglion cells in the mouse. *Nature* 529, 345–350. <https://doi.org/10.1038/nature16468>
- Baden, T., Osorio, D., 2019. The Retinal Basis of Vertebrate Color Vision 24.
- Baden, T., Schubert, T., Chang, L., Wei, T., Zaichuk, M., Wissinger, B., Euler, T., 2013. A Tale of Two Retinal Domains: Near-Optimal Sampling of Achromatic Contrasts in Natural Scenes through Asymmetric Photoreceptor Distribution. *Neuron* 80, 1206–1217. <https://doi.org/10.1016/j.neuron.2013.09.030>
- Barlow, H.B., Levick, W.R., 1965. The mechanism of directionally selective units in rabbit's retina. *The Journal of Physiology* 178, 477–504. <https://doi.org/10.1113/jphysiol.1965.sp007638>
- Barnett, A.H., Magland, J.F., Greengard, L.F., 2016. Validation of neural spike sorting algorithms without ground-truth information. *Journal of Neuroscience Methods* 264, 65–77. <https://doi.org/10.1016/j.jneumeth.2016.02.022>
- Bartel, P., Yoshimatsu, T., Janiak, F.K., Baden, T., 2021. Spectral inference reveals principal cone-integration rules of the zebrafish inner retina. *Current Biology* 31, 5214–5226.e4. <https://doi.org/10.1016/j.cub.2021.09.047>
- Baudin, J., Angueyra, J.M., Sinha, R., Rieke, F., 2019. S-cone photoreceptors in the primate retina are functionally distinct from L and M cones. *eLife* 8. <https://doi.org/10.7554/eLife.39166>
- Behrens, C., Schubert, T., Haverkamp, S., Euler, T., Berens, P., 2016. Connectivity map of bipolar cells and photoreceptors in the mouse retina 20. <https://doi.org/10.7554/eLife.20041.001>
- Behrens, C., Zhang, Y., Yadav, S.C., Haverkamp, S., Irsen, S., Korympidou, M.M., Schaedler, A., Dedek, K., Smith, R.G., Euler, T., Berens, P., Schubert, T., 2019. Retinal horizontal cells use different synaptic sites for global feedforward and local feedback signaling (preprint). *Neuroscience*. <https://doi.org/10.1101/780031>
- Bennett, M.R., Farnell, L., Gibson, W.G., 2008. A Quantitative Model of Cortical Spreading Depression Due to Purinergic and Gap-Junction Transmission in Astrocyte Networks. *Biophysical Journal* 95, 5648–5660. <https://doi.org/10.1529/biophysj.108.137190>

- Bliss, T.V.P., Lømo, T., 1973. Long-lasting potentiation of synaptic transmission in the dentate area of the anaesthetized rabbit following stimulation of the perforant path. *The Journal of Physiology* 232, 331–356. <https://doi.org/10.1113/jphysiol.1973.sp010273>
- Boije, H., Shirazi Fard, S., Edqvist, P.-H., Hallböök, F., 2016. Horizontal Cells, the Odd Ones Out in the Retina, Give Insights into Development and Disease. *Frontiers in Neuroanatomy* 10. <https://doi.org/10.3389/fnana.2016.00077>
- Borst, A., 2000. Models of motion detection 1.
- Bowmaker, J.K., 2008. Evolution of vertebrate visual pigments. *Vision Research* 48, 2022–2041. <https://doi.org/10.1016/j.visres.2008.03.025>
- Bowmaker, J.K., 1977. The visual pigments, oil droplets and spectral sensitivity of the pigeon. *Vision Research* 17, 1129–1138. [https://doi.org/10.1016/0042-6989\(77\)90147-X](https://doi.org/10.1016/0042-6989(77)90147-X)
- Bowmaker, J.K., Knowles, A., 1977. The visual pigments and oil droplets of the chicken retina. *Vision Research* 17, 755–764. [https://doi.org/10.1016/0042-6989\(77\)90117-1](https://doi.org/10.1016/0042-6989(77)90117-1)
- Brackbill, N., Rhoades, C., Kling, A., Shah, N.P., Sher, A., Litke, A.M., Chichilnisky, E., 2020. Reconstruction of natural images from responses of primate retinal ganglion cells. *eLife* 9, e58516. <https://doi.org/10.7554/eLife.58516>
- Brombas, A., Kalita-de Croft, S., Cooper-Williams, E.J., Williams, S.R., 2017. Dendro-dendritic cholinergic excitation controls dendritic spike initiation in retinal ganglion cells. *Nature Communications* 8. <https://doi.org/10.1038/ncomms15683>
- Campbell, R.A.A., King, A.J., 2004. Auditory Neuroscience: A Time for Coincidence? *Current Biology* 14, R886–R888. <https://doi.org/10.1016/j.cub.2004.09.070>
- Chapot, C.A., Euler, T., Schubert, T., 2017. How do horizontal cells ‘talk’ to cone photoreceptors? Different levels of complexity at the cone-horizontal cell synapse: How do horizontal cells ‘talk’ to cone photoreceptors? *The Journal of Physiology* 595, 5495–5506. <https://doi.org/10.1113/JP274177>
- Chase, S.M., Young, E.D., 2007. First-spike latency information in single neurons increases when referenced to population onset. *Proceedings of the National Academy of Sciences* 104, 5175–5180. <https://doi.org/10.1073/pnas.0610368104>
- Chen, A., 2003. Chicken retinal ganglion cells response characteristics: multi-channel electrode recording study. *Science in China Series C* 46, 414. <https://doi.org/10.1360/02yc0053>
- Chen, Y., Naito, J., 1999. A Quantitative Analysis of Cells in the Ganglion Cell Layer of the Chick Retina. *Brain, Behavior and Evolution* 53, 75–86. <https://doi.org/10.1159/000006584>
- Chichilnisky, E.J., 2001. A simple white noise analysis of neuronal light responses 15.
- Coombs, J.S., Eccles, J.C., Fatt, P., 1955. The specific ionic conductances and the ionic movements across the motoneuronal membrane that produce the inhibitory post-synaptic potential. *The Journal of Physiology* 130, 326–373. <https://doi.org/10.1113/jphysiol.1955.sp005412>
- Country, M.W., 2017. Retinal metabolism: A comparative look at energetics in the retina. *Brain Research* 8.

- Cowan, C.S., Renner, M., De Gennaro, M., Gross-Scherf, B., Goldblum, D., Hou, Y., Munz, M., Rodrigues, T.M., Krol, J., Szikra, T., Cuttat, R., Walddt, A., Papasaikas, P., Diggelmann, R., Patino-Alvarez, C.P., Galliker, P., Spirig, S.E., Pavlinic, D., Gerber-Hollbach, N., Schuierer, S., Srdanovic, A., Balogh, M., Panero, R., Kusnyerik, A., Szabo, A., Stadler, M.B., Orgül, S., Picelli, S., Hasler, P.W., Hierlemann, A., Scholl, H.P.N., Roma, G., Nigsch, F., Roska, B., 2020. Cell Types of the Human Retina and Its Organoids at Single-Cell Resolution. *Cell* 182, 1623-1640.e34. <https://doi.org/10.1016/j.cell.2020.08.013>
- Cronin, T.W., 2014. Visual ecology. Princeton University Press, Princeton.
- Crook, J.D., Manookin, M.B., Packer, O.S., Dacey, D.M., 2011. Horizontal Cell Feedback without Cone Type-Selective Inhibition Mediates “Red-Green” Color Opponency in Midget Ganglion Cells of the Primate Retina. *Journal of Neuroscience* 31, 1762–1772. <https://doi.org/10.1523/JNEUROSCI.4385-10.2011>
- Crook, J.D., Peterson, B.B., Packer, O.S., Robinson, F.R., Troy, J.B., Dacey, D.M., 2008. Y-Cell Receptive Field and Collicular Projection of Parasol Ganglion Cells in Macaque Monkey Retina. *Journal of Neuroscience* 28, 11277–11291. <https://doi.org/10.1523/JNEUROSCI.2982-08.2008>
- da Silva, S., Cepko, C.L., 2017. Fgf8 Expression and Degradation of Retinoic Acid Are Required for Patterning a High-Acuity Area in the Retina. *Developmental Cell* 42, 68-81.e6. <https://doi.org/10.1016/j.devcel.2017.05.024>
- Dacey, D., 1993. The mosaic of midget ganglion cells in the human retina. *J. Neurosci.* 13, 5334–5355. <https://doi.org/10.1523/JNEUROSCI.13-12-05334.1993>
- Dacey, D.M., Lee, B.B., 1994. The “blue-on” opponent pathway in primate retina originates from a distinct bistratified ganglion cell type. *Nature* 367, 731–735. <https://doi.org/10.1038/367731a0>
- Dacey, D.M., Packer, O.S., 2003. Colour coding in the primate retina: diverse cell types and cone-specific circuitry. *Current Opinion in Neurobiology* 13, 421–427. [https://doi.org/10.1016/S0959-4388\(03\)00103-X](https://doi.org/10.1016/S0959-4388(03)00103-X)
- Delius, J.D., Delius, J.A.M., Lee, J.M., 2017. Symmetry recognition by pigeons: Generalized or not? *PLoS ONE* 12, e0187541. <https://doi.org/10.1371/journal.pone.0187541>
- DeVries, S.H., 2000. Bipolar Cells Use Kainate and AMPA Receptors to Filter Visual Information into Separate Channels. *Neuron* 28, 847–856. [https://doi.org/10.1016/S0896-6273\(00\)00158-6](https://doi.org/10.1016/S0896-6273(00)00158-6)
- Diedrich, E., Schaeffel, F., 2009. Spatial resolution, contrast sensitivity, and sensitivity to defocus of chicken retinal ganglion cells *in vitro*. *Visual Neuroscience* 26, 467–476. <https://doi.org/10.1017/S0952523809990253>
- Dolan, T., Fernández-Juricic, E., 2010. Retinal Ganglion Cell Topography of Five Species of Ground-Foraging Birds. *Brain, Behavior and Evolution* 75, 111–121. <https://doi.org/10.1159/000305025>
- Edqvist, P.-H.D., Lek, M., Boije, H., Lindbäck, S.M., Hallböök, F., 2008. Axon-bearing and axonless horizontal cell subtypes are generated consecutively during chick retinal development from progenitors that are sensitive to follistatin. *BMC Developmental Biology* 8, 46. <https://doi.org/10.1186/1471-213X-8-46>

- Ehrlich, D., 1989. Regional specialization of the chick retina as revealed by the size and density of neurons in the ganglion cell layer. *The Journal of Comparative Neurology* 195, 643–657. <https://doi.org/10.1002/cne.901950408>
- Enroth-Cugell, C., Robson, J.G., 1966. The contrast sensitivity of retinal ganglion cells of the cat. *The Journal of Physiology* 187, 517–552. <https://doi.org/10.1113/jphysiol.1966.sp008107>
- Eriksson, J., Larson, G., Gunnarsson, U., Bed'hom, B., Tixier-Boichard, M., 2008. Identification of the Yellow Skin Gene Reveals a Hybrid Origin of the Domestic Chicken. *PLoS Genetics* 4, 8.
- Euler, T., Haverkamp, S., Schubert, T., Baden, T., 2014. Retinal bipolar cells: elementary building blocks of vision. *Nature Reviews Neuroscience* 15, 507–519. <https://doi.org/10.1038/nrn3783>
- Evans, C.S., Evans, L., 1999. Chicken food calls are functionally referential. *Animal Behaviour* 58, 307–319. <https://doi.org/10.1006/anbe.1999.1143>
- Farkas, R.H., Qian, J., Goldberg, J.L., Quigley, H.A., Zack, D.J., 2004. Gene Expression Profiling of Purified Rat Retinal Ganglion Cells. *Invest. Ophthalmol. Vis. Sci.* 45, 2503. <https://doi.org/10.1167/iovs.03-1391>
- Farrow, K., Masland, R.H., 2011. Physiological clustering of visual channels in the mouse retina. *Journal of Neurophysiology* 105, 1516–1530. <https://doi.org/10.1152/jn.00331.2010>
- Feldkaemper, M.P., Schaeffel, F., 2002. Evidence for a potential role of glucagon during eye growth regulation in chicks. *Visual Neuroscience* 19, 755–766. <https://doi.org/10.1017/S0952523802196064>
- Field, G.D., Chichilnisky, E.J., 2007. Information Processing in the Primate Retina: Circuitry and Coding 32.
- Field, G.D., Gauthier, J.L., Sher, A., Greschner, M., Machado, T.A., Jepson, L.H., Shlens, J., Gunning, D.E., Mathieson, K., Dabrowski, W., Paninski, L., Litke, A.M., Chichilnisky, E.J., 2010. Functional connectivity in the retina at the resolution of photoreceptors. *Nature* 467, 673–677. <https://doi.org/10.1038/nature09424>
- Fischer, A.J., McGuire, J.J., Schaeffel, F., Stell, W.K., 1999. Light- and focus-dependent expression of the transcription factor ZENK in the chick retina. *Nature Neuroscience* 2, 706–712. <https://doi.org/10.1038/11167>
- Fischer, A.J., Stanke, J.J., Aloisio, G., Hoy, H., Stell, W.K., 2007. Heterogeneity of horizontal cells in the chicken retina. *The Journal of Comparative Neurology* 500, 1154–1171. <https://doi.org/10.1002/cne.21236>
- Fischer, A.J., Stell, W.K., 1999. Nitric oxide synthase-containing cells in the retina, pigmented epithelium, choroid, and sclera of the chick eye. *The Journal of Comparative Neurology* 405, 1–14. [https://doi.org/10.1002/\(SICI\)1096-9861\(19990301\)405:1<1::AID-CNE1>3.0.CO;2-U](https://doi.org/10.1002/(SICI)1096-9861(19990301)405:1<1::AID-CNE1>3.0.CO;2-U)
- Franke, K., Maia Chagas, A., Zhao, Z., Zimmermann, M.J., Bartel, P., Qiu, Y., Szatko, K.P., Baden, T., Euler, T., 2019. An arbitrary-spectrum spatial visual stimulator for vision research. *eLife* 8, e48779. <https://doi.org/10.7554/eLife.48779>
- Fumihito, A., Miyake, T., Sumi, S., Takada, M., Ohno, S., Kondo, N., 1994. One subspecies of the red junglefowl (*Gallus gallus gallus*) suffices as the matriarchic ancestor of all domestic breeds.

- Proceedings of the National Academy of Sciences 91, 12505–12509.
<https://doi.org/10.1073/pnas.91.26.12505>
- Gallego, A., Baron, M., Gayoso, M., 1975. Organization of the outer plexiform layer of the diurnal and nocturnal bird retinae. *Vision Research* 15, 1027-1037.
[https://doi.org/10.1016/0042-6989\(75\)90246-1](https://doi.org/10.1016/0042-6989(75)90246-1)
- Gehring, W.J., Ikeya, K., 1999. Pax 6: mastering eye morphogenesis and eye evolution. *Trends in Genetics* 15, 371–377. [https://doi.org/10.1016/S0168-9525\(99\)01776-X](https://doi.org/10.1016/S0168-9525(99)01776-X)
- Gisbert, S., Schaeffel, F., 2018. M to L cone ratios determine eye sizes and baseline refractions in chickens. *Experimental Eye Research* 172, 104–111.
<https://doi.org/10.1016/j.exer.2018.03.029>
- Goetz, J., Jessen, Z.F., Jacobi, A., Mani, A., Cooler, S., Greer, D., Segal, J., Shekhar, K., Sanes, J., Schwartz, G.W., 2021. Unified classification of mouse retinal ganglion cells using function, morphology, and gene expression 29.
- Goldsmith, T.H., Collins, J.S., Licht, S., 1984. The cone oil droplets of avian retinas. *Vision Research* 24, 1661–1671. [https://doi.org/10.1016/0042-6989\(84\)90324-9](https://doi.org/10.1016/0042-6989(84)90324-9)
- Govardovskii, V.I., Fyhrquist, N., Reuter, T., Kuzmin, D.G., Donner, K., 2000. In search of the visual pigment template. *Visual Neuroscience* 17, 509–528.
<https://doi.org/10.1017/S0952523800174036>
- Graef, K., 2017. Verarbeitung von Defokussierung durch retinale Ganglienzellen beim Haushuhn. PhD Thesis 128.
- Grünert, U., Martin, P.R., 2020. Cell types and cell circuits in human and non-human primate retina. *Progress in Retinal and Eye Research* 78, 100844.
<https://doi.org/10.1016/j.preteyeres.2020.100844>
- Günther, A., Dedek, K., Haverkamp, S., Irsen, S., Briggman, K.L., Mouritsen, H., 2021. Double Cones and the Diverse Connectivity of Photoreceptors and Bipolar Cells in an Avian Retina. *J. Neurosci.* 41, 5015–5028. <https://doi.org/10.1523/JNEUROSCI.2495-20.2021>
- Hamill, O.P., Marty, A., Neher, E., Sakmann, B., Sigworth, F.J., 1981. Improved patch-clamp techniques for high-resolution current recording from cells and cell-free membrane patches. *Pflügers Arch - Eur J Physiol* 391, 85–100. <https://doi.org/10.1007/BF00656997>
- Hart, N.S., 2001. The visual ecology of avian photoreceptors. *Progress in Retinal and Eye Research* 20, 675–703. [https://doi.org/10.1016/S1350-9462\(01\)00009-X](https://doi.org/10.1016/S1350-9462(01)00009-X)
- Hart, N.S., Lisney, T.J., Collin, S.P., 2006. Cone photoreceptor oil droplet pigmentation is affected by ambient light intensity. *Journal of Experimental Biology* 209, 4776–4787.
<https://doi.org/10.1242/jeb.02568>
- Hart, N.S., Vorobyev, M., 2005. Modelling oil droplet absorption spectra and spectral sensitivities of bird cone photoreceptors. *Journal of Comparative Physiology A: Neuroethology, Sensory, Neural, and Behavioral Physiology* 191, 381–392. <https://doi.org/10.1007/s00359-004-0595-3>

- Hartline, H.K., 1938. THE RESPONSE OF SINGLE OPTIC NERVE FIBERS OF THE VERTEBRATE EYE TO ILLUMINATION OF THE RETINA. *American Journal of Physiology-Legacy Content* 121, 400–415. <https://doi.org/10.1152/ajplegacy.1938.121.2.400>
- Heesy, C.P., Hall, M.I., 2010. The Nocturnal Bottleneck and the Evolution of Mammalian Vision. *Brain Behav Evol* 75, 195–203. <https://doi.org/10.1159/000314278>
- Hilgen, G., Kartsaki, E., Kartysh, V., Cessac, B., Sernagor, E., 2022. A novel approach to the functional classification of retinal ganglion cells. *Open Biol.* 12, 210367. <https://doi.org/10.1098/rsob.210367>
- Hilgen, G., Pirmoradian, S., Pamplona, D., Kornprobst, P., Cessac, B., Hennig, M.H., Sernagor, E., 2017a. Pan-retinal characterisation of Light Responses from Ganglion Cells in the Developing Mouse Retina. *Scientific Reports* 7. <https://doi.org/10.1038/srep42330>
- Hilgen, G., Sorbaro, M., Pirmoradian, S., Muthmann, J.-O., Kepiro, I.E., Ullo, S., Ramirez, C.J., Puente Encinas, A., Maccione, A., Berdondini, L., Murino, V., Sona, D., Cella Zanacchi, F., Sernagor, E., Hennig, M.H., 2017b. Unsupervised Spike Sorting for Large-Scale, High-Density Multielectrode Arrays. *Cell Reports* 18, 2521–2532. <https://doi.org/10.1016/j.celrep.2017.02.038>
- Hodgkin, A.L., Huxley, A.F., 1952. A quantitative description of membrane current and its application to conduction and excitation in nerve. *The Journal of Physiology* 117, 500–544. <https://doi.org/10.1113/jphysiol.1952.sp004764>
- Hubel, D.H., Wiesel, T.N., 1959. Receptive fields of single neurones in the cat's striate cortex. *The Journal of Physiology* 148, 574–591. <https://doi.org/10.1113/jphysiol.1959.sp006308>
- Johnson, K.O., Hsiao, S.S., Yoshioka, T., 2002. Review: Neural Coding and the Basic Law of Psychophysics. *Neuroscientist* 8, 111–121. <https://doi.org/10.1177/107385840200800207>
- Jones, C.D., Osorio, D., 2004. Discrimination of oriented visual textures by poultry chicks. *Vision Research* 44, 83–89. <https://doi.org/10.1016/j.visres.2003.08.014>
- Jones, I.L., Russell, T.L., Farrow, K., Fiscella, M., Franke, F., Müller, J., Jäckel, D., Hierlemann, A., 2015. A method for electrophysiological characterization of hamster retinal ganglion cells using a high-density CMOS microelectrode array. *Frontiers in Neuroscience* 9, 1–16. <https://doi.org/10.3389/fnins.2015.00360>
- Jouty, J., Hilgen, G., Sernagor, E., Hennig, M.H., 2018. Non-parametric physiological classification of retinal ganglion cells in the mouse retina. <https://doi.org/10.1101/407635>
- Kalloniatis, M., Fletcher, E.L., 1993. Immunocytochemical localization of the amino acid neurotransmitters in the chicken retina. *The Journal of Comparative Neurology* 336, 174–193. <https://doi.org/10.1002/cne.903360203>
- Kanginakudru, S., Metta, M., Jakati, R., Nagaraju, J., 2008. Genetic evidence from Indian red jungle fowl corroborates multiple domestication of modern day chicken. *BMC Evolutionary Biology* 8, 174. <https://doi.org/10.1186/1471-2148-8-174>
- Kelber, A., 2019. Bird colour vision – from cones to perception. *Current Opinion in Behavioral Sciences* 30, 34–40. <https://doi.org/10.1016/j.cobeha.2019.05.003>

- Klee, M.R., Pierau, F.-K., Faber, D.S., 1974. Temperature effects on resting potential and spike parameters of cat motoneurons. *Exp Brain Res* 19. <https://doi.org/10.1007/BF00236112>
- Kolb, H., Marshak, D., 2003. The midget pathways of the primate retina 106, 15.
- Kölsch, Y., Hahn, J., Sappington, A., Stemmer, M., Fernandes, A.M., Helmbrecht, T.O., Lele, S., Butrus, S., Laurell, E., Arnold-Ammer, I., Shekhar, K., Sanes, J.R., Baier, H., 2021. Molecular classification of zebrafish retinal ganglion cells links genes to cell types to behavior. *Neuron* 109, 645-662.e9. <https://doi.org/10.1016/j.neuron.2020.12.003>
- König, P., Engel, A.K., Singer, W., 1996. Integrator or coincidence detector? The role of the cortical neuron revisited. *Trends in Neurosciences* 19, 130–137. [https://doi.org/10.1016/S0166-2236\(96\)80019-1](https://doi.org/10.1016/S0166-2236(96)80019-1)
- Kram, Y.A., Mantey, S., Corbo, J.C., 2010. Avian cone photoreceptors tile the retina as five independent, self-organizing mosaics. *PLoS ONE* 5. <https://doi.org/10.1371/journal.pone.0008992>
- Krauss, A., Neumeier, C., 2003. Wavelength dependence of the optomotor response in zebrafish (*Danio rerio*). *Vision Research* 43, 1275–1284. [https://doi.org/10.1016/S0042-6989\(03\)00090-7](https://doi.org/10.1016/S0042-6989(03)00090-7)
- Krieger, B., Qiao, M., Rousso, D.L., Sanes, J.R., Meister, M., 2017. Four alpha ganglion cell types in mouse retina: Function, structure, and molecular signatures. *PLoS ONE* 12, e0180091. <https://doi.org/10.1371/journal.pone.0180091>
- Kuffler, S.W., 1953. DISCHARGE PATTERNS AND FUNCTIONAL ORGANIZATION OF MAMMALIAN RETINA. *Journal of Neurophysiology* 16, 37–68. <https://doi.org/10.1152/jn.1953.16.1.37>
- Laboissonniere, L.A., Goetz, J.J., Martin, G.M., Bi, R., Lund, T.J.S., Ellson, L., Lynch, M.R., Mooney, B., Wickham, H., Liu, P., Schwartz, G.W., Trimarchi, J.M., 2019. Molecular signatures of retinal ganglion cells revealed through single cell profiling. *Sci Rep* 9, 15778. <https://doi.org/10.1038/s41598-019-52215-4>
- Lamb, T.D., 2019. Evolution of the genes mediating phototransduction in rod and cone photoreceptors. *Progress in Retinal and Eye Research* 100823. <https://doi.org/10.1016/j.preteyeres.2019.100823>
- Lamb, T.D., 2016. Why rods and cones? *Eye* 30, 179–185. <https://doi.org/10.1038/eye.2015.236>
- Lamb, T.D., Collin, S.P., Pugh, E.N., 2007. Evolution of the vertebrate eye: opsins, photoreceptors, retina and eye cup. *Nature Reviews Neuroscience* 8, 960–976. <https://doi.org/10.1038/nrn2283>
- Lefebvre, P.C., Seifert, M., Stumpner, A., 2018. Auditory DUM neurons in a bush-cricket: A filter bank for carrier frequency. *Journal of Comparative Neurology* 526, 1166–1182. <https://doi.org/10.1002/cne.24399>
- Li, Y.N., Matsui, J.I., Dowling, J.E., 2009. Specificity of the horizontal cell-photoreceptor connections in the zebrafish (*Danio rerio*) retina. *The Journal of Comparative Neurology* 516, 442–453. <https://doi.org/10.1002/cne.22135>

- Lindstrom, S.H., Nacsa, N., Blankenship, T., Fitzgerald, P.G., Weller, C., Vaney, D.I., Wilson, M., 2009. Distribution and structure of efferent synapses in the chicken retina. *Visual Neuroscience* 26, 215–226. <https://doi.org/10.1017/S0952523809090063>
- Lisney, T.J., Ekesten, B., Tauson, R., Håstad, O., Ödeen, A., 2012. Using electroretinograms to assess flicker fusion frequency in domestic hens *Gallus gallus domesticus*. *Vision Research* 62, 125–133. <https://doi.org/10.1016/j.visres.2012.04.002>
- Lisney, T.J., Rubene, D., Rózsa, J., Løvlie, H., Håstad, O., Ödeen, A., 2011. Behavioural assessment of flicker fusion frequency in chicken *Gallus gallus domesticus*. *Vision Research* 51, 1324–1332. <https://doi.org/10.1016/j.visres.2011.04.009>
- López-López, R., López-Gallardo, M., Pérez-Álvarez, M.J., Prada, C., 2008. Isolation of chick retina cones and study of their diversity based on oil droplet colour and nucleus position. *Cell and Tissue Research* 332, 13–24. <https://doi.org/10.1007/s00441-007-0572-6>
- Maloney, L.T., 1986. Evaluation of linear models of surface spectral reflectance with small numbers of parameters. *J. Opt. Soc. Am. A* 3, 1673. <https://doi.org/10.1364/JOSAA.3.001673>
- Mankowska, N.D., Marcinkowska, A.B., Waskow, M., Sharma, R.I., Kot, J., Winklewski, P.J., 2021. Critical Flicker Fusion Frequency: A Narrative Review. *Medicina* 57, 1096. <https://doi.org/10.3390/medicina57101096>
- Mariani, A.P., 1987. Neuronal and synaptic organization of the outer plexiform layer of the pigeon retina. *American Journal of Anatomy* 179, 25–39. <https://doi.org/10.1002/aja.1001790105>
- Mariani, A.P., Leure-Dupree, A.E., 1978. Photoreceptors and oil droplet colors in the red area of the pigeon retina. *The Journal of Comparative Neurology* 182, 821–837. <https://doi.org/10.1002/cne.901820506>
- Martin, G.R., 2017. What Drives Bird Vision? Bill Control and Predator Detection Overshadow Flight. *Frontiers in Neuroscience* 11. <https://doi.org/10.3389/fnins.2017.00619>
- Martins-Ferreira, H., Nedergaard, M., Nicholson, C., 2000. Perspectives on spreading depression. *Brain Research Reviews* 32, 215–234. [https://doi.org/10.1016/S0165-0173\(99\)00083-1](https://doi.org/10.1016/S0165-0173(99)00083-1)
- Masland, R.H., 2012. The Neuronal Organization of the Retina. *Neuron* 76, 266–280. <https://doi.org/10.1016/j.neuron.2012.10.002>
- Masland, R.H., 2001. The fundamental plan of the retina. *Nature Neuroscience* 4, 877–886. <https://doi.org/10.1038/nn0901-877>
- Mathis, U., Schaeffel, F., 2007. Glucagon-related peptides in the mouse retina and the effects of deprivation of form vision. *Graefes' Archive for Clinical and Experimental Ophthalmology* 245, 267–275. <https://doi.org/10.1007/s00417-006-0282-x>
- McMains, E., Krishnan, V., Prasad, S., Gleason, E., 2011. Expression and Localization of CLC Chloride Transport Proteins in the Avian Retina. *PLoS ONE* 6, e17647. <https://doi.org/10.1371/journal.pone.0017647>
- Meier, A., Nelson, R., Connaughton, V.P., 2018. Color Processing in Zebrafish Retina. *Frontiers in Cellular Neuroscience* 12. <https://doi.org/10.3389/fncel.2018.00327>

- Meister, M., 1996. Multineuronal codes in retinal signaling. *Proc. Natl. Acad. Sci. U.S.A.* 93, 609–614. <https://doi.org/10.1073/pnas.93.2.609>
- Meister, M., Berry, M.J., 1999. The Neural Code of the Retina. *Neuron* 22, 435–450. [https://doi.org/10.1016/S0896-6273\(00\)80700-X](https://doi.org/10.1016/S0896-6273(00)80700-X)
- Miles, F.A., 1972. Centrifugal control of the avian retina. I. Receptive field properties of retinal ganglion cells. *Brain Research* 48, 65–92. [https://doi.org/10.1016/0006-8993\(72\)90171-0](https://doi.org/10.1016/0006-8993(72)90171-0)
- Millar, T., Ishimoto, I., Johnson, C.D., Epstein, M.L., Chubb, I.W., Morgan, I.G., 1985. Cholinergic and acetylcholinesterase-containing neurons of the chicken retina. *Neuroscience Letters* 61, 311–316. [https://doi.org/10.1016/0304-3940\(85\)90482-3](https://doi.org/10.1016/0304-3940(85)90482-3)
- Millar, T.J., Ishimoto, I., Chubb, I.W., Epstein, M.L., Johnson, C.D., Morgan, I.G., 1987. Cholinergic amacrine cells of the chicken retina: A light and electron microscope immunocytochemical study. *Neuroscience* 21, 725–743. [https://doi.org/10.1016/0306-4522\(87\)90033-9](https://doi.org/10.1016/0306-4522(87)90033-9)
- Mitkus, M., Olsson, P., Toomey, M.B., Corbo, J.C., Kelber, A., 2017. Specialized photoreceptor composition in the raptor fovea. *Journal of Comparative Neurology* 525, 2152–2163. <https://doi.org/10.1002/cne.24190>
- Mollon, J.D., 1989. The uses and origins of primate colour vision. *The company of biologists limited* 146, 20.
- Morgan, I.G., 1983. The Organization of Amacrine Cell Types Which Use Different Transmitters in Chicken Retina, in: *Progress in Brain Research*. Elsevier, pp. 191–199. [https://doi.org/10.1016/S0079-6123\(08\)60020-5](https://doi.org/10.1016/S0079-6123(08)60020-5)
- Morris, V.B., 1982. An afoveate area centralis in the chick retina. *The Journal of Comparative Neurology* 210, 198–203. <https://doi.org/10.1002/cne.902100210>
- Morris, V.B., Shorey, C.D., 1967. An electron microscope study of types of receptor in the chick retina. *The Journal of Comparative Neurology* 129, 313–339. <https://doi.org/10.1002/cne.901290404>
- Mulansky, M., Kreuz, T., 2016. PySpike—A Python library for analyzing spike train synchrony. *SoftwareX* 5, 183–189. <https://doi.org/10.1016/j.softx.2016.07.006>
- Naito, J., Chen, Y., 2004a. Morphologic analysis and classification of ganglion cells of the chick retina by intracellular injection of lucifer yellow and retrograde labeling with Dil. *The Journal of Comparative Neurology* 469, 360–376. <https://doi.org/10.1002/cne.11010>
- Naito, J., Chen, Y., 2004b. Morphological features of chick retinal ganglion cells. *Anatomical Science International* 79, 213–225. <https://doi.org/10.1111/j.1447-073x.2004.00084.x>
- Nakanishi, T., Norris, F.H., 1970. Effect of local temperature on the resting membrane potential in rat muscle. *Electroencephalography and Clinical Neurophysiology* 28, 633–636. [https://doi.org/10.1016/0013-4694\(70\)90206-3](https://doi.org/10.1016/0013-4694(70)90206-3)
- Nedergaard, M., Cooper, A.J.L., Goldman, S.A., 1995. Gap junctions are required for the propagation of spreading depression. *J. Neurobiol.* 28, 433–444. <https://doi.org/10.1002/neu.480280404>

- Nelson, R., Connaughton, V., 2012. Bipolar Cell Pathways in the Vertebrate Retina, in: Webvision: The Organization of the Retina and Visual System [Internet]. Kolb H, Fernandez E, Nelson R.
- Nilsson, D.-E., 2013. Eye evolution and its functional basis. *Vis Neurosci* 30, 5–20. <https://doi.org/10.1017/S0952523813000035>
- Nilsson, D.-E., Arendt, D., 2008. Eye Evolution: The Blurry Beginning. *Current Biology* 18, R1096–R1098. <https://doi.org/10.1016/j.cub.2008.10.025>
- Niven, J.E., Laughlin, S.B., 2008. Energy limitation as a selective pressure on the evolution of sensory systems. *Journal of Experimental Biology* 211, 1792–1804. <https://doi.org/10.1242/jeb.017574>
- Noë, A., 2006. Action in perception, 1. MIT Press paperback ed. ed, Representation and mind. MIT Press, Cambridge, Mass.
- Okano, T., Fukada, Y., Artamonov, I.D., Yoshizawa, T., 1989. Purification of cone visual pigments from chicken retina. *Biochemistry* 28, 8848–8856. <https://doi.org/10.1021/bi00448a025>
- Okano, T., Kojima, D., Fukada, Y., Shichida, Y., Yoshizawa, T., 1992. Primary structures of chicken cone visual pigments: vertebrate rhodopsins have evolved out of cone visual pigments. *Proceedings of the National Academy of Sciences* 89, 5932–5936. <https://doi.org/10.1073/pnas.89.13.5932>
- Olsson, P., Lind, O., Kelber, A., 2015. Bird colour vision: behavioural thresholds reveal receptor noise. *Journal of Experimental Biology* 218, 184–193. <https://doi.org/10.1242/jeb.111187>
- Osorio, D., Miklósi, A., Gonda, Zs., 1999. Visual Ecology and Perception of Coloration Patterns by Domestic Chicks. *Evolutionary Ecology* 13, 673–689. <https://doi.org/10.1023/A:1011059715610>
- Osorio, D., Vorobyev, M., 2008. A review of the evolution of animal colour vision and visual communication signals. *Vision Research* 48, 2042–2051. <https://doi.org/10.1016/j.visres.2008.06.018>
- Pang, J.-J., Gao, F., Wu, S.M., 2007. Cross-talk between ON and OFF channels in the salamander retina: Indirect bipolar cell inputs to ON–OFF ganglion cells. *Vision Research* 47, 384–392. <https://doi.org/10.1016/j.visres.2006.09.021>
- Pang, J.-J., Gao, F., Wu, S.M., 2002. Relative contributions of bipolar cell and amacrine cell inputs to light responses of ON, OFF and ON–OFF retinal ganglion cells. *Vision Research* 42, 19–27. [https://doi.org/10.1016/S0042-6989\(01\)00258-9](https://doi.org/10.1016/S0042-6989(01)00258-9)
- Patterson, S.S., Neitz, M., Neitz, J., 2019. Reconciling Color Vision Models With Midget Ganglion Cell Receptive Fields. *Front. Neurosci.* 13, 865. <https://doi.org/10.3389/fnins.2019.00865>
- Pearlman, A.L., Hughes, C.P., 1976. Functional role of efferents to the avian retina. II. Effects of reversible cooling of the isthmo-optic nucleus. *The Journal of Comparative Neurology* 166, 123–131. <https://doi.org/10.1002/cne.901660109>

- Peichel, L., Wässel, A., 1981. Morphological identification of on- and off-centre brisk transient (Y) cells in the cat retina. *Proc. R. Soc. Lond. B.* 212, 139–153.
<https://doi.org/10.1098/rspb.1981.0030>
- Pignatelli, V., Champ, C., Marshall, J., Vorobyev, M., 2010. Double cones are used for colour discrimination in the reef fish, *Rhinecanthus aculeatus*. *Biology Letters* 6, 537–539.
<https://doi.org/10.1098/rsbl.2009.1010>
- Portelli, G., Barrett, J.M., Hilgen, G., Masquelier, T., Maccione, A., Di Marco, S., Berdondini, L., Kornprobst, P., Sernagor, E., 2016. Rank Order Coding: a Retinal Information Decoding Strategy Revealed by Large-Scale Multielectrode Array Retinal Recordings. *eneuro* 3, ENEURO.0134-15.2016. <https://doi.org/10.1523/ENEURO.0134-15.2016>
- Potier, S., Mitkus, M., Kelber, A., 2018. High resolution of colour vision, but low contrast sensitivity in a diurnal raptor. *Proceedings of the Royal Society B: Biological Sciences* 285, 20181036. <https://doi.org/10.1098/rspb.2018.1036>
- Querubin, A., Lee, H.R., Provis, J.M., O'Brien, K.M.B., 2009. Photoreceptor and ganglion cell topographies correlate with information convergence and high acuity regions in the adult pigeon (*Columba livia*) retina. *The Journal of Comparative Neurology* 517, 711–722.
<https://doi.org/10.1002/cne.22178>
- Quesada, A., Génis-Gálvez, J.M., 1985. Morphological and structural study of Landolt's club in the chick retina: LANDOLT'S CLUB IN CHICK RETINA. *Journal of Morphology* 184, 205–214.
<https://doi.org/10.1002/jmor.1051840210>
- Quesada, A., Prada, F.A., Genis-Galvez, J.M., 1988. Bipolar cells in the chicken retina. *Journal of Morphology* 197, 337–351. <https://doi.org/10.1002/jmor.1051970308>
- Quinn, N., Csincsik, L., Flynn, E., Curcio, C.A., Kiss, S., Saddy, S.R., Hogg, R., Peto, T., Lengyel, I., 2019. The clinical relevance of visualising the peripheral retina. *Progress in Retinal and Eye Research* 68, 83–109. <https://doi.org/10.1016/j.preteyeres.2018.10.001>
- Randall, W.C., Hiestand, W.A., 1939. PANTING AND TEMPERATURE REGULATION IN THE CHICKEN. *American Journal of Physiology-Legacy Content* 127, 761–767.
<https://doi.org/10.1152/ajplegacy.1939.127.4.761>
- Reinhard, K., Münch, T.A., 2021. Visual properties of human retinal ganglion cells. *PLoS ONE* 16, e0246952. <https://doi.org/10.1371/journal.pone.0246952>
- Reinhard, K., Tikidji-Hamburyan, A., Seitter, H., Idrees, S., Mutter, M., Benkner, B., Münch, T.A., 2014. Step-By-Step Instructions for Retina Recordings with Perforated Multi Electrode Arrays. *PLoS ONE* 9, e106148. <https://doi.org/10.1371/journal.pone.0106148>
- Repérant, J., Ward, R., Miceli, D., Rio, J.P., Médina, M., Kenigfest, N.B., Vesselkin, N.P., 2006. The centrifugal visual system of vertebrates: A comparative analysis of its functional anatomical organization. *Brain Research Reviews* 52, 1–57.
<https://doi.org/10.1016/j.brainresrev.2005.11.008>
- Rheume, B.A., Jereen, A., Bolisetty, M., Sajid, M.S., Yang, Y., Renna, K., Sun, L., Robson, P., Trakhtenberg, E.F., 2018. Single cell transcriptome profiling of retinal ganglion cells identifies cellular subtypes. *Nat Commun* 9, 2759. <https://doi.org/10.1038/s41467-018-05134-3>

- Rocha, F.A.F., Saito, C.A., Silveira, L.C.L., De Souza, J.M., Ventura, D.F., 2008. Twelve chromatically opponent ganglion cell types in turtle retina. *Vis Neurosci* 25, 307–315. <https://doi.org/10.1017/S0952523808080516>
- Rubene, D., Hastad, O., Tauson, R., Wall, H., Odeen, A., 2010. The presence of UV wavelengths improves the temporal resolution of the avian visual system. *Journal of Experimental Biology* 213, 3357–3363. <https://doi.org/10.1242/jeb.042424>
- Ruderman, D.L., Cronin, T.W., Chiao, C.-C., 1998. Statistics of cone responses to natural images: implications for visual coding. *J. Opt. Soc. Am. A* 15, 2036. <https://doi.org/10.1364/JOSAA.15.002036>
- Sanes, J.R., Masland, R.H., 2015. The Types of Retinal Ganglion Cells: Current Status and Implications for Neuronal Classification. *Annu. Rev. Neurosci.* 38, 221–246. <https://doi.org/10.1146/annurev-neuro-071714-034120>
- Schaeffel, F., Rohrer, B., Lemmer, T., Zrenner, E., 1991. Diurnal control of rod function in the chicken. *Vis. Neurosci.* 6, 641–653. <https://doi.org/10.1017/s0952523800002637>
- Seifert, M., Baden, T., Osorio, D., 2020. The retinal basis of vision in chicken. *Seminars in Cell & Developmental Biology.* <https://doi.org/10.1016/j.semcdb.2020.03.011>
- Shatillo, A., Salo, R.A., Giniatullin, R., Gröhn, O.H., 2015. Involvement of NMDA receptor subtypes in cortical spreading depression in rats assessed by fMRI. *Neuropharmacology* 93, 164–170. <https://doi.org/10.1016/j.neuropharm.2015.01.028>
- Sinha, R., Hoon, M., Baudin, J., Okawa, H., Wong, R.O.L., Rieke, F., 2017. Cellular and Circuit Mechanisms Shaping the Perceptual Properties of the Primate Fovea. *Cell* 168, 413-426.e12. <https://doi.org/10.1016/j.cell.2017.01.005>
- Smith, R.L., Nishimura, Y., Raviola, G., 1985. Interreceptor junction in the double cone of the chicken retina. *J. Submicrosc. Cytol.* 17, 183–186.
- Stavenga, D.G., Wilts, B.D., 2014. Oil droplets of bird eyes: Microlenses acting as spectral filters. *Philosophical Transactions of the Royal Society B: Biological Sciences* 369. <https://doi.org/10.1098/rstb.2013.0041>
- Stett, A., Barth, W., Weiss, S., Haemmerle, H., Zrenner, E., 2000. Electrical multisite stimulation of the isolated chicken retina. *Vision Research* 40, 1785–1795. [https://doi.org/10.1016/S0042-6989\(00\)00005-5](https://doi.org/10.1016/S0042-6989(00)00005-5)
- Storey, A.A., Athens, J.S., Bryant, D., Carson, M., Emery, K., deFrance, S., Higham, C., Huynen, L., Intoh, M., Jones, S., Kirch, P.V., Ladefoged, T., McCoy, P., Morales-Muñiz, A., Quiroz, D., Reitz, E., Robins, J., Walter, R., Matisoo-Smith, E., 2012. Investigating the Global Dispersal of Chickens in Prehistory Using Ancient Mitochondrial DNA Signatures. *PLoS ONE* 7, e39171. <https://doi.org/10.1371/journal.pone.0039171>
- Sun, H., Crossland, W.J., 2000. Quantitative assessment of localization and colocalization of glutamate, aspartate, glycine, and GABA immunoreactivity in the chick retina. *The Anatomical Record* 260, 158–179. [https://doi.org/10.1002/1097-0185\(20001001\)260:2<158::AID-AR60>3.0.CO;2-V](https://doi.org/10.1002/1097-0185(20001001)260:2<158::AID-AR60>3.0.CO;2-V)
- Sun, H.-J., Frost, B.J., 1997. Motion processing in pigeon tectum: equiluminant chromatic mechanisms: *Experimental Brain Research* 116, 434–444. <https://doi.org/10.1007/PL00005771>

- Sun, W., Deng, Q., Levick, W.R., He, S., 2006. ON direction-selective ganglion cells in the mouse retina: ON DSGCs in the mouse retina. *The Journal of Physiology* 576, 197–202. <https://doi.org/10.1113/jphysiol.2006.115857>
- Tadano, R., Kinoshita, K., Mizutani, M., Tsudzuki, M., 2014. Comparison of microsatellite variations between Red Junglefowl and a commercial chicken gene pool. *Poultry Science* 93, 318–325. <https://doi.org/10.3382/ps.2013-03547>
- Tanabe, K., 2006. Cadherin is required for dendritic morphogenesis and synaptic terminal organization of retinal horizontal cells. *Development* 133, 4085–4096. <https://doi.org/10.1242/dev.02566>
- Thoreson, W.B., Mangel, S.C., 2012. Lateral interactions in the outer retina. *Progress in Retinal and Eye Research* 31, 407–441. <https://doi.org/10.1016/j.preteyeres.2012.04.003>
- Toomey, M.B., Collins, A.M., Frederiksen, R., Cornwall, M.C., Timlin, J.A., Corbo, J.C., 2015. A complex carotenoid palette tunes avian colour vision. *Journal of The Royal Society Interface* 12, 20150563. <https://doi.org/10.1098/rsif.2015.0563>
- Torrente, D., Mendes-da-Silva, R.F., Lopes, A.A.C., González, J., Barreto, G.E., Guedes, R.C.A., 2014. Increased calcium influx triggers and accelerates cortical spreading depression in vivo in male adult rats. *Neuroscience Letters* 558, 87–90. <https://doi.org/10.1016/j.neulet.2013.11.004>
- v. Campenhausen, M., Kirschfeld, K., 1998. Spectral sensitivity of the accessory optic system of the pigeon. *Journal of Comparative Physiology A: Sensory, Neural, and Behavioral Physiology* 183, 1–6. <https://doi.org/10.1007/s003590050229>
- van Hateren, J.H., 1993. Spatial, temporal and spectral pre-processing for colour vision. *Proc. R. Soc. Lond. B* 251, 61–68. <https://doi.org/10.1098/rspb.1993.0009>
- Van Wyk, M., Wässle, H., Taylor, W.R., 2009. Receptive field properties of ON- and OFF-ganglion cells in the mouse retina. *Vis Neurosci* 26, 297–308. <https://doi.org/10.1017/S0952523809990137>
- Ventura, D.F., 2001. Ultraviolet colour opponency 8.
- Verkhatsky, A., Krishtal, O.A., Petersen, O.H., 2006. From Galvani to patch clamp: the development of electrophysiology. *Pflugers Arch - Eur J Physiol* 453, 233–247. <https://doi.org/10.1007/s00424-006-0169-z>
- Victor, J.D., 2005. Analyzing receptive fields, classification images and functional images: challenges with opportunities for synergy. *Nature Neuroscience* 8, 1651–1656. <https://doi.org/10.1038/nn1607>
- Volgyi, B., 2004. Convergence and Segregation of the Multiple Rod Pathways in Mammalian Retina. *Journal of Neuroscience* 24, 11182–11192. <https://doi.org/10.1523/JNEUROSCI.3096-04.2004>
- Wahlin, K.J., Hackler, L., Adler, R., Zack, D.J., 2010. Alternative splicing of neuroligin and its protein distribution in the outer plexiform layer of the chicken retina. *The Journal of Comparative Neurology* 518, 4938–4962. <https://doi.org/10.1002/cne.22499>

- Wai, M.S.M., Lorke, D.E., Kung, L.S., Yew, D.T.W., 2006. Morphogenesis of the different types of photoreceptors of the chicken (*Gallus domesticus*) retina and the effect of amblyopia in neonatal chicken. *Microscopy Research and Technique* 69, 99–107.
<https://doi.org/10.1002/jemt.20279>
- Wai, S.M., Kung, L.S., Yew, D.T., 2002. Novel Identification of the Different Types of Cones in the Retina of the Chicken. *Cellular and Molecular Neurobiology* 8.
- Waldner, D.M., Visser, F., Fischer, A.J., Bech-Hansen, N.T., Stell, W.K., 2019. Avian Adeno-Associated Viral Transduction of the Postembryonic Chicken Retina. *Translational Vision Science & Technology* 8, 1. <https://doi.org/10.1167/tvst.8.4.1>
- Walls, G.L., 1942. The vertebrate eye and its adaptive radiation [by] Gordon Lynn Walls. Cranbrook Institute of Science, Bloomfield Hills, Mich.,. <https://doi.org/10.5962/bhl.title.7369>
- Wang, M.M., Janz, R., Belizaire, R., Frishman, L.J., Sherry, D.M., 2003. Differential distribution and developmental expression of synaptic vesicle protein 2 isoforms in the mouse retina. *J. Comp. Neurol.* 460, 106–122. <https://doi.org/10.1002/cne.10636>
- Wang, M.-S., Zhang, R., Su, L.-Y., Li, Y., Peng, M.-S., Liu, H.-Q., Zeng, L., Irwin, D.M., Du, J.-L., Yao, Y.-G., Wu, D.-D., Zhang, Y.-P., 2016. Positive selection rather than relaxation of functional constraint drives the evolution of vision during chicken domestication. *Cell Research* 26, 556–573. <https://doi.org/10.1038/cr.2016.44>
- Warrant, E.J., Nilsson, D.-E., 1998. Absorption of white light in photoreceptors. *Vision Research* 38, 195–207. [https://doi.org/10.1016/S0042-6989\(97\)00151-X](https://doi.org/10.1016/S0042-6989(97)00151-X)
- Wässle, H., 2004. Parallel processing in the mammalian retina. *Nat Rev Neurosci* 5, 747–757. <https://doi.org/10.1038/nrn1497>
- Weller, C., Lindstrom, S.H., De Grip, W.J., Wilson, M., 2009. The area centralis in the chicken retina contains efferent target amacrine cells. *Visual Neuroscience* 26, 249–254. <https://doi.org/10.1017/S0952523808080917>
- Wells-Gray, E.M., Choi, S.S., Bries, A., Doble, N., 2016. Variation in rod and cone density from the fovea to the mid-periphery in healthy human retinas using adaptive optics scanning laser ophthalmoscopy. *Eye* 30, 1135–1143. <https://doi.org/10.1038/eye.2016.107>
- Weng, S., Sun, W., He, S., 2005. Identification of ON-OFF direction-selective ganglion cells in the mouse retina: ON-OFF DSGCs in the mouse retina. *The Journal of Physiology* 562, 915–923. <https://doi.org/10.1113/jphysiol.2004.076695>
- Werblin, F.S., Dowling, J.E., 1969. Organization of the retina of the mudpuppy, *Necturus maculosus*. II. Intracellular recording. *Journal of Neurophysiology* 32, 339–355. <https://doi.org/10.1152/jn.1969.32.3.339>
- Westheimer, G., 2008. Directional sensitivity of the retina: 75 years of Stiles–Crawford effect. *Proceedings of the Royal Society B: Biological Sciences* 275, 2777–2786. <https://doi.org/10.1098/rspb.2008.0712>
- Wilby, D., Roberts, N.W., 2017. Optical influence of oil droplets on cone photoreceptor sensitivity. *The Journal of Experimental Biology* 220, 1997–2004. <https://doi.org/10.1242/jeb.152918>

- Wilby, D., Toomey, M.B., Olsson, P., Frederiksen, R., Cornwall, M.C., Oulton, R., Kelber, A., Corbo, J.C., Roberts, N.W., 2015. Optics of cone photoreceptors in the chicken (*Gallus gallus domesticus*). *Journal of the Royal Society, Interface / the Royal Society* 12, 20150591. <https://doi.org/10.1098/rsif.2015.0591>
- Wisely, C.E., Sayed, J.A., Tamez, H., Zelinka, C., Abdel-Rahman, M.H., Fischer, A.J., Cebulla, C.M., 2017. The chick eye in vision research: An excellent model for the study of ocular disease. *Progress in Retinal and Eye Research* 61, 72–97. <https://doi.org/10.1016/j.preteyeres.2017.06.004>
- Yamagata, M., Yan, W., Sanes, J.R., 2021. A cell atlas of the chick retina based on single-cell transcriptomics. *eLife* 10, e63907. <https://doi.org/10.7554/eLife.63907>
- Yan, W., Peng, Y.-R., van Zyl, T., Regev, A., Shekhar, K., Juric, D., Sanes, J.R., 2020. Cell Atlas of the Human Fovea and Peripheral Retina (preprint). *Neuroscience*. <https://doi.org/10.1101/2020.02.11.943779>
- Yau, K.-W., Hardie, R.C., 2009. Phototransduction Motifs and Variations. *Cell* 139, 246–264. <https://doi.org/10.1016/j.cell.2009.09.029>
- Yger, P., Spampinato, G.L., Esposito, E., Lefebvre, B., Deny, S., Gardella, C., Stimberg, M., Jetter, F., Zeck, G., Picaud, S., Duebel, J., Marre, O., 2018. A spike sorting toolbox for up to thousands of electrodes validated with ground truth recordings in vitro and in vivo. *eLife* 7. <https://doi.org/10.7554/eLife.34518>
- Yokoyama, S., 2008. Evolution of Dim-Light and Color Vision Pigments. *Annual Review of Genomics and Human Genetics* 9, 259–282. <https://doi.org/10.1146/annurev.genom.9.081307.164228>
- Yokoyama, S., 2002. Molecular evolution of color vision in vertebrates. *Gene* 300, 69–78. [https://doi.org/10.1016/S0378-1119\(02\)00845-4](https://doi.org/10.1016/S0378-1119(02)00845-4)
- Yoshimatsu, T., Schröder, C., Nevala, N.E., Berens, P., Baden, T., 2019. Cellular and molecular mechanisms of photoreceptor tuning for prey capture in larval zebrafish (preprint). *Neuroscience*. <https://doi.org/10.1101/744615>
- Zhang, Y., Kim, I.-J., Sanes, J.R., Meister, M., 2012. The most numerous ganglion cell type of the mouse retina is a selective feature detector. *Proc. Natl. Acad. Sci. U.S.A.* 109. <https://doi.org/10.1073/pnas.1211547109>
- Zhou, M., Bear, J., Roberts, P.A., Janiak, F.K., Semmelhack, J., Yoshimatsu, T., Baden, T., 2020. Zebrafish Retinal Ganglion Cells Asymmetrically Encode Spectral and Temporal Information across Visual Space. *Current Biology*. <https://doi.org/10.1016/j.cub.2020.05.055>
- Zimmermann, M.J.Y., Nevala, N.E., Yoshimatsu, T., Osorio, D., Nilsson, D.-E., Berens, P., Baden, T., 2018. Zebrafish Differentially Process Color across Visual Space to Match Natural Scenes. *Current Biology* 28, 2018-2032.e5. <https://doi.org/10.1016/j.cub.2018.04.075>